CANADIAN THESES ON MICROFICHE

I.S.B.N.

THESES CANADIENNES SUR MICROFICHE

National Library of Canada
Collections Development Branch

Canadian Theses on
Microfiche Service

Ottawa, Canada
K1A 0N4

Bibliothèque nationale du Canada
Direction du développement des collections

Service des thèses canadiennes
sur microfiche

NOTICE

The quality of this microfiche is heavily dependent upon the quality of the original thesis submitted for microfilming. Every effort has been made to ensure the highest quality of reproduction possible.

If pages are missing, contact the university which granted the degree.

Some pages may have indistinct print especially if the original pages were typed with a poor typewriter ribbon or if the university sent us a poor photocopy.

Previously copyrighted materials (journal articles, published tests, etc.) are not filmed.

Reproduction in full or in part of this film is governed by the Canadian Copyright Act, R.S.C. 1970, c. C-30. Please read the authorization forms which accompany this thesis.

THIS DISSERTATION
HAS BEEN MICROFILMED
EXACTLY AS RECEIVED

AVIS

La qualité de cette microfiche dépend grandement de la qualité de la thèse soumise au microfilmage. Nous avons tout fait pour assurer une qualité supérieure de reproduction.

S'il manque des pages, veuillez communiquer avec l'université qui a conféré le grade.

La qualité d'impression de certaines pages peut laisser à désirer, surtout si les pages originales ont été dactylographiées à l'aide d'un ruban usé ou si l'université nous a fait parvenir une photocopie de mauvaise qualité.

Les documents qui font déjà l'objet d'un droit d'auteur (articles de revue, examens publiés, etc.) ne sont pas microfilmés.

La reproduction, même partielle, de ce microfilm est soumise à la Loi canadienne sur le droit d'auteur, SRC 1970, c. C-30. Veuillez prendre connaissance des formules d'autorisation qui accompagnent cette thèse.

LA THÈSE A ÉTÉ
MICROFILMÉE TELLE QUE
NOUS L'AVONS REÇUE

NL-339 (r. 82/08)

Canada

109

0-315-16018-7

National Library of Canada | Bibliothèque nationale du Canada

Canadian Theses Division | Division des thèses canadiennes

Ottawa, Canada
K1A 0N4

63927

PERMISSION TO MICROFILM — AUTORISATION DE MICROFILMER

• Please print or type — Écrire en lettres moulées ou dactylographier

Full Name of Author — Nom complet de l'auteur

SAEID SHAMMAS

Date of Birth — Date de naissance

SEPT 9, 1949.

Country of Birth — Lieu de naissance

IRAN

Permanent Address — Résidence fixe

901, 1220 MERIVALE ROAD
OTTAWA, ONTARIO K1Z 8P2

Title of Thesis — Titre de la thèse

Numerical Methods in Microwave Integrated Circuits

University — Université

Univ of Alberta

Degree for which thesis was presented — Grade pour lequel cette thèse fut présentée

Ph. D.

Year this degree conferred — Année d'obtention de ce grade

Spring 1983

Name of Supervisor — Nom du directeur de thèse

P. Gaud

Permission is hereby granted to the NATIONAL LIBRARY OF CANADA to microfilm this thesis and to lend or sell copies of the film.

The author reserves other publication rights, and neither the thesis nor extensive extracts from it may be printed or otherwise reproduced without the author's written permission.

L'autorisation est, par la présente, accordée à la BIBLIOTHÈQUE NATIONALE DU CANADA de microfilmer cette thèse et de prêter ou de vendre des exemplaires du film.

L'auteur se réserve les autres droits de publication; ni la thèse ni de longs extraits de celle-ci ne doivent être imprimés ou autrement reproduits sans l'autorisation écrite de l'auteur.

Date

April 5 / 83

Signature

Saeid Shammas

NL-91 (4/77)

THE UNIVERSITY OF ALBERTA

NUMERICAL METHODS IN MICROWAVE INTEGRATED CIRCUITS

by

© SAEID SHAMMAS

A THESIS

SUBMITTED TO THE FACULTY OF GRADUATE STUDIES AND RESEARCH

IN PARTIAL FULFILMENT OF THE REQUIREMENTS FOR THE DEGREE

OF DOCTOR OF PHILOSOPHY

DEPARTMENT OF ELECTRICAL ENGINEERING

EDMONTON, ALBERTA

SPRING, 1983

MICRO

THE UNIVERSITY OF ALBERTA

RELEASE FORM

NAME OF AUTHOR Saeid Shammas

TITLE OF THESIS Numerical Methods in Microwave Integrated Circuits

DEGREE FOR WHICH THESIS WAS PRESENTED Doctor of Philosophy

YEAR THIS DEGREE GRANTED Spring 1983

Permission is hereby granted to THE UNIVERSITY OF ALBERTA LIBRARY to reproduce single copies of this thesis and to lend or sell such copies for private, scholarly or scientific research purposes only.

The author reserves other publication rights, and neither the thesis nor extensive extracts from it may be printed or otherwise reproduced without the author's written permission.

(Signed) Saeid Shammas

PERMANENT ADDRESS:

#901 - 1220 Merivale Road
Ottawa, Ontario
K1Z 8P2

DATED March 21, 1983

THE UNIVERSITY OF ALBERTA

FACULTY OF GRADUATE STUDIES AND RESEARCH

The undersigned certify that they have read, and recommend to the Faculty of Graduate Studies and Research, for acceptance, a thesis entitled Numerical Methods in Microwave Integrated Circuits submitted by Saeid Shammas in partial fulfilment of the requirements for the degree of Doctor of Philosophy.

Saeid A. Ford.
Supervisor

F.E. Vermeulen

W. Ismail

C. G. Englefield

Alaaddin Saleh
External Examiner

Date 83.03.21

To my wife, Shaunie

ABSTRACT

In this thesis, novel numerical methods are devised for analyzing microwave integrated circuits. A review of current methods shows a need for new methods that are efficient and yet flexible to handle various types of microstrip structures. Microstrip lines in the quasi-TEM (transverse electromagnetic) regime are analyzed by the boundary element method (BEM). The accuracy of the obtained results is comparable to other methods but the required computer space/time is decreased significantly (15 x 15 matrix for microstrip lines, 35 x 35 matrix for coupled microstrip lines). A new method is developed for analyzing microstrip lines, which can be considered as a generalization of Green's functions. A closed-form solution for the characteristic impedance of microstrip lines is obtained which exhibits reasonable accuracy (typically 5%). An exact analysis of microstrip lines is presented in which only one potential function is required rather than the customary choice of two potential functions. This reduction in the number of variables is accompanied by generalizing the developed numerical method; the domain of integration in the integral equation is the dielectric air interface (DAI). The numerical results are in good agreement with other methods, while a relatively small matrix size is needed for computation (of the order of 8x8). In order to generalize this method for analyzing microstrip resonators, the method is modified so that the domain

of integration is the area along the strips. As an example, a rectangular microstrip resonator is analyzed. The accuracy of this method is good at high frequencies, but decreases as frequency decreases. This method results in small matrix sizes (e.g., 4 x 4), shows reasonable accuracy within a specified frequency range, and is shown to be flexible since it can be used to analyze microstrip lines as well as microstrip resonators.

ACKNOWLEDGEMENTS

I wish to thank Dr. P.A. Goud for his constant help and encouraging advice throughout the work. My appreciation is also extended to Dr. W. Israel who has given me his constant support and understanding. Thanks are also extended to the members of my examining committee for reviewing this work. Finally, I wish to thank Mrs. Giff of Ottawa for typing the thesis.

TABLE OF CONTENTS

Chapter		Page
I.	Historical Review of Numerical Methods Applied to Microstrips	1
	A. Introduction	1
	B. Microstrip Lines	8
	Quasi-TEM (Transverse Electromagnetic) Analysis	8
	Exact Analysis of Microstrip Lines	20
	Open Microstrip Lines	25
	C. Quasi-TEM (Transverse Electromagnetic) Analysis of Coupled Microstrip Lines	27
	Preliminary Discussion	27
	Green's Function	28
	Mode Matching	30
	Variational Method	30
	Variational Method in the Fourier Transform Domain	31
	D. Microstrip Resonators	32
	Transmission Line Models	32
	Magnetic Wall Models	35
	Fringing Effects	37
	Exact Formulation	37
	E. Review Conclusions	39
	F. Thesis Organization	40
II.	Boundary Element Method	42
	A. Introduction	42

B. Formulation..... 43
C. Microstrip Line with $\varepsilon_r=1$..... 51
D. Final Assembly of the Matrix Equation..... 55
E. Microstrip Line with $\varepsilon_r\neq1$..... 56
F. Coupled Microstrip Lines..... 59
G. Coupled Lines with $\varepsilon_r=1$..... 67
H. Summary..... 70
I. Conclusions..... 77
III. An Alternative Integral Equation Method..... 78
A. Introduction..... 78
B. Formulation..... 78
C. Single Microstrip Line..... 82
D. Coupled Microstrip Lines..... 87
E. Numerical Results..... 89
F. Summary..... 94
G. Conclusions..... 95
IV. Wave Analysis of Microstrip Lines..... 97
A. Introduction..... 97
B. Formulation..... 97
C. An Integral Equation Formulation..... 99
D. Evaluation of the Kernel $K(\xi)$..... 103
E. Numerical Solution..... 106
F. Summary..... 109
G. Conclusions..... 113
V. An Alternative Integral Equation Method for the Wave Analysis of Microstrips..... 114

A. Introduction..... 114
B. Formulation..... 114
C. Single Microstrip Line..... 120
D. Microstrip Resonators..... 124
E. Numerical Results..... 129
F. Summary..... 134
G. Conclusions..... 135
VI. Conclusions..... 136
References..... 139
Appendices
Appendix A..... 145
Appendix B..... 153
Appendix C..... 163
Appendix D..... 168

LIST OF FIGURES

Figure	Caption	Page
1-1	(a) open microstrip line; (b) shielded microstrip line; (c) coupled microstrip line; (d) shielded microstrip resonator.	3
1-2	Sketch of the electric field configuration at a microstrip line cross section (a) the case $\epsilon_r = 1$; (b) the case $\epsilon_r \neq 1$, the electric field lines have a break at the DAI (dielectric air interface).	12
1-3	(a) Sketch of the charge distribution on the microstrip line (taken from [12]); (b) Sketch of the potential distribution at the y=h plane (taken from [12]).	19
1-4	(a) LSE (longitudinal section electric) model for a microstrip line; (b) general behavior of the effective dielectric constant, ϵ_e, as a function of frequency, obtained from the LSE model.	22

1-5	Transmission line models for microstrip resonators; (a) rectangular resonator; (b) transmission line model neglecting fringing fields; (c) transmission line model with fringing fields; (d) transmission line model with fringing fields; due to odd symmetry, half of model (c) is sufficient; (e) open-ring resonator which can be modelled by (d).	33
1-6	(a) Ring resonator at y=h plane [33]. (b) magnetic wall model of ring resonator.	36
2-1	(a) Unshielded microstrip line; (b) an equivalent structure	44
2-2	Equivalent structure for the microstrip line used for BEM (Boundary Element Method); R is assumed to be infinitely large.	46
2-3	DAI deformed in the vicinity of (x_i, y_i) in order to find the limit of $\partial\psi/\partial y$ as (x,y) approaches (x_i, h) (Eq. 2-11).	49
2-4	$x(\zeta)$ discretized to facilitate the numerical solution of Eqs. 2-22.	53

2-5	Demonstration of ζ-axis divided into various segments using the data for numerical integration. (ζ-axis is the path defined by the y=h plane in a microstrip line cross-section)	57
2-6	Potential distribution of a microstrip line on the DAI vs. normalized distance with ε_r=9.9 and w/h=1.0; results coincide with those of [12].	60
2-7	Surface charge of a microstrip line vs. normalized distance on the MIC with ε_r=9.9 and w/h=1.0; results coincide with those of [12].	61
2-8	Characteristic impedance of a microstrip line vs. w/h for various ε_r, results coincide with those of [8].	62
2-9	Normalized wavelength of a microstrip line vs. w/h for various ; results coincide with those of [8].	63
2-10	(a) Coupled microstrip lines; (b) coupled microstrip lines with normalized x-axis.	65
2-11	Even- and odd-mode characteristic impedance of coupled microstrip lines vs. w/h for various values of s/h and ε_r=9.0; results coincide with [4] and [26].	71

2-12	Even- and odd-mode ϵ_e of coupled microstrip lines vs. w/h for various values of s/h and ϵ_r=9.0.	72
2-13	Even- and odd-mode surface charge vs. normalized distance on coupled microstrip lines; ϵ_r=9.0, w/h=1.0 and s/h=0.3.	73
2-14	Even- and odd-mode potential distribution of coupled microstrip lines on the DAI vs. normalized distance; ϵ_r =9.0, w/h=1.0 and s/h=0.3.	74
2-15	Even- and odd-mode ϵ_e of coupled microstrip lines vs. s/h; w/h=1.0 and ϵ_r=9.0.	75
3-1	Open microstrip line; R is assumed infinitely large.	79
3-2	Characteristic impedence of a microstrip line vs. w/h.	85
3-3	Normalized wavelength of a microstrip line vs. w/h.	86
3-4	Even- and odd-mode characteristic impedence vs. w/h for s/h=2.0; coupled microstrip lines with ϵ_r=9.0.	90
3-5	Percent error in final value of ϵ_e vs. N_m (N_m is the number of terms to which the sum of Eq. 3-24 is truncated)	92

	w/h=1.5, s/h=0.3, ϵ_r=9.0 and L_m=5 (L_m is the final matrix size)	
3-6	Percent error in Z_o vs. L_m; (L_m is the final matrix size) w/h=1.5, s/h=1.0, ϵ_r=9.0 and N_m=40 (N_m is the number of terms to which the sum of Eq. 3-24 is truncated).	93
4-1	A single microstrip line shielded on top by a metallic plane.	100
4-2	Countour for the complex integration of Eq. 4-23b; γ_o is used to find a complimentary kernel.	104
4-3	ξ-axis divided into various segments for the numerical integration of Eqs. 4-23a and 30.	107
4-4	ϵ_e of a single microstrip line vs. normalized frequency; ϵ_{eo} is obtained from quasi-TEM methods.	110
4-5	ϵ_e of a single microstrip line vs. normalized frequency; ϵ_r=10.1 and w/h=2.5; ϵ_{eo} is obtained from quasi-TEM methods.	111
5-1	Microstrip line shielded on top by a metallic plane; f(x) of Eq. 5-4 is non-zero on $-(x_i + d_i)$ to.	116

	$-(x_i - d'_i)$, and $(x_i - d'_i)$ to $(x_i + d'_i)$.	
5-2	Countour for the integral of Eq. 5-5a.	118
5-3	MIC divided into several intervals for the numerical integration of Eq. 5-15.	122
5-4	Rectangular microstrip resonator with even mode of resonance.	125
5-5	Countour for the integration of Eq. 5-30.	127
5-6	Effective dielectric constant of a microstrip line vs. normalized frequency; ε_r=11.7 and w/h=0.96.	130
5-7	Effective dielectric constant vs. Nx, (Nx is the number of terms to which Eq. 5-10a is truncated). fh=40.0 GHxmm, w/h=0.96, ε_r=11.7 and Mr=4 (Mr is the final matrix size).	131
5-8	Calculated effective dielectric constant vs. final matrix size, Mr; fh=40.0 GHz · mm, w/h=0.96, ε_r=11.7 and Nx=500. (Nx is the number of terms to which Eq. 5-10a is truncated)	132

LIST OF SYMBOLS

$\hat{a}_x, \hat{a}_y, \hat{a}_z$:	Unit vectors along the x-, y-, and z-axes
h:	Substrate height
h^-:	$=\lim_{\substack{y < h \\ y \to h}} y$
h^+:	$=\lim_{\substack{y > h \\ y \to h}} y$
c:	Speed of light in free space
C:	Capacitance of the microstrip line per unit length
C_o:	Capacitance of the microstrip line per unit length assuming that the dielectric substance is removed
$\vec{E}$:	Electric field vector
$\vec{H}$:	Magnetic field vector
f:	Frequency
$k=2\pi f/c$	Propagation constant of an electromagnetic wave in free space
t:	Strip thickness
w:	Strip width
Z:	Characteristic impedance of the microstrip line
Z_o:	Characteristic impedance of the microstrip line when $\epsilon_r=1$
Z_e:	Even-mode characteristic impedance of coupled lines
Z_o:	Odd-mode characteristic impedance of coupled lines

β	Propagation constant along the microstrip line
ϵ	Dielectric constant of free space
ϵ_e	Effective relative dielectric constant
ϵ_{e0}	Zero frequency ϵ_e
$\epsilon_{e,e}$	Even-mode ϵ_e of coupled lines
$\epsilon_{e,o}$	Odd-mode ϵ_e of coupled lines
ϵ_r	Relative dielectric constant of the substrate (Fig. 1-1)
λ_g	The guide wavelength of the microstrip line
$\kappa = \epsilon_r$	In dielectric
$\kappa = 1$	In vacuo
η	$=w/(2h)$, Figs. 1-1a, 1b, and 1c
σ	$=(s+w)/(2h)$, Fig. 1-1c
ρ	Charge distribution per unit length on strip
μ	Magnetic constant of free space
ω	Radian frequency
$\partial/\partial n$	Normal derivative (to surface)

Subscripts and Superscripts

a:	Air
d:	Dielectric
e:	Even (in case of coupled microstrip lines)
o:	Odd (in case of coupled microstrip lines)
t:	Transverse component (with respect to the direction of propagation)
tan:	Tangential component
nor:	Normal component

Abbreviations

BEM:	Boundary element method
DAI:	Dielectric air interface
LSE:	Longitudinal section electric
LSM:	Longitudinal section magnetic
MIC:	Metallic portion of the y=h plane in Fig. 1-1
TE:	Transverse electric
TEM:	Transverse electromagnetic
TLM:	Transmission line matrix
TM:	Transverse magnetic

I. HISTORICAL REVIEW OF NUMERICAL METHODS APPLIED TO MICROSTRIPS

A. Introduction

Microstrips are microwave circuits which are constructed by printed circuit techniques. Prior to the development of printed circuit technology, structures formed of conducting surfaces of various configurations were used as electromagnetic waveguides. Microstrip circuits have been favoured over waveguide technology for many applications, due to their low cost and compactness. Also, microstrips are of interest since, in principle, the same microstrip circuit can be used for a very broad frequency range. Extensive research has been carried out on microstrip structures. During the decade spanning the years 1945 to 1955, this field of research grew so rapidly that a special issue of the IRE Transactions on Microwave Theory and Techniques was totally devoted to this field [1].

The basic microstrip structure consists of a dielectric sheet, called the substrate, which is bounded by a ground plane on one side and by a thin, metallic circuit on the other side. The geometry of this circuit determines the electromagnetic properties of the microstrip structure. Significant circuit size reduction can be accomplished by using an appropriate dielectric material; the relative dielectric constant of substrates is typically about 10.

At the heart of many complicated microstrip circuits lie three basic microstrip structures, namely, lines, coupled

lines and resonators, as shown in Fig. 1-1. These structures are analyzed numerically in this thesis.

Microstrip lines (Fig. 1-1a) are the "second generation" of printed transmission lines. The original version, called "stripline", was introduced in 1949, [2]. A stripline is similar to a microstrip line, except that it has an additional dielectric and ground plane above the strip conductor. Striplines are no longer commonly used, since they are harder to manufacture than microstrip lines.

A microstrip line (Fig. 1-1a) is assumed to extend to infinity in the z-direction (i.e., the direction of propagation of the electromagnetic waves). In practice, the microstrip line exhibits a characteristic impedance, Z, which is used to terminate the line. In this way, the reflection of electromagnetic waves is avoided. Thus, a line of finite length can be treated in the same way as one that is infinitely long.

Microstrip lines are normally placed in a grounded metallic box having dimensions which are usually considerably larger than the line width; the resulting structure is called a shielded microstrip line (Fig. 1-1b). By shielding a microstrip line, electromagnetic interference problems can be avoided. The effect of these shielding walls on the properties of microstrip lines is usually negligible.

A coupled microstrip line consists of a pair of closely spaced parallel metallic strips bonded to the dielectric

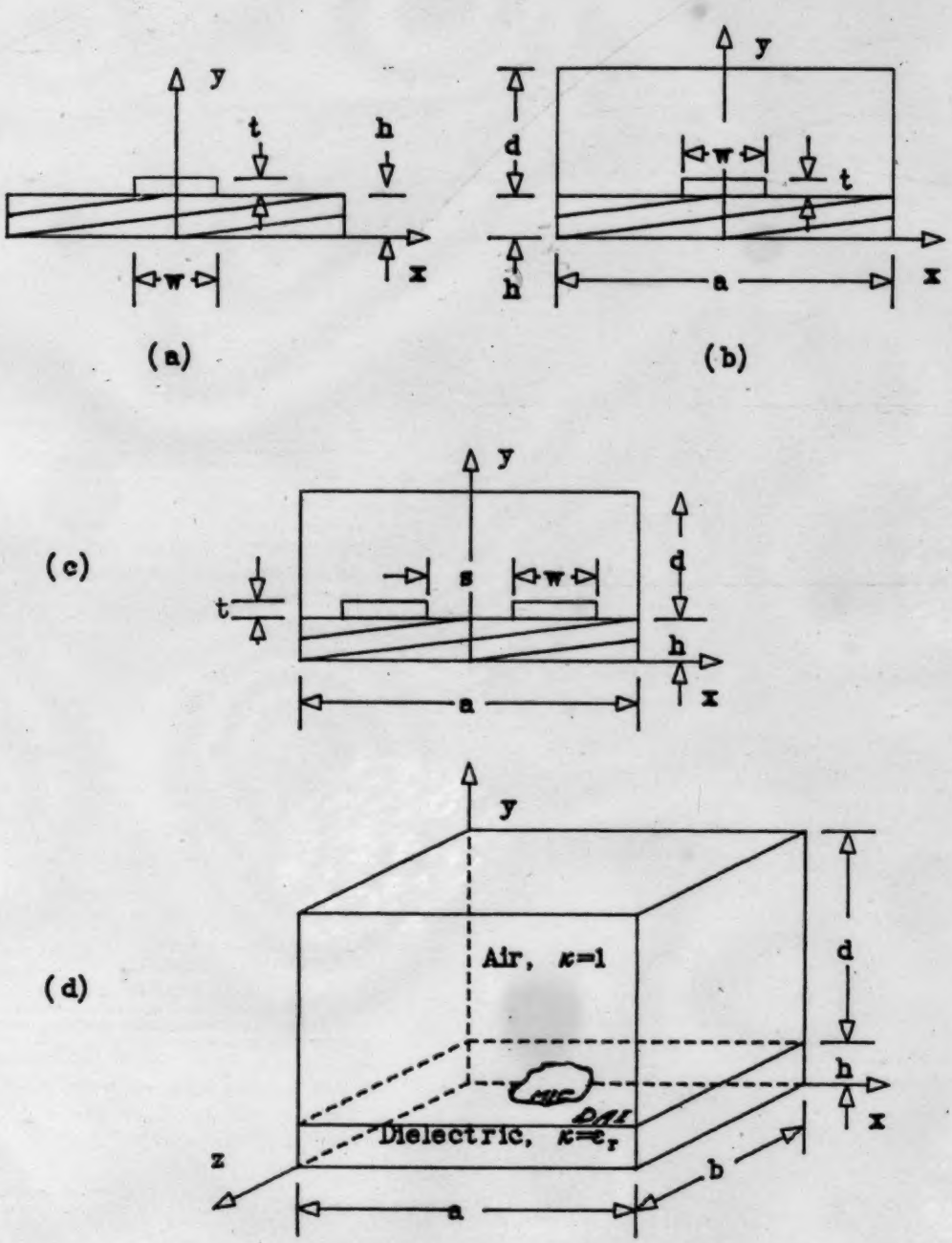

Fig.1-1 (a) Open microstrip line;
(b) shielded microstrip line;
(c) coupled microstrip line;
(d) shielded microstrip resonator.

substrate at the y=h plane (Fig. 1-1c). The ground plane lies on the opposite side of the substrate. With two conducting strips and a ground plane, the structure has two independent modes of propagation.

Microstrip resonators (Fig. 1-1d) consist of a metallized area in the y=h plane (rectangular, circular, elliptical or triangular shapes are commonly used); the dimensions of this metallized area are usually of the order of a wavelength at the frequency at which the resonator resonates.

Advances in semiconductor technology have created an interest in the integration of microwave circuits. Monolithic microwave integrated circuits are active circuits operating at microwave frequencies in which the solid state devices and the microwave circuit have been integrated. In recent years, the terms "stripline", "microstrip" and "microwave integrated circuits" have come to be used interchangeably. However, the term "monolithic microwave integrated circuits" refers only to the active circuit described above. In this thesis, only microstrip structures are analyzed (i.e., microstrip lines, coupled lines and microstrip resonators).

Rapid advances in microstrip technology have stimulated much theoretical research; an important goal of this field is the computer-aided design of microstrips. The main objective of this thesis is to develop computer algorithms which may eventually lead to the analysis of a wide variety

of microstrip structures. The basic concepts underlying the different theoretical methods used to analyze these structures are presented. These methods are important for the design of microstrips. It is hoped that these theoretical methods will lead to the computer-aided design of microstrips.

In order to analyze microstrip lines, the type of electromagnetic waves which propagate in the lines must first be determined. A microstrip line resembles a two-conductor transmission line and thus, at first, it may appear that the structure supports TEM (transverse electromagnetic) waves. However, this is true only if the relative dielectric constant of the dielectric substrate, ε_r, tends to unity. Otherwise, the line cannot support TEM waves, since the phase velocity of the waves in the substrate will be different from that in the air. When the operating frequency approaches zero, the electromagnetic fields approach a TEM configuration (even when $\varepsilon_r \neq 1$), which is referred to as the quasi-TEM regime [2]. The microstrip can be assumed to be in the quasi-TEM regime when the wavelength of the propagating waves is larger than the microstrip line width and the substrate height [3].

In the quasi-TEM regime, the parameters of a microstrip line can be calculated with the simplifying assumption that the propagating waves in the microstrip line are TEM. Coupled microstrip lines can be treated similarly. Quasi-TEM methods are useful not only as a first step towards the exact analysis of microstrips, but also as engineering design aids. For example, a 50Ω microstrip line can be treated as a TEM line

up to approximately 10 GHz. Thus, several quasi-TEM methods which are frequently used are explained briefly in this chapter.

With the continuing advances of semiconductor technology, microstrips are being designed for operation at ever higher frequencies, where the quasi-TEM approximation may not be justified. An exact analysis of microstrips thus becomes necessary. Moreover, quasi-TEM approximations can be used only for some resonator shapes, such as rectangular resonators. In this chapter, some mathematical procedures which have been applied to date to the analysis of microwave integrated circuits (Fig. 1-1) are discussed. The merits of each method (e.g., the accuracy of the results and the computer space and time requirements) are also discussed whenever such data have been given in the original papers. However, it is necessary to emphasize that some of the methods are more analytical in nature and that the time spent in formulating them may overshadow considerations of the final matrix size and computer efficiency. Such analytical methods are important if they can be generalized to a wide variety of microstrip structures. Thus, a number of methods used by engineers are explained in this chapter and the possibility of generalizing them to more complicated problems is also discussed.

Other aspects of microstrips, which deal with higher order modes, radiation from sharp edges, microstrip loss, surface waves, and box resonances are not included in this work.

The basic concepts necessary to formulate and analyze

microstrips are discussed first. Next, the mathematical methods applied by others to microstrips are summarized. The methods are classified and discussed according to their application to microstrip lines, coupled lines and resonators. These methods are quite diverse and few of them can be used to analyze all the microstrip structures shown in Fig. 1-1.

Sec. B, titled "Microstrip Lines", is based on the work done by Mittra and Itoh [2]. A modified discussion is presented, which includes more recent publications. The approach has been to avoid mathematical detail, while, at the same time, to give a sufficiently comprehensive review of each method to communicate its essence. Some quasi-TEM methods are presented first. Next, a semi-empirical model is explained which describes the frequency behavior of microstrip lines. Subsequently, the works of other researchers dealing with the exact analysis of microstrip lines are presented.

Sec. C (Coupled Microstrip Lines) is similarly a modification of the work of Weiss [4], together with the review of several works published in recent years.

In Sec. D (Microstrip Resonators), some approximate methods for evaluating the resonant frequencies of microstrip resonators are explained. Such approximate methods are applicable to simple resonator geometries, such as rectangular-, circular-, or ring-resonators. Subsequently, other exact formulations are reviewed.

Sec. E (Review Conclusions) compares the methods discussed

in this chapter. It is argued that methods involving integral equations are better suited for analyzing microstrips than other methods. Furthermore, this section introduces the methods that are developed in this thesis.

B. Microstrip Lines

Quasi-TEM Analysis

Preliminary Discussion

For sinusoidal time variations, the electric and magnetic field components of the waves propagating in microstrip lines must satisfy the steady-state Maxwell's equations

$$\nabla \times \vec{E} = -j\omega\mu\vec{H}, \tag{1-1a}$$

$$\nabla \times \vec{H} = j\omega\varepsilon\kappa\vec{E}, \tag{1-1b}$$

$$\nabla \cdot \vec{E} = 0, \tag{1-1c}$$

$$\nabla \vec{H} = 0. \tag{1-1d}$$

where

$\vec{E}$ is the electric field intensity,

$\vec{H}$ is the magnetic field intensity,

μ is the magnetic permeability of free space,

ε is the dielectric constant of free space,

ε_r is the relative dielectric constant;

$$\kappa = \begin{cases} 1 \text{ in air,} \\ \varepsilon_r \text{ in dielectric .} \end{cases}$$

and

$$\omega = 2\pi f .$$

where f is the frequency.

In the analysis of microstrip lines, it is assumed that the lines are lossless and infinitely long. Consequently, the fields travelling along the positive z-axis are assumed to vary as $\exp(-j\beta z)$. β is called the propagation constant in the z-direction. Eqs. 1, together with the assumption that the fields vary as $\exp(-j\beta z)$ in the z-direction, result in Helmholtz's equation for $\vec{E}$ and $\vec{H}$ in the microstrip line cross section (i.e., the x-y-plane):

$$\nabla_t^2\vec{E}+(\epsilon_r k^2-\beta^2)\vec{E}=0, \qquad (1\text{-}2a)$$

and

$$\nabla_t^2\vec{H}+(\epsilon_r k^2-\beta^2)\vec{H}=0, \qquad (1\text{-}2b)$$

where

$$\nabla_t^2=(\partial/\partial x)^2+(\partial/\partial y)^2, \qquad (1\text{-}2c)$$

$$k=2\pi f/c, \qquad (1\text{-}2d)$$

and c is the speed of light in free space.

Microstrip lines can be fully analyzed by solving Eqs. 1-2, subject to the boundary and continuity conditions for $\vec{E}$ and $\vec{H}$. However, it has been customary to solve Helmholtz's equation for two properly chosen potential functions and to obtain the field components from these potential functions. This approach will be more fully explained in the section "Exact Analysis of Microstrip Lines" (p. 20).

In this section, the simpler case of the quasi-TEM regime is studied. When $\epsilon_r=1$, the lowest order solution

of Eqs. 1-2 is of the TEM form [2] and [4], with $\beta=k$. It is then possible to obtain the field components from a potential function which satisfies Laplace's equation in the cross section

$$\nabla_t^2\varphi(x,y)=0. \qquad (1\text{-}2e)$$

where φ is the electrical potential distribution in the microstrip cross section.

When $\varepsilon_r \neq 1$, the fields approach a TEM configuration for lower frequencies [2]. This assumption, as explained above, is only valid when f and thus k is small, since for $\varepsilon_r \neq 1$, $\beta \to k$ only as $k \to 0$.

In order to describe the boundary conditions imposed on φ, two definitions are introduced: DAI connotes the dielectric air interface at the y=h plane in Fig. 1-1, and MIC refers to the metallic portions of the microwave integrated circuits at the y=h plane (Fig. 1-1). These acronyms will be used throughout the thesis.

The boundary conditions imposed on $\varphi(x,y)$ are as follows (Fig. 1-1a):

$$\varphi(x,0)=0, \qquad (1\text{-}3a)$$

$$\varphi(x,h)=V \text{ volts on the MIC} \qquad (1\text{-}3b)$$

The continuity of the displacement vector at the DAI implies

$$\varepsilon_r\, \partial\varphi(x,h^-)/\partial y = \partial\varphi(x,h^+)/\partial y, \qquad (1\text{-}3c)$$

where

$$\bar{h}=\lim_{\substack{y\to h\\ y<h}} y \qquad (1\text{-}3d)$$

and

$$\bar{\bar{h}}=\lim_{\substack{y\to h\\ y>h}} y \qquad (1\text{-}3e)$$

Furthermore, the strip thickness, t, of Fig. 1-1a and 1b is usually assumed to be negligible. With this assumption, the free electrons in the strip can be regarded as a surface charge layer $\rho(x)$; therefore

$$\varepsilon_r \partial\varphi(x,\bar{h})/\partial y - \partial\varphi(x,\bar{\bar{h}})/\partial y = \rho(x)/\varepsilon. \qquad (1\text{-}3f)$$

The electric field distribution at a microstrip line cross section is illustrated in Fig. 1-2. Fig. 1-2a shows the field distribution for the case $\varepsilon_r=1$.

When $\varepsilon_r\neq 1$, due to the boundary condition of Eq. 1-3c, the electric field lines refract at the DAI (Fig. 1-2b).

At this point, the parameters used to characterize microstrip lines are introduced [2]. The capacitance, C, per unit length of the line is defined as

$$C=Q/V, \qquad (1\text{-}4a)$$

where V is the potential on the strip (Eq. 1-3b) and Q is the total charge on the strip given by

$$Q=\int_{-w/2}^{w/2}\rho(x)\,dx. \qquad (1\text{-}4b)$$

When $\varepsilon_r=1$, the capacitance per unit length is denoted by C_0. The characteristic impedance of a microstrip

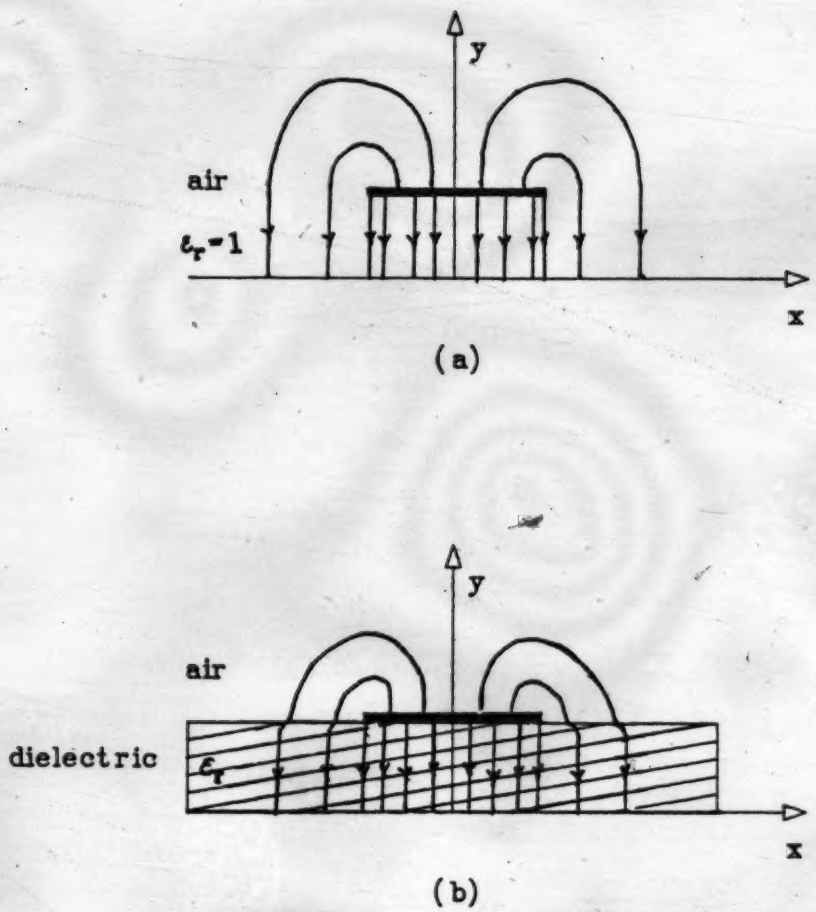

Fig. 1-2 Sketch of the electric field configuration at a microstrip line cross section

(a) the case ε_r=1;

(b) the case $\varepsilon_r \neq 1$; the electric field lines refract at the DAI (dielectric air interface).

line with $\varepsilon_r=1$ is defined as

$$\bar{Z}_o=1/(cC_o). \qquad (1\text{-}4c)$$

For the case $\varepsilon_r\neq 1$, the characteristic impedance is

$$Z=\bar{Z}_o(C_o/C)^{1/2} \qquad (1\text{-}4d)$$

The propagation constant along the z-axis is related to the wavenumber, k, as follows

$$\beta=k(C/C_o)^{1/2} \qquad (1\text{-}4e)$$

The factor (C/C_o) is called the effective dielectric constant and is denoted by ε_e. Thus,

$$\beta=\sqrt{\varepsilon_e}k, \qquad (1\text{-}4f)$$

The physical meaning of ε_e, is as follows: Assume that the dielectric substrate of Figs. 1-1a, b, or c is removed and the whole region around the conductors is filled with a dielectric material with a relative dielectric constant equal to ε_e, then Z and β will still be given by Eqs. 1-4. However, ε_e is frequency dependent. In the quasi-TEM approximation, the value of ε_e at zero frequency is obtained.

Summarizing, in the quasi-TEM method, the Laplace equation (Eq. 1-2e) is solved for the potential distribution, φ, at the microstrip line cross section. The boundary conditions imposed on φ are described in Eqs. 1-3. The characteristic impedance, Z, and the effective dielectric constant, ε_e, of the line is calculated from (Eqs. 1-4). In the following sections, the methods used by different authors for the quasi-TEM analysis of microstrip lines are summarized.

Quasi-TEM Methods

Wheeler [1] has used conformal mapping for solving the Laplace equation at the microstrip line cross section.

The mapping transforms the original microstrip line into a parallel-plate structure bounded by two vertical magnetic side walls (i.e., a surface on which the normal component of $\vec{E}$ is zero). The DAI is mapped into a curved surface. The curved DAI is then approximated by straight lines parallel to the coordinate axes. Microstrip lines are classified into three categories, according to their width. Different mapping functions are used for each category.

The results obtained by Wheeler [1] are extensively used in microstrip designs, because of their low cost and ease of programming. Unfortunately, the method cannot be generalized to the exact analysis of microstrips, since conformal mapping is applicable to Laplace's equation only.

In the finite difference (relaxation) method, the unknown field distribution is quantized at discrete intersections of coordinate grids called the net - or mesh-points [5]. The potential function can be expanded in a Taylor series about each mesh-point.

The potentials at the conductors are known. In this way, a matrix equation is obtained which can be solved by a matrix inversion. However, when the

number of mesh-points is large, the matrix inversion becomes very time consuming.

A superior method which reduces the computer time for finding the unknowns is the relaxation method [6] and [7]. The relaxation method is a numerical algorithm for finding the unknowns by the method of successive approximations.

The finite difference method is easy to formulate and program. The method can be easily generalized to the exact analysis of microstrips, but the final matrix size is usually large (c.f. Finite Difference Method applied to the wave analysis described on page 23).

In the variational method in the Fourier Transform domain [8], the strip is considered as an infinitely thin layer of charge. Thus, Poisson's equation is solved in the cross section of a microstrip line (Fig. 1-1a)

$$\nabla_t^2 \varphi(x, y) = -(1/\varepsilon)\rho(x)\delta(y-h), \qquad (1\text{-}5)$$

Taking the Fourier transform of Eq. 1-5 in the x-direction and applying the boundary conditions yields

$$\tilde{\varphi}(\gamma, h) = \tilde{\rho}(\gamma)/\{\varepsilon|\gamma|[1+\varepsilon_r \coth(|\gamma|h)]\}. \qquad (1\text{-}6)$$

Eq. 1-6 leads to a variational form for the capacitance per unit length, C, in the Fourier domain.

The variational method has the property of including only the charge distribution in the final equation. The accuracy of the results depends on the assumed

charge distribution. The method does, in general, provide a lower bound to the value of the capacitance.

The typical computer (CPU) time needed is less than 10 secs. on an IBM 7094 computer [8].

The integral equation method uses Green's functions and can be used in cases where the strip thickness cannot be neglected [9] and [10]. Define

$$G(x, y; x_o, y_o)$$

such that

$$\nabla_t^2 G(x, y; x_o, y_o) = -(1/\varepsilon)\,\delta(x-x_o)\,\delta(y-y_o). \qquad (1\text{-}7)$$

G is the potential at (x,y) due to a charge located at (x_o, y_o). Applying the superposition principle, the potential can be expressed as

$$\varphi(x, y) = \int_{MIC} G(x, y; x_o, y_o)\,\rho(x_o, y_o)\,dl_o. \qquad (1\text{-}8)$$

The potential distribution is known on the MIC, say $\varphi = V$; Eq. 1-8 is an integral equation with unknown ρ, and can be solved by discretizing the equation. The typical computer time needed is 30 secs. for a resulting matrix size of 30 X 30.

The method of moments [11] is closely related to the integral equation method. In this method, a function similar to the Green's function is found for a very narrow but finite line. In this way, the integral of Eq. 1-8 is discretized.

In the generalized Wiener-Hopf method [12] and [13], the potential and the charge distributions are found by considering their properties in the Fourier domain.

This method uses Eq. 1-6 obtained above.

Taking the potential of the strip as 1V, we can express φ at the y=h plane as

$$\varphi(x, h) = h(x-w/2)\,u(x-w/2) + [u(x+w/2) - u(x-w/2)] + h(-x-w/2)\,u(-x-w/2). \quad (1\text{-}9)$$

where u(x) is a unit step function and h(x) is the unknown potential function on the DAI. Taking the Fourier transform of Eq. 1-9 with respect to x we obtain

$$\tilde{\varphi}(\gamma, h) = 2[\sin(\gamma w/2)/\gamma] + \exp(j\gamma w/2)\,H(\gamma) + \exp(-j\gamma w/2)\,H(-\gamma), \quad (1\text{-}10)$$

where $H(\gamma)$ is the Fourier transform of h(x)u(x). Comparing Eqs. 1-6 and 1-10 we obtain

$$\tilde{\rho}(\gamma)/\{\varepsilon|\gamma|[1+\varepsilon_r \coth(|\gamma|h)]\} = 2\sin(\gamma w/2)/\gamma + \exp(j\gamma w/2)\,H(\gamma) + \exp(-j\gamma w/2)\,H(-\gamma). \quad (1\text{-}11)$$

Eq. 1-11 includes two unknown functions, $\tilde{\rho}(\gamma)$ and $H(\gamma)$, but both can be found by considering the properties of the complex functions involved. Firstly, $\tilde{\rho}(\gamma)$ has no poles in the entire complex γ-plane, since $\rho(x)$ is a function which is nonzero on the MIC only. Secondly, $H(\gamma)$ must have all its singularities in the lower γ-plane, since h(x) is nonzero for x greater than w/2 only. $H(\gamma)$ and $H(-\gamma)$ are thus expanded in terms of their poles which must coincide with the poles of the expression in the left-hand side of Eq. 1-11.

Evaluating Eq. 1-11 at the known zeros of the left-hand side results in a set of equations in terms of the unknown coefficients of expansion for $H(\gamma)$. These equations are then transformed into a much more rapidly converging set of equations.

Sketches of the charge and potential distribution obtained by the Wiener-Hopf method [12] are shown in Fig. 1-3. The method gives accurate results even for very small matrix equations (~5x5), and provides the charge and the potential distributions. However, the Wiener-Hopf method is, in general, difficult to formulate and cannot be used as a prescription when applied to new problems. The generalization of the method to coupled microstrip lines and resonators seems very difficult.

In the mode-matching method [3], the cross section of a shielded microstrip line is divided into several rectangular regions. In each rectangular region the fields are expanded in terms of known solutions of the Laplace equation with unknown coefficients. The application of the boundary and continuity conditions yield the unknown coefficients. The resulting matrix size is large (40 x 40 in [3]). The accuracy of the results oscillates as a function of the resulting matrix size [3].

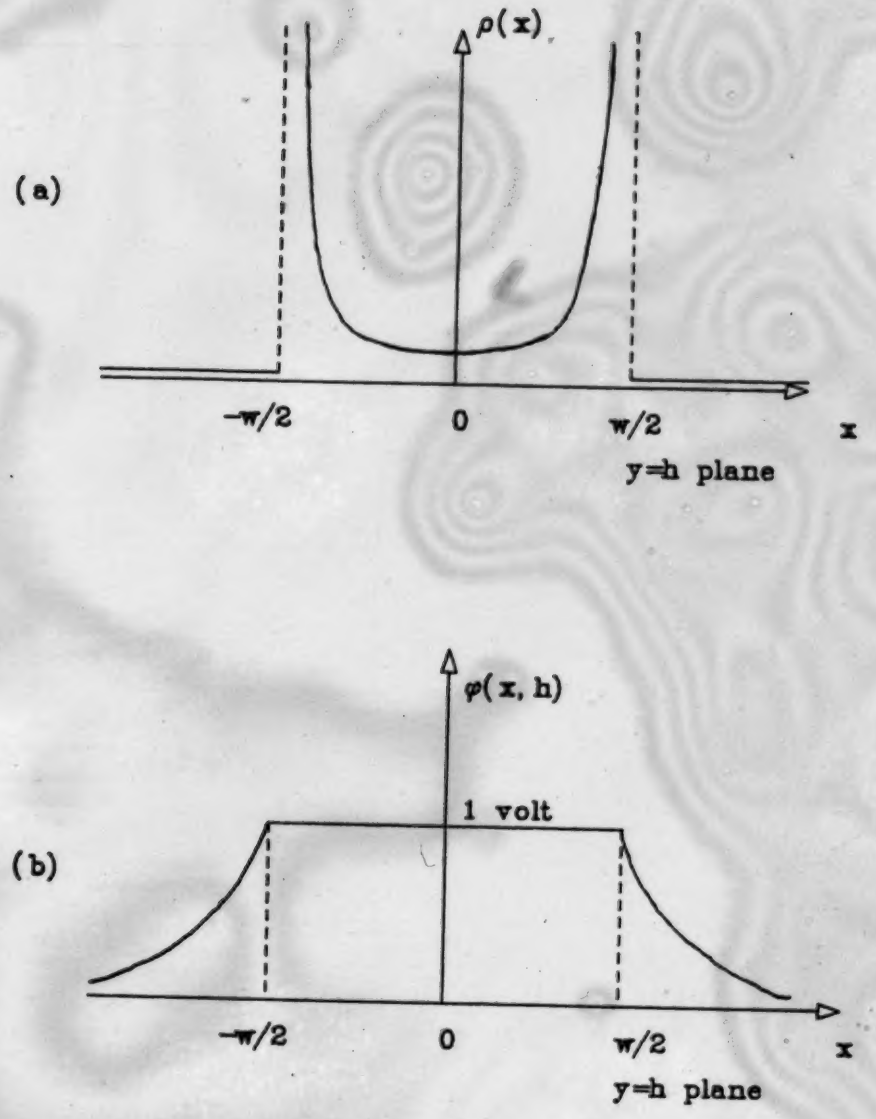

Fig. 1-3 (a) Sketch of the charge distribution on a microstrip line (taken from [12]);
(b) sketch of the potential distribution at the y=h plane (taken from [12]).

Exact Analysis of Microstrip Lines

Preliminary Discussion

In the previous section, the quasi-TEM approach to microstrip lines and the concept of ε_e were introduced. However, since the wave velocity in the dielectric is different from that in free space, it is impossible to support a TEM mode in the microstrip line; as the frequency is increased, ε_e and consequently Z are changed.

In the exact analysis of microstrip lines, called the wave analysis, the field components are usually expressed in terms of a superposition of the TE (transverse electric) and TM (transverse magnetic) fields, which are, in turn, derivable from two scalar potentials [14], namely,

$$\psi^{(e)} \text{ and } \psi^{(h)}$$

which satisfy the Helmholtz equation (i.e., Eqs. 1-2) such that

$$E_z = j[(\kappa k^2 - \beta^2)/\beta]\psi^{(e)}(x, y)\exp(-j\beta z) \qquad (1\text{-}12a)$$

$$H_z = j[(\kappa k^2 - \beta^2)/\beta]\psi^{(h)}(x, y)\exp(-j\beta z) \qquad (1\text{-}12b)$$

$$E_t = \nabla_t\psi^{(e)}\exp(-j\beta z) - (\omega\mu/\beta)\hat{a}_z \times \nabla_t\psi^{(h)}\exp(-j\beta z) \qquad (1\text{-}12c)$$

$$H_t = (\omega\kappa\varepsilon/\beta)\hat{a}_z \times \nabla_t\psi^{(e)}\exp(-j\beta z) + \nabla_t\psi^{(h)}\exp(-j\beta z) \qquad (1\text{-}12d)$$

where $\vec{E}$ is the electric field and $\vec{H}$ is the magnetic field; the indices z and t denote the z- and the transverse-components. $\hat{a}_z$ is the unit vector along the z-axis. The boundary and continuity conditions on the field components are obtainable by Eqs. 1-12. The lowest-order mode approaches the quasi-TEM mode, as explained above.

In the following sections, methods used for the wave analysis of microstrip lines are summarized. The strip thickness, t, is assumed to be negligible, unless otherwise specified.

LSE (Longitudinal Section Electric) Model

Based on the field configurations in a microstrip line, Getsinger [15] has proposed a model for the microstrip line which supports LSE (longitudinal section electric) waves, shown in Fig. 1-4a. It is easier to analyze this model than the actual microstrip line. The solution for the structure of Fig. 1-4 is found and yields

$$\varepsilon_e = \varepsilon_r - (\varepsilon_r - \varepsilon_{eo}) / [1 + G(f/f_p)^2] \qquad (1\text{-}13)$$

where ε_{eo} is the zero frequency limit of ε_e (obtainable by quasi-TEM methods) and G and f_p are parameters that depend on the characteristic impedance.

Eq. 1-13 shows the general behavior of the dispersion relation (i.e., ε_e vs. f); it is drawn in Fig. 1-4b. The slope of ε_e goes to zero as the frequency approaches zero. The dispersion curve possesses an inflection point at

$$f_i = f_p / \sqrt{3G}$$

and asymptotically approaches ε_r as the frequency

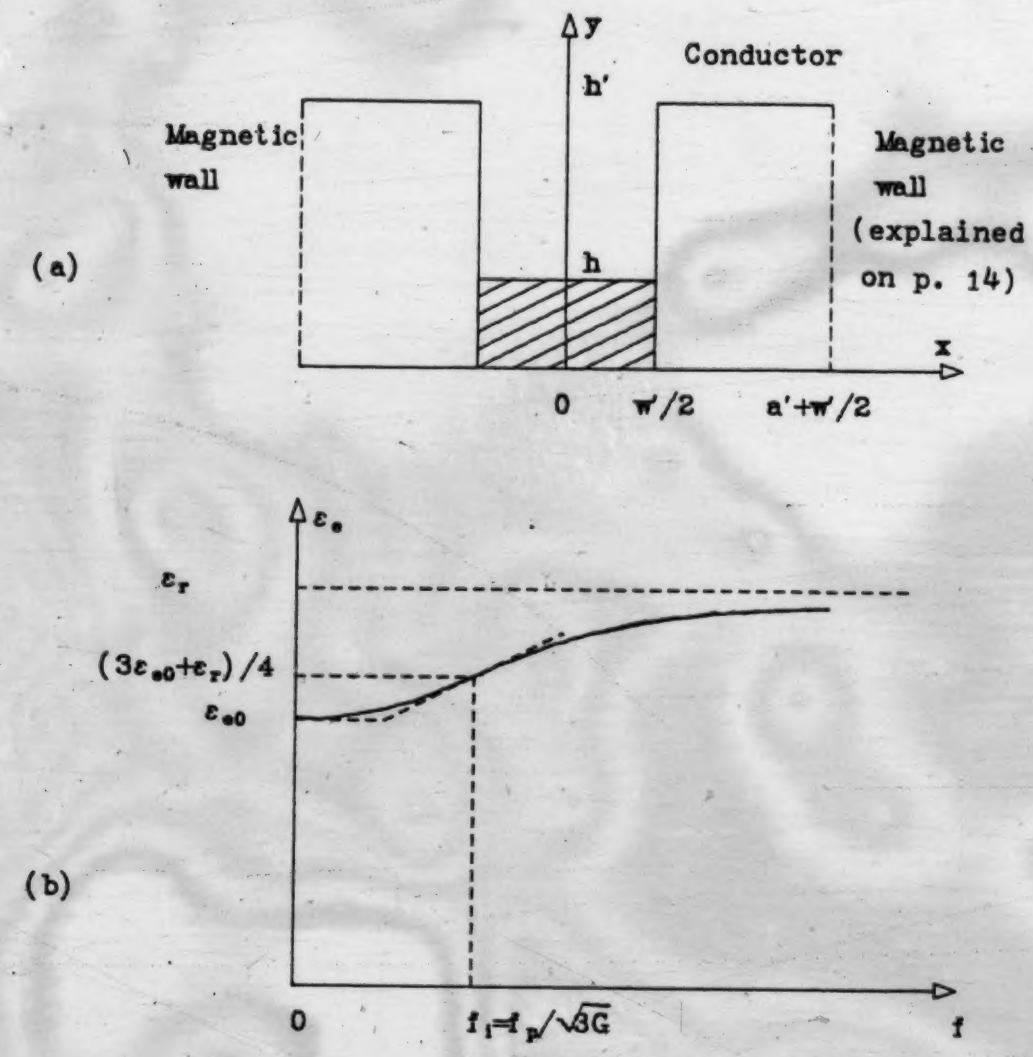

Fig. 1-4 (a) LSE (longitudinal section electric) model for a microstrip line;

(b) general behavior of the effective dielectric constant, ε_e, as a function of frequency obtained from the LSE model.

goes to infinity. In the following sections, more rigorous methods of obtaining the dispersion relation are summarized.

Exact Methods

The two potential functions

$$\psi^{(e)} \text{ and } \psi^{(h)}$$

of Eqs. 1-12 satisfy a two-dimensional wave equation in the microstrip line cross section (Fig. 1-1b); thus, they can be expanded in terms of known solutions to the Helmholtz equation in dielectric and in air. The imposition of the boundary and continuity conditions on $\vec{E}$ and $\vec{H}$ yields a pair of coupled integral equations [16]. These equations may be transformed into a matrix equation and solved numerically, yielding the dispersion relation. The final matrix size and accuracy depend on which boundary and continuity conditions on the six electromagnetic components are chosen and how they are manipulated. Similar methods are presented in [17] and [18].

The finite difference method discussed in the quasi-TEM approach can be extended to apply to the wave analysis of microstrip lines.

After properly applying the discretized version of the wave equation and the boundary conditions at all of the mesh-points, an eigenvalue matrix equation is obtained.

The algorithm in this method is straightforward, but the final eigenvalue matrix is large (e.g., 100 x 100 or larger [19]) and the results are less accurate than those obtained by integral equation methods [2].

The mode matching method discussed in the quasi-TEM approach can also be applied to the wave analysis of microstrip lines [20]. The dielectric and air regions in the cross section of a microstrip line are divided into a few rectangles. In each rectangle, the two potential functions are expanded in terms of solutions to the Helmholtz equation. The functions are chosen so that the boundary conditions on the electric and magnetic walls are satisfied. Using the conditions for the continuity of the electromagnetic field components, the solutions written in the rectangular subregions can be matched. In this way, a set of equations for the unknown coefficients is obtained. The final matrix required for reasonable accuracy is 42 x 42, [2].

In the finite element method, the differential equations and the boundary conditions are transformed into a variational expression, which yields the field distributions and ϵ_e when optimized. The microstrip line cross section is subdivided into a number of arbitrarily shaped triangles; each corner of a triangle is called a node. In each triangle, the fields are written in terms of known linear functions of x and y and unknown nodal values of the potential functions.

Since the potential functions are linearized in each triangle, it is possible to integrate the variational expression.

The resulting expression is then optimized with respect to the unknown nodal values, yielding an eigenvalue matrix equation in terms of ε_e. The resulting matrix size may be as large as 126 x 126; the obtained results are accurate within a few percent [21].

In the transmission line matrix method (TLM), the microstrip line cross section is subdivided into a mesh as in the finite difference method. However, the functions are not linearized in between the mesh-points; the distance between any two adjacent pairs of mesh-points which lie along the coordinate axes is considered to be a segment of transmission line. The response to an impulse applied at a node is calculated by letting the impulse scatter in the mesh and reflect back and forth a large number of times.

This method is easily capable of handling losses and discontinuities. The dimension of the final matrix size is typically 270 X 270. The iteration number is 200, the required time is 2.16 min. on an ICL 1906A computer, and the required memory space is 20k words [22].

Open Microstrip Lines

The effect of the enclosing walls on the properties of a shielded microstrip line is usually negligible (by

design). However, some mathematical methods are simplified when applied to open microstrip lines (Fig. 1-1a).

In the integral equation method [23], the Fourier transform of the Helmholtz equation for the potential functions of Eqs. 1-12 is taken with respect to x. The Fourier transforms of the two potential functions are expressed in terms of known solutions of the Helmholtz equation. Separate solutions are written in dielectric and in air, which satisfy the boundary conditions on the ground plane and at infinity.

The following conditions at the y=h plane (Fig. 1-1a) are used to match the solutions obtained for the dielectric and the air regions

$$E_t(x,h^-)=E_t(x,h^+), \text{ on the DAI}$$

$$E_t(x,h^-)=E_t(x,h^+)=0, \text{ on the MIC}$$

$$H_z(x,h^-)-H_z(x,h^+)=J_x(x), \text{ on the MIC}$$

$$H_x(x,h^-)-H_x(x,h^+)=J_z(x), \text{ on the MIC}$$

where E_t is the tangential component of the electric field, H_x and H_z are the x- and z-components of the magnetic field, and J_x and J_z are the x- and z-components of the current distribution on the MIC, respectively.

The matching procedure results in a set of equations in terms of the current distribution on the MIC. The resulting equations are then solved by trying suitable functions with unknown coefficients which approximate the actual current distributions. This method of expressing the unknown fields in terms of the current distribution on the MIC is widely used in microstrip analyses.

The resulting matrix equation can be solved, yielding ε_e. The size of the final matrix equation is usually small and depends on the assumed current distribution [23].

In Galerkin's method [24] the final equations are solved in the Fourier transform domain. The tangential component of the current distribution along the z-axis, J_z, is non-zero only on the MIC (Fig. 1-1a); E_z is non-zero only on the DAI. Thus, the product of $J_z(x)$ and $E_z(x,h)$ is identically zero. Applying Parseval's theorem, we have

$$\int_{-\infty}^{\infty} J_z(x)\, E_z^*(x, h)\, dx = 1/(2\pi) \int_{-\infty}^{\infty} \tilde{J}_z(\gamma)\, \tilde{E}_z^*(\gamma, h)\, d\gamma = 0. \qquad (1\text{-}14)$$

A similar equation can be obtained in terms of J_x. Eq. 1-14 can be used as a boundary condition yielding a pair of coupled integral equations in terms of $\tilde{J}_x$ and $\tilde{J}_z$. The equations are then solved by expanding $\tilde{J}_x$ and $\tilde{J}_z$ in terms of known basis functions with unknown coefficients. The merits of this method are similar to the integral equation method described in the previous section.

C. Quasi-TEM Analysis of Coupled Microstrip Lines

Preliminary Discussion

Due to the symmetry of the coupled lines about the y-axis (Fig. 1-1c) there are two normal modes for the structure, namely, the even mode and the odd mode. In the quasi-TEM regime, the mode with equal voltages on the left and the right strips is called even, and the

mode with equal amplitude voltages but of opposite sign is called odd.

Since the field configurations are different for the two modes, it is expected that there are two values for Z and ε_e, namely

Z_e : even-mode characteristic impedance,

Z_o : odd-mode characteristic impedance,

$\varepsilon_{e,e}$: even-mode ε_e

$\varepsilon_{e,o}$: odd-mode ε_e

The numerical methods applied to the coupled microstrip lines in the quasi-TEM regime are presented in the following sections.

Green's Function

In the Fourier integral method, a function $g(x,y;x',h)$ is found, where $g(x,y;x';h)$ refers to the electrostatic potential at point (x,y) due to a line charge at (x',h), [25]. In practice, it is easier to consider a charge element of nonzero width and finite charge density.

The strips may be regarded as a parallel arrangement of such charge elements. Using the superposition principle,

$$\varphi(x,y)=\int_{-\infty}^{\infty} g(x,y;x',h)\rho(x')\,dx', \qquad (1\text{-}15)$$

where ρ is the charge distribution over the microstrip lines. Let $R(\gamma)$ be the Fourier transform of $\rho(x)$ and

$G(x,y;\gamma)$ be the Fourier transform with respect to x' of $g(x,y;x',h)$ then Eq. 1-15 can also be written as

$$\varphi(x,y)=\int_{-\infty}^{\infty} G(x,y;\gamma)R(\gamma)\,d\gamma. \qquad (1\text{-}16)$$

For the normal modes, the potential values on the strips are known. The charge distribution can be found from Eq. 1-16.

$G(x,y;\gamma)$ can be interpreted as the potential distribution due to the surface charge

$$\rho_s(x)=(1/2\pi)\exp(-j\gamma x), \qquad (1\text{-}17)$$

since

$$G(x,y;\gamma)=(1/2\pi)\int_{-\infty} g(x,y;x',h)\exp(-j\gamma x)\,dx'. \qquad (1\text{-}18)$$

Thus, G can be obtained. An alternate method for finding the Green's function is described below:

In the bound charge method, the Green's function is first approximated by a function $g_o(x,y;x',h)$. $g_o(x,y;x',h)$ is the same as the actual Green's function when the substrate is removed [26]. The error in this assumption is a function $g_c(x,y;x',h)$ such that

$$g(x,y;x',h)=g_o(x,y;x',h)+g_c(x,y;x',h). \qquad (1\text{-}19)$$

Since g_o is the solution for the structure without the dielectric, it will be the solution to the actual structure, provided that there is a charge distribution at the y=h plane given by

$$\rho_c(x;x')=\varepsilon(\varepsilon_r-1)\bar{a}_y\cdot\nabla g_o(x,h;x',h). \qquad (1\text{-}20)$$

We may place a compensating bound charge

$$\rho_c(x;x') \text{ at } y=h$$

so that g satisfies the DAI continuity condition. The next step is to find $\rho_c(x;x')$ and $g_c(x,y;x',h)$. g_c is given by

$$g_c(x,y;x',h) = (1/4\pi\varepsilon) \int_L \rho_c(x';x'') g_o(x,y;x'',h)\, dx'', \quad (1\text{-}21)$$

where L is the line described by y=h (Fig. 1-1a).

Applying the continuity condition at the DAI to g yields an integral equation in terms of the unknown ρ_c.

Having found ρ_c, Eq. 1-21 can then be used to obtain g_c. The desired Green's function is eventually found from Eq. 1-19 by adding g_o to g_c. The time needed on an IBM 360/67 computer is 0.72 + 21.4NT, where NT is the number of the lines of data produced (e.g., 214.72 secs. for 10 lines of data). The computer space needed is 64,000 bytes [26].

Mode Matching

This method is the same in principle as the mode matching method described under the quasi-TEM analysis of microstrip lines on p. 18, 3 , only this time for coupled microstrip lines.

Variational Method

The Laplace equation can be transformed into the

variational expression

$$W = \varepsilon \iint_S [(\partial\varphi/\partial x)^2 + (\partial\varphi/\partial y)^2]\, dx dy, \qquad (1\text{-}22)$$

where S is the cross section of the microstrip line. W can be interpreted as the stored electric energy. If a function φ is found such that W is minimized, then φ satisfies the Laplace equation.

The trial field φ can be chosen to be the same functions as used in the mode matching method above [27]. After the necessary boundary and continuity conditions are imposed on the solutions, a set of unknown coefficients remain. W of Eq. 1-22 is then optimized with respect to these coefficients, yielding a set of linear equations in terms of the coefficients. The final matrix size is about 4x4. The method provides the upper-bound values of the capacitance. The results are poor for very narrow microstrip lines, but the accuracy increases for moderately wide microstrip lines [27]. This work is complementary to that of Yamashita and Mittra [8], in that their results provide lower bound values for the capacitance.

Variational Method in the Fourier Transform Domain

This is exactly the same method as explained in the quasi-TEM analysis of the single microstrip lines [28]. For coupled microstrip lines the method should be modified slightly to accommodate for the even and the odd modes. The charge distribution is identical

on the two strips for the even modes. For the odd modes the charge distributions on the two strips are equal in magnitude but are opposite in polarity.

The required computer time per data point is 32 secs. on a Univac 1108 computer. The efficiency of this method depends on which function is chosen to represent the charge distribution [28].

D. Microstrip Resonators

Transmission Line Models

One of the simplest microstrip resonators is a length of microstrip line called the rectangular resonator (Fig. 1-5a). Assuming perfect open circuits at both ends (Fig. 1-5b), the resonator will resonate at frequencies for which

$$L=n(\lambda_g/2), \quad n=1, 2, \cdots. \tag{1-21}$$

Considering that the guide wavelength is given by

$$\lambda_g=c/(f\sqrt{\epsilon_e}), \tag{1-22}$$

we obtain

$$f=nc/(2L\sqrt{\epsilon_e}), \quad n=1, 2, \cdots. \tag{1-23}$$

ϵ_e is in turn a function of f. The resonant frequencies can be found from Eq. 1-21 and the dispersion relation. The results obtained by Eq. 1-21 are accurate within a few percent, the inaccuracy being primarily caused by the fringing fields at the resonator ends.

A more accurate transmission line model is shown in Fig. 1-5c. The end effects are taken into account

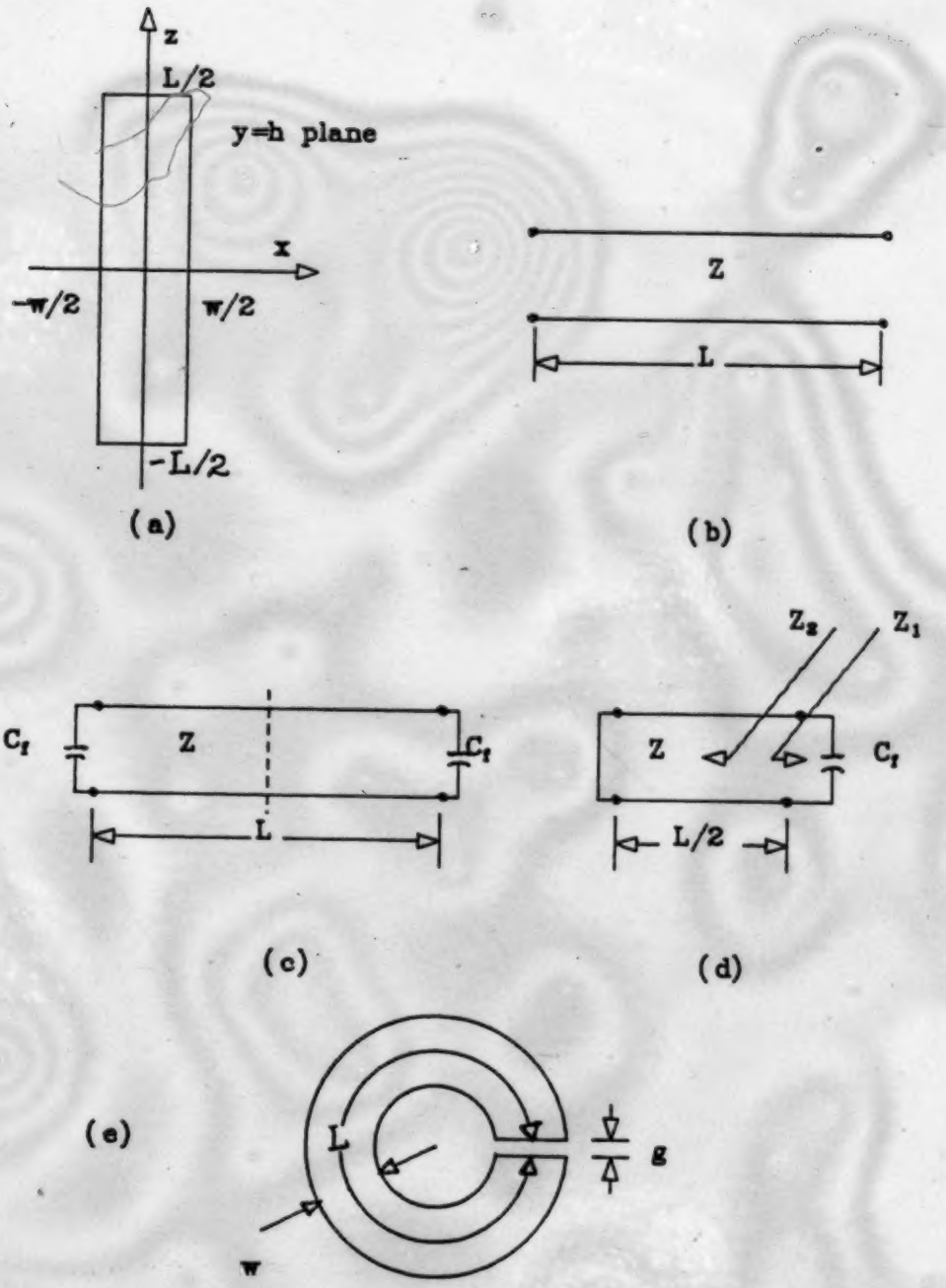

Fig. 1-5 Transmission line models for microstrip resonators;

(a) rectangular resonator;

(b) transmission line model neglecting fringing fields;

(c) transmission line model with fringing fields;

(d) transmission line model with fringing fields; due to odd symmetry, half of model (c) is sufficient;

(e) open-ring resonator which can be modelled by (d).

by adding the capacitors C_f at the ends. The values of C_f are calculated and are available in [29] and [30].

If the rectangular resonator is "bent" so that the two ends come close to each other, the open-ring resonator shown in Fig. 1-5e is obtained [31]. The transmission line model for this resonator is shown in Fig. 1-5d, [32]. This resonator shows interesting properties [31], especially for the principal mode (i.e., n=1 in Eq. 1-21). For this mode, the resonator has an odd symmetry with respect to the z=0 plane; Fig. 1-5c can be short circuited in the middle. The resulting model is shown in Fig. 1-5d.

The resonant frequency can be obtained by letting the impedance at the right and the left at any cross section of the transmission line add up to zero (Fig. 1-5d).

$$Z_1+Z_2=0, \tag{1-24}$$

where

$$Z_1=1/(j\omega C_f), \tag{1-25}$$

and

$$Z_2=Z/\tan[\omega\sqrt{\epsilon_e}L/(2C)] \tag{1-26}$$

Substituting Eqs. 1-25 and 26 into 24 we get

$$\tan[\omega\sqrt{\epsilon_e}L/(2C)]=\omega C_f Z. \tag{1-27}$$

Eq. 1-27 yields the odd mode resonant frequencies of the resonator. The accuracy of this method is typically 4% or better [32].

Transmission-line modelling can also be applied to the ring resonator of Fig. 1-6a; the resonator resonates at frequencies at which L, the mean length, is an integral multiple of λ_g. The model gives accurate results only when $w/L \leq 0.05$, [33].

Magnetic Wall Models

The effect of w and curvature in the ring resonators are not negligible. For this reason, ϵ_e as calculated for a straight microstrip line is not necessarily the same for the ring resonator [33]. The effect of curvature in the ring resonator is included by regarding the resonator as a cavity with electric walls on the top and the bottom, and magnetic walls on the sides (Fig. 1-6b). The cavity is assumed to be filled with the substrate dielectric material.

Moreover, it is assumed that the variation of fields in the y-direction is negligible; the fields are TH with respect to the y-axis; Maxwell's equations yield

$$J_n'(\epsilon_r k r_0) Y_n'(\epsilon_r k r_1) - J_n'(\epsilon_r k r_1) Y_n'(\epsilon_r k r_0) = 0. \quad (1\text{-}28)$$

where J_n and Y_n are Bessel functions [33].

This model gives accurate results when $w/L \leq 0.05$, [33]. Based on this theory, the mode chart for the resonator is obtained in [34].

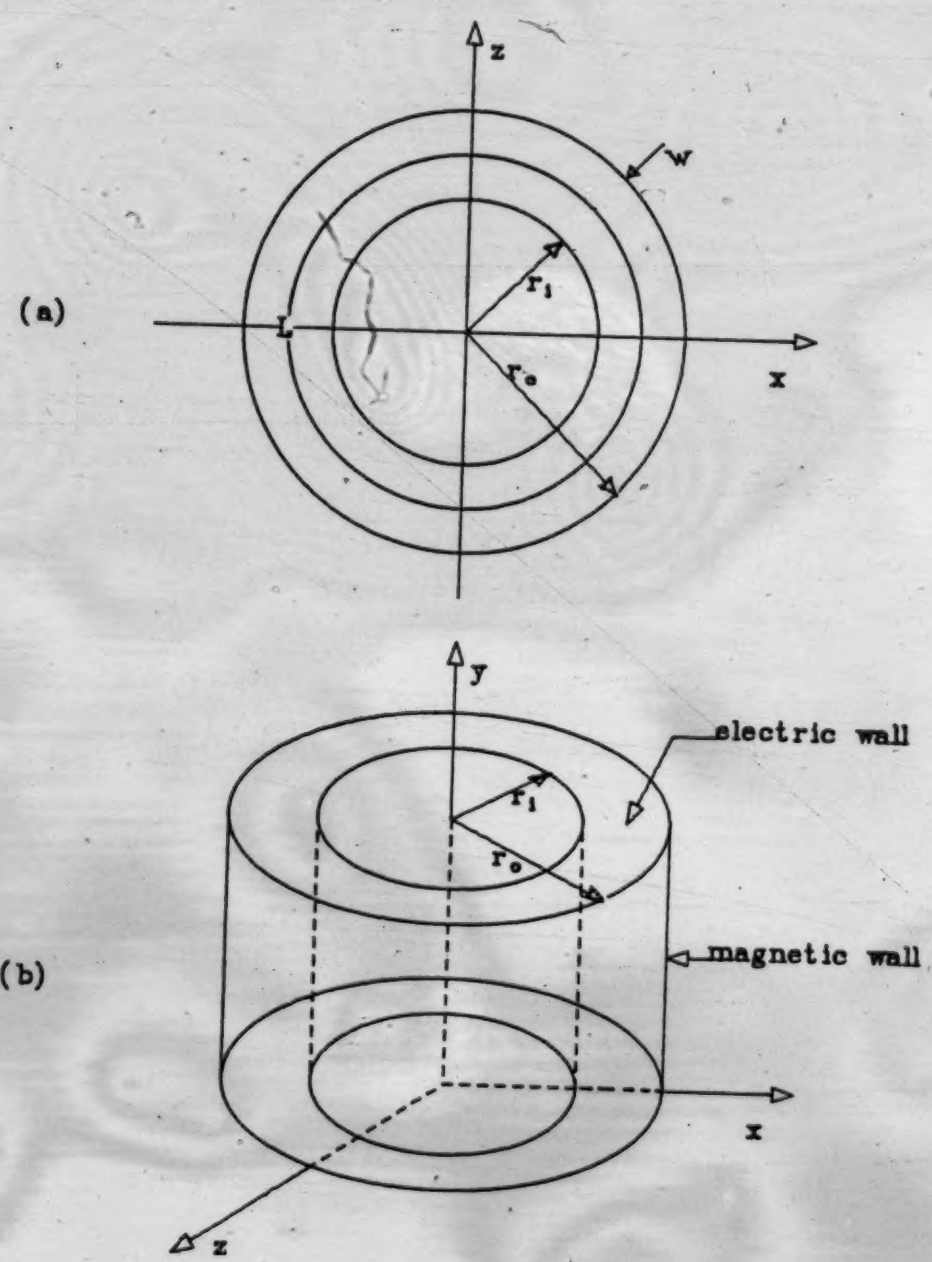

Fig. 1-6 (a) Ring resonator at y=h plane [33];
(b) magnetic wall model of ring resonator.

Fringing Effects

The resonant frequencies calculated by the magnetic wall modelling can be inaccurate up to several per cent [35] (e.g., up to 10% for the open-ring resonator [36]), since the fringing fields at the resonator edges are not negligible.

The effect of the fringing fields can be taken into account by regarding the resonator as a capacitor. The theoretical calculation of the capacitance reveals an effective change in the resonator dimensions due to fringing. Furthermore, an effective dielectric constant is found which reflects the nonuniform charge distribution in the resonator, which is different from the DC charge distribution. Finally, to obtain the resonant frequency, a magnetic wall model is considered for which the effective dimensions are obtained theoretically and is filled with a dielectric material with the effective dielectric constant.

The results of the above theory show good agreement with experiments [36].

Exact Formulation

In this section, the exact methods which have been applied to microstrip resonators are summarized, namely, the mode-matching, self-reaction, Galerkin and TLM methods.

The mode matching method, as described above, can be applied to the disc resonator. The size of the resulting matrix equation is 20x20. With this matrix size, the results are accurate to within 1%. The computer time on a TELEFUNKEN computer TR440 is 0.666 secs. [37].

In the self-reaction method as mentioned above, the reaction of the field on its own source, should be zero. The ring resonator has been analyzed by this method [38]. However, the generalization of this method to other geometries seems impossible.

Rectangular resonators have been analyzed by Galerkin's method [39] which is a generalization of the Galerkin method described previously. The typical computer time on CDC G-20 computer is 200 secs. per structure. More time is required for analyzing narrower rectangular resonators.

In [40], the six component Maxwell equations are solved, including the loss in the dielectric and the metals by the TLM method.

This method can be applied to microstrip resonators of any geometry. The size of the resulting matrix is 704 x 704 and the iteration number is 400. The computer time on the ICL 1906A computer is 11.26 mins. The computer space needed is 46k words.

E. Review Conclusions

In the previous sections, methods for obtaining the properties of microstrip lines, coupled lines, and resonators were reviewed. Few of these methods can be easily generalized so that they will include the three structures of Fig. 1-1.

Since microstrip technology is advancing rapidly, a need exists for accurate methods which can be easily programmed, which are sufficiently flexible to include all three basic microstrip structures, and which are cheap and efficient in terms of computer time and memory space. In this thesis, novel numerical methods are developed which attempt to fulfil these requirements.

Due to the sharp edges of the MIC, some of the field components can be expected to become singular near these edges [41]. For this reason, any numerical method which does not include these singularities will likely result in large matrices. However, since the total energy around the edges remains finite, it must be possible to remove the singularities. Following this reasoning, it can be deduced that methods which employ integral equations are intrinsically better suited for analyzing microstrips (since integration is performed over the singularity). Many such methods, including methods using Green's functions, were discussed in the previous sections. In some cases, such as in the "Bound Charge Method", it is a major undertaking to obtain the Green's functions.

In order to utilize the interesting properties of

Green's functions, while at the same time keeping the effort of finding these functions minimal, it is possible to modify the integral equations in such a manner that simpler Green's functions can be employed. One such method is the BEM (boundary element method) [42] and [43]. This method, as well as other novel methods, are applied to the analysis of microstrips.

The analysis of microstrip resonators is a complex problem. Therefore, simpler structures are analyzed first. The methods developed for analyzing single and coupled microstrip lines are then applied to the analysis of microstrip resonators. However, each method is useful and applicable to engineering design.

F. Thesis Organization

Chap. 2 deals with the quasi-TEM analysis of microstrip lines and coupled lines. The boundary value problem is first transformed into an integral equation which is then solved by the BEM. Chap. 2 introduces two new concepts. First, the thin MIC sheet is included in the integral equation and is represented as a charge layer, and the singularity in the charge distribution on the MIC is explicitly included in the integral equation. Second, the integral equation is formulated in such a manner that a simple free-space Green's function can be used, regardless of the dielectric substrate; therefore, no method of images is necessary to find more complicated Green's functions.

However, the generalization of the method presents some difficulties. For this reason, the integral equation method of Chap. 2 is further modified in Chap. 3. In this chapter, Green's functions are generalized and are made more flexible so that they can be applied more easily to the wave analysis of microstrips.

In Chap. 4 the generalized Green's functions developed in Chap. 3 are employed. Moreover, Chap. 4 introduces a new approach to the wave analysis of microstrips. It is shown that boundary conditions for E_y, the y-component of the electric field (Fig. 1-1), can be totally separated from the other components of the electromagnetic fields. Thus, instead of using two potential functions $\psi^{(e)}$ and $\psi^{(h)}$ (introduced in this chapter), it is possible to solve the boundary value problem for E_y. The parameters of engineering interest, such as ϵ_e for the microstrip lines, and the resonant frequency of resonators, can be obtained from E_y alone. This greatly reduces the effort of analyzing microstrips.

The domain of integration of the integral equation derived in Chap. 4 is the DAI. It seems difficult, if not impossible, to generalize this method to microstrip resonators. For this reason, the method of Chap. 4 is modified in Chap. 5 so that the domain of integration will be that of the MIC. Chap. 5 also gives an example of how this method can be applied to microstrip resonators.

In Chap. 6, the overall conclusions of this thesis are summarized and recommendations are made for further research.

II. A BOUNDARY ELEMENT METHOD

A. Introduction

In this chapter, microstrip lines and coupled lines in the quasi-TEM regime are analyzed by the boundary element method (BEM). The BEM is a method in which a boundary value problem is first converted into a boundary integral equation, integrated over the boundaries of a domain. The boundary is then divided into a set of elements over which the functions under consideration can vary in different ways, as in the method of finite elements [42] and [43].

The BEM offers important advances over the finite element and finite difference methods; the resulting system of equations is much smaller, less time is required to solve a problem, and the accuracy is greater than in the "domain" type methods, i.e., finite elements 42 and 43. Moreover, the BEM can be applied to problems with infinite domains.

The classical boundary solution known as the boundary integral method is closely related to the BEM [42], [43], and [44].

As noted in Chap. 1, a boundary value problem can be transformed into an integral equation by many different ways. A good formulation can greatly reduce the effort for solving a problem. One possible formulation uses Green's functions. However, as Beckenbach [45] has stated, "in actual boundary-value problems it is often difficult to

determine the Green's function and in many cases it is easier to solve the problem directly by numerical methods than by the use of the general theory".

To analyze microstrip lines in the quasi-TEM regime, the Laplace equation for the potential function at the microstrip cross section is transformed into an integral equation. The domain of integration of the integral equation is the y=h plane (Fig. 1-1). In this way, the boundary conditions for the thin MIC sheet are imbedded in the integral equation and are represented in the form of a charge distribution. Moreover, the integral equation is formulated in such a way that the free-space Green's function can be used, regardless of the dielectric substrate; thus, the method of images is not required to find a more complicated Green's function. Finally, the obtained integral equation is applied to coupled microstrip lines.

B. Formulation

For a microstrip line in the quasi-TEM regime, it is required to solve the Laplace equation

$$\nabla_t^2 \varphi = 0, \tag{2-1}$$

in the microstrip cross section (Fig. 2-1a). It is assumed that the microstrip is unshielded, the ground plane potential is zero, and the strip potential is unity. The boundary conditions at the y=h plane are as follows: The continuity of the potential implies that

$$\varphi|_{y=h^-} = \varphi|_{y=h^+} \tag{2-2a}$$

Further, the continuity of the normal component of the

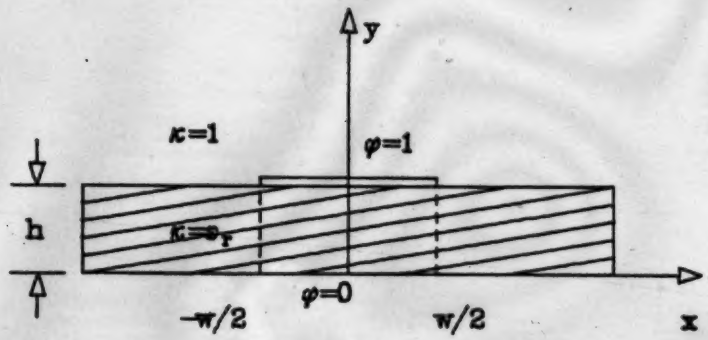

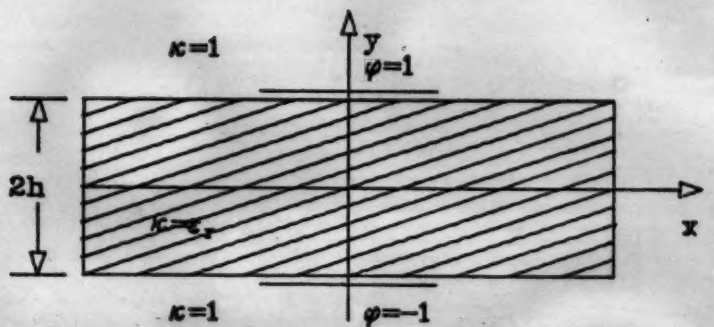

(b)

Fig. 2-1 (a) Unshielded microstrip line;
(b) an equivalent structure.

displacement vector on the DAI implies that

$$\varepsilon_r(\partial\varphi/\partial y|_{y=-h^-}) = (\partial\varphi/\partial y|_{y=-h^+}). \qquad (2\text{-}2b)$$

Moreover, on the MIC

$$\varepsilon_r(\partial\varphi/\partial y|_{y=-h^-}) - (\partial\varphi/\partial y|_{y=-h^+}) = \rho(x), \qquad (2\text{-}2c)$$

where $\rho(x)$ is the charge distribution on the MIC. The microstrip structure in Fig. 2-1a is equivalent to that of Fig. 2-1b, [1]. The boundary and the continuity conditions on the y=-h plane in Fig. 2-1b resemble Eqs. 2-2.

The infinite geometry of Fig. 2-1b is first approximated by the finite geometry of Fig. 2-2, enclosed within a circle of radius R; the two geometries become identical when R tends to infinity. Consider Green's second identity

$$\int_S(\varphi\nabla_t^2\psi - \psi\nabla_t^2\varphi)\,dS =$$

$$\int_C[\varphi(\partial\psi/\partial n) - \psi(\partial\varphi/\partial n)]\,dC \qquad (2\text{-}3)$$

where S is the area enclosed by the curve C, and $\partial/\partial n$ designates the normal derivative. In this work φ is the potential function, and ψ is an auxiliary function called the fundamental solution. This is similar to a Green's function, by means of which φ can be obtained. The procedure is explained below.

Applying Eqs. 2-3 to regions S_1, S_2, and S_3 yields

$$\int_{S_1}(\varphi\nabla_t^2\psi - \psi\nabla_t^2\varphi)\,dS =$$

$$\int_{C_1 \cup r_1}[\varphi(\partial\psi/\partial n) - \psi(\partial\varphi/\partial n)]\,dC \qquad (2\text{-}4a)$$

$$\int_{S_2}(\varphi\nabla_t^2\psi - \psi\nabla_t^2\varphi)\,dS =$$

$$\int_{r_2 \cup C_2 \cup r_3 \cup C_4}[\varphi(\partial\psi/\partial n) - \psi(\partial\varphi/\partial n)]\,dC, \qquad (2\text{-}4b)$$

$$\int_{S_3}(\varphi\nabla_t^2\psi - \psi\nabla_t^2\varphi)\,dS =$$

$$\int_{r_4 \cup C_3}[\varphi(\partial\psi/\partial n) - \psi(\partial\varphi/\partial n)]\,dC. \qquad (2\text{-}4c)$$

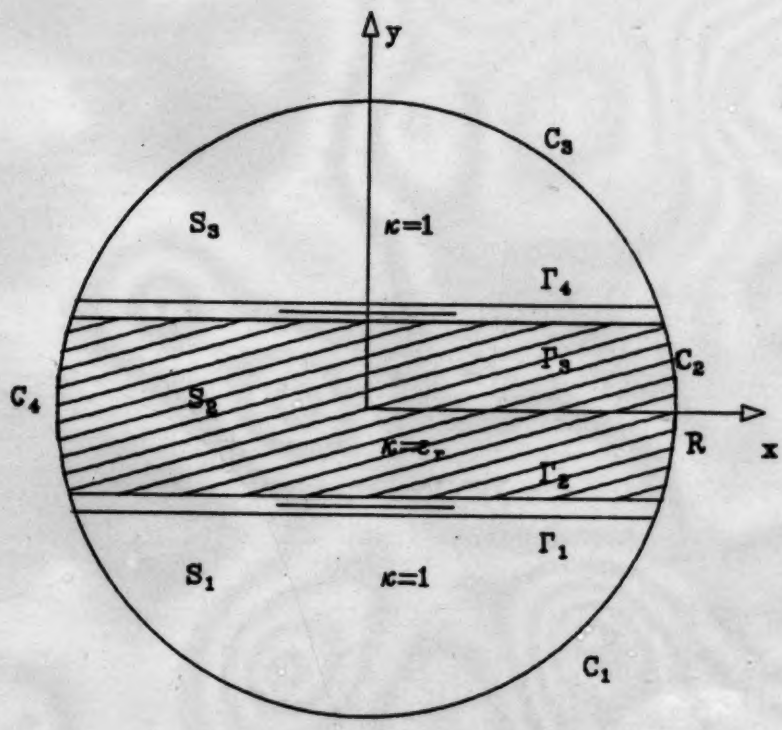

Fig. 2-2 Equivalent structure for the microstrip line used for BEM (Boundary Element Method); R is assumed to be infinitely large.

where $\cup$ designates the union of two sets. Thus $C_1 \cup \Gamma_1$ is the curve which encloses S_1 (Fig. 2-2).

Multiplying Eq. 2-4b by ε_r and adding it to Eqs. 2-4a and 4c results in

$$\int_{S_1 \cup S_3} (\varphi \nabla_t^2 \psi - \psi \nabla_t^2 \varphi)\, dS + \int_{S_2} \varepsilon_r (\varphi \nabla_t^2 \psi - \psi \nabla_t^2 \varphi)\, dS =$$
$$\int_{C_1 \cup \Gamma_1 \cup \Gamma_4 \cup C_3} [\varphi (\partial\psi/\partial n) - \psi (\partial\varphi/\partial n)]\, dC$$
$$+ \int_{\Gamma_2 \cup C_2 \cup \Gamma_3 \cup C_4} [\varphi (\partial\psi/\partial n) - \psi (\partial\varphi/\partial n)]\, dC. \qquad (2\text{-}5)$$

The fundamental solution is assumed to satisfy

$$\nabla_t^2 \psi = -\delta(x - x_i)\, \delta(y - y_i), \qquad (2\text{-}6)$$

regardless of the boundary conditions. Considering Eqs. 2-1 and 6, the left hand side of Eq. 2-5 reduces to $-a_i \varphi_i$ where

$$a_i = \begin{cases} 1 & \text{if } (x_i, y_i) \text{ is in the air,} \\ \varepsilon_r & \text{if } (x_i, y_i) \text{ is in the dielectric,} \end{cases} \qquad (2\text{-}7)$$

and

$$\varphi_i = \varphi(x_i, y_i). \qquad (2\text{-}8)$$

If (x_i, y_i) is chosen to have a nonzero distance from the origin, then as R tends to infinity, the integrands of the right hand side of Eq. 2-5 vanish on $C_1 \cup C_2 \cup C_3 \cup C_4$. Thus, as $R \to \infty$, Eq. 2-5 yields

$$-a_i \varphi_i = \int_{-\infty}^{\infty} [\varphi (\partial\psi/\partial y) - \psi (\partial\varphi/\partial y)]_{y=-h^+} (-dx)$$
$$+ \int_{-\infty}^{\infty} \varepsilon_r [\varphi (-\partial\psi/\partial y) - \psi (-\partial\varphi/\partial y)]_{y=-h^-} dx$$
$$+ \int_{-\infty}^{\infty} \varepsilon_r [\varphi (\partial\psi/\partial y) - \psi (\partial\varphi/\partial y)]_{y=h^-} (-dx)$$
$$+ \int_{-\infty}^{\infty} [\varphi (-\partial\psi/\partial y) - \psi (-\partial\varphi/\partial y)]_{y=h^+} dx. \qquad (2\text{-}9)$$

Considering Eqs. 2-2, Eq. 2-9 results in

$$-a_i \varphi_i = -(\varepsilon_r - 1) \int_{-\infty}^{\infty} [\varphi (\partial\psi/\partial y)]_{y=-h^+} dx - \int_{-\infty}^{\infty} (\rho/\varepsilon)[\psi]_{y=-h^+}^{y=h^-} dx$$
$$+ (\varepsilon_r - 1) \int_{-\infty}^{\infty} [\varphi (\partial\psi/\partial y)]_{y=h^+} dx + \int_{-\infty}^{\infty} (\rho/\varepsilon)[\psi]_{y=h^-}^{y=h^+} dx, \qquad (2\text{-}10)$$

where ρ is the charge distribution over the upper strip in Fig. 2-2. Considering the odd symmetry of φ with respect to the y=0 plane (Fig. 2-1b), Eq. 2-10 reduces to

$$-a_i\varphi_i=(\varepsilon_r-1)\int_{-\infty}^{\infty}[\varphi]_{y=h}[(\partial\psi/\partial y|_{y=h^+})-(\partial\psi/\partial y|_{y=h^+})]\,dx$$
$$+\int_{-w/2}^{w/2}(\rho/\varepsilon)(\psi|_{y=h^+}-\psi|_{y=h^+})\,dx \qquad (2\text{-}11)$$

The solution to Eq. 2-6 is [42]

$$\psi=-(1/2\pi)\ln r_i=-(1/4\pi)\ln[(x-x_i)^2+(y-y_i)^2], \qquad (2\text{-}12)$$

where

$$r_i=\sqrt{(x-x_i)^2+(y-y_i)^2}. \qquad (2\text{-}13)$$

Thus

$$\partial\psi/\partial y=-(1/\pi)\{(y-y_i)/[(x-x_i)^2+(y-y_i)^2]\}. \qquad (2\text{-}14)$$

Eq. 2-11 should be modified if (x_i, y_i) is chosen to lie on y=h, since Eq. 2-14 becomes indefinite as (x,y) approaches (x_i, y_i). Therefore, Γ_3 and Γ_4 must be deformed into a semicircle with radius r, in the vicinity of (x_i, y_i) as shown in Fig. 2-3; the limit of the first integral at the right of Eq. 2-11 is found as r tends to zero.

It can be shown that, if y=h, then

$$\int_{\Gamma_4}\varphi(\partial\psi/\partial n)\,dC+\varepsilon_r\int_{\Gamma_3}\varphi(\partial\psi/\partial n)\,dC=-(\varepsilon_r-1)\varphi_i/2. \qquad (2\text{-}15)$$

Eq. 2-11 should thus be modified to

$$(1/2)(\varepsilon_r+1)\varphi_i=(\varepsilon_r-1)\int_{-\infty}^{\infty}(\varphi|_{y=h^+})[(\partial\psi/\partial y|_{y=h^+})-(\partial\psi/\partial y|_{y=h^+})]\,dx$$
$$+\int_{-w/2}^{w/2}(\rho/\varepsilon)(\psi|_{y=h^+}-\psi|_{y=h^+})\,dx. \qquad (2\text{-}16)$$

Substituting the results of Eqs. 2-12 and 14 into 16 yields

$$-(1/2)(\varepsilon_r+1)\varphi(x_i, h^+)=$$
$$(\varepsilon_r-1)\int_{-\infty}^{\infty}\varphi(x, h^+)(h/\pi)\{1/[(x-x_i)^2+(2h)^2]\}\,dx$$
$$-\int_{-w/2}^{w/2}[\rho(x)/(4\pi\varepsilon)]\ln\{(x-x_i)^2/[(x-x_i)^2+(2h)^2]\}\,dx \qquad (2\text{-}17)$$

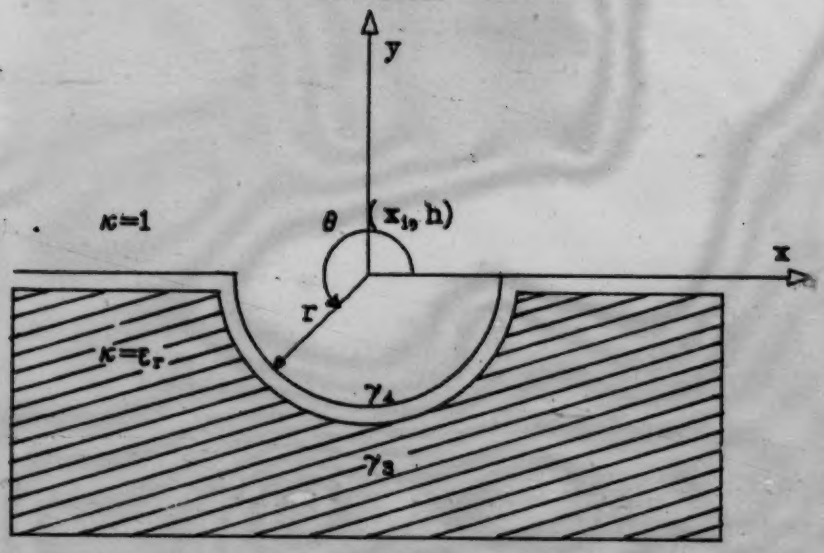

Fig. 2-3 DAI deformed in the vicinity of (x_i, y_i) in order to find the limit of $\partial\Psi/\partial y$ as (x,y) approaches (x_i, h), (Eq. 2-11).

Eq. 2-17 is an integral equation which is equivalent to the Laplace equation and the boundary conditions described by Eqs. 2-2. To make this integral equation suitable for numerical solutions, three additional modifications are required:

- the fact that $\rho(x)$ is singular at $\pm w/2$ must be included,
- there must be a change of units to simplify the integrals, and
- the symmetry of the microstrip line about the y-axis must be taken into consideration.

The fact that the energy should be finite in the vicinity of the microstrip edges leads to the conclusion that $\rho(x)$ should vary as $r^{-1/2}$ at the edges, [41] and [46], where r is the distance from the MIC edges; thus let the charge distribution be explicitly expressed in terms of these singularities at $x=\pm w/2$;

$$\rho(x) = \epsilon \bar{\chi}(x) / \sqrt{1-(2x/w)^2}, \qquad (2\text{-}18)$$

where $\bar{\chi}(x)$ is a slowly varying function which describes the behavior of the charge distribution away from the singular edges of the MIC. The factor ϵ is included in the definition in order to make the computations easier. An explicit representation of the singularity in ρ greatly reduces the numerical effort and leads to a higher computational accuracy with smaller matrix sizes [47].

The change of units

$$\zeta = 2x/w \qquad (2\text{-}19)$$

together with substitution of Eq. 2-18 in 17 results in

$$-2\pi(\varepsilon_r+1)\Phi_i=(2/\eta)(\varepsilon_r-1)\int_{-\infty}^{\infty}\varphi(\zeta)\{1/[(\zeta-\zeta_i)^2+(2/\eta)^2]\}d\zeta$$
$$-\eta\int_{-1}^{1}[\chi(\zeta)/\sqrt{1-\zeta^2}]\ln\{(\zeta-\zeta_i)^2/[(\zeta-\zeta_i)^2+(2/\eta)^2]\}d\zeta, \quad (2\text{-}20)$$

where

$$\eta=w/(2h), \quad (2\text{-}21a)$$

$$\zeta_i=2x_i/w, \quad (2\text{-}21b)$$

$$\Phi(\zeta)=\varphi(w\zeta/2, h^+), \quad (2\text{-}21c)$$

$$\Phi_i=\Phi(\zeta_i), \quad (2\text{-}21d)$$

and

$$\chi(\zeta)=\bar{\chi}(w\zeta/2). \quad (2\text{-}21e)$$

Eq. 2-20 can be solved numerically by the usual BEM procedures combined with quadrature formulae for integration.

In the following sections the algorithm for solving Eq. 2-20 is presented for special cases and is then generalized to include the analysis of single and coupled microstrip lines.

C. Microstrip Lines with $\varepsilon_r=1$

When $\varepsilon_r=1$, Eq. 2-20 reduces to

$$4\pi/\eta=G_1+G_2, \quad (2\text{-}22a)$$

where

$$G_1=-\int_{-1}^{1}[\chi(\zeta)/\sqrt{1-\zeta^2}]\ln[(\zeta-\zeta_i)^2+(2/\eta)^2]d\zeta, \quad (2\text{-}22b)$$

$$G_2=\int_{-1}^{1}[\chi(\zeta)/\sqrt{1-\zeta^2}]\ln(\zeta-\zeta_i)^2 d\zeta. \quad (2\text{-}22c)$$

Note that $\Phi_i=1$ on the MIC.

Eqs. 2-22 are the same as those obtained by Acton [47] using Green's functions. The techniques presented by Acton [47] to treat the singularities are very helpful in solving Eqs. 2-22. The integral Eqs. 2-22, when discretized, yield a set of linear equations. The domains of integration of

Eqs. 2-22 should be transformed to remove the singularities. The singularities of Eq. 2-22b occur at

$$\zeta=\pm 1;$$

The following transformation removes this singularity:

$$\zeta=\sin 0.5\pi\nu \tag{2-23}$$

Considering this transformation and the even symmetry of the quasi-TEM mode about the y-axis, and using the quadrature formulae for integration [48], we can write

$$G_1\approx(\pi/2)\sum_j W_j\,\chi_j\ln\{[(\zeta_j-\zeta_i)^2+(2/\eta)^2][(\zeta_j+\zeta_i)^2+(2/\eta)^2]\} \tag{2-24}$$

where

$$\zeta_i=\sin 0.5\pi\nu_j, \tag{2-25a}$$

and χ_j is the value of χ at ζ_j

$$\chi_j=\chi(\zeta_j). \tag{2-25b}$$

W_j and ν_j are the parameters of the quadrature formulae for integration given in [48]. The computer program for evaluating G_1 is called FIRST and appears in App. A. The singularities of Eq. 2-22c lie at

$$\zeta=\pm 1,$$

and at

$$\zeta=\zeta_i;$$

To discretize the integral of Eq. 2-22c it is assumed that the slowly varying function $\chi(\zeta)$ is constant at small intervals containing ζ_j as shown in Fig. 2-4. Thus, equation 2-22c can be discretized as

$$G_2=\sum_j \chi_j\int_{\zeta_j}^{\zeta_{j+1}}(1/\sqrt{1-\zeta^2})\ln(\zeta^2-\zeta_i^2)^2 d\zeta. \tag{2-26}$$

By the transformation

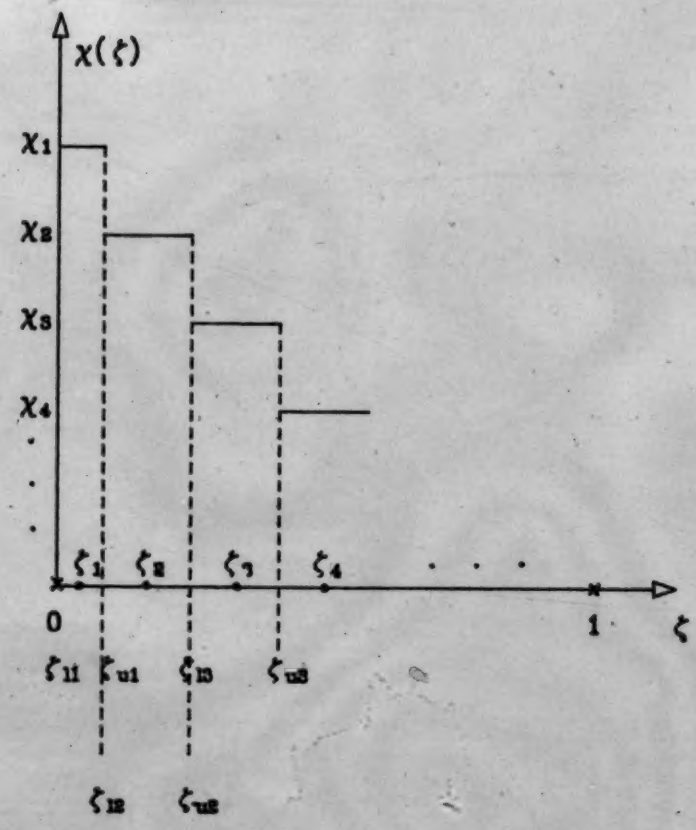

Fig. 2-4 $\chi(\zeta)$ discretized to facilitate the numerical solution of Eqs. 2-22.

$$\zeta=\sin\theta, \tag{2-27}$$

the integral in Eq. 2-26 can be rearranged as

$$\int_{\zeta_{ij}}\left(1/\sqrt{1-\zeta^2}\right)\ln\left(\zeta^2-\zeta_i^2\right)^2 d\zeta=\int_{\theta_1}^{\theta_2}\ln\left(\sin^2\theta-\sin^2\theta_i\right)^2 d\theta$$

$$=\int_{\theta_1}^{\theta_2}\ln\{[\sin(\theta-\theta_i)/(\theta-\theta_i)][\sin((\theta+\theta_i)/2)/((\theta+\theta_i)/2)]$$

$$[\sin((\pi/2)-((\theta+\theta_i)/2))/((\pi/2)-((\theta+\theta_i)/2))]\}^2 d\theta$$

$$+\int_{\theta_1}^{\theta_2}\ln(\theta-\theta_i)^2 d\theta+\int_{\theta_1}^{\theta_2}\ln(\theta+\theta_i)^2 d\theta$$

$$+\int_{\theta_1}^{\theta_2}\ln(\theta+\theta_1-\pi)^2 d\theta-(\ln 4)(\theta_2-\theta_1) \tag{2-28}$$

where

$$\theta_1=\sin^{-1}\zeta_{ij}, \tag{2-29a}$$

$$\theta_2=\sin^{-1}\zeta_{uj}, \tag{2-29b}$$

and

$$\theta_i=\sin^{-1}\zeta_i. \tag{2-29c}$$

The last step is performed to remove the singularities at

$$\theta=\theta_i,\quad (\theta+\theta_i)/2=0,\quad \text{and}\quad (\theta+\theta_i)/2=\pi/2.$$

Let

$$A=\theta-\theta_i\ (\text{thus e.g. } A_2=\theta_2-\theta_1), \tag{2-30a}$$

$$B=(\theta+\theta_i)/2, \tag{2-30b}$$

and

$$\bar{C}=(\theta+\theta_i-\pi)/2. \tag{2-30c}$$

To use the quadrature formulae for integration, the integration domain has to be between -1 and +1, thus the following transformation is employed

$$\theta=((\theta_2+\theta_1)/2)+\nu((\theta_2-\theta_1)/2) \tag{2-31}$$

Then Eq. 2-28 can be rewritten as

$$\int_{\zeta_{ij}}\left(1/\sqrt{1-\zeta^2}\right)\ln\left(\zeta^2-\zeta_i^2\right)^2 d\zeta=$$

$$(\theta_2-\theta_1)\int_{-1}^{1}\ln[(\sin A/A)(\sin B/B)(\sin\bar{C}/\bar{C})]\,d\nu$$

$$+2\ln\left|\left(A_2^{A_2}/A_1^{A_1}\right)\left(B_2^{B_2}/B_1^{B_1}\right)\left(\bar{C}_2^{\bar{C}_2}/\bar{C}_1^{\bar{C}_1}\right)\right|$$

$$-(6+\ln 4)(\theta_2-\theta_1). \tag{2-32}$$

Considering Eq. 2-32, the results are presented in terms of forms like

$$\sin A/A \text{ and } A_1^{A_1},$$

since as A or A_1 tend to zero, these forms tend to unity; in the programming language, APL, these indeterminate forms are defined as unity. In this way, no extra branchings are required in the computer programs when A_1, A_2, etc., are zero in Eq. 2-32. The program to perform the integration of Eq. 2-32 is called INT and appears in App. A.

D. Final Assembly of the Matrix Equation

The different parts of Eq. 2-22 can be assembled to form the final matrix equations. Letting i and j vary over all the possible values, Eq. 2-24 results in

$$[G_1]\{\chi\},$$

where, from Eq. 2-24

$$G_{1,ij} = -(\pi/2) W_j \ln\{[(\zeta_j-\zeta_i)^2+(2/\eta)^2][(\zeta_j+\zeta_i)^2+(2/\eta)^2]\}. \quad (2\text{-}33)$$

$\{\chi\}$ is a column matrix containing χ_1, χ_2, ...

Similarly, Eqs. 2-26 and 31 result in

$$[G_2]\{\chi\}.$$

Thus, in matrix form, Eqs. 2-22 can be written as

$$\{F\} = ([G_1] + [G_2])\{x\}, \quad (2\text{-}34)$$

where $\{F\}$ is a column matrix, all elements of which are equal to $4\pi/\eta$ (Eq. 2-22a). The program FNL in App. A forms and solves the matrix Eq. 2-34.

The capacitance per unit length of a microstrip line with $\varepsilon_r=1$ is the total charge per unit length divided by the strip potential, which is assumed to be unity. To find C the total charge, ρ must be integrated over the strip, thus

$$C=\int_{-\eta}^{\eta}\rho\,dx=\varepsilon\eta\int_{-1}^{1}\chi/\sqrt{1-\zeta^2}\,d\zeta, \qquad (2\text{-}35a)$$

or

$$C_0\approx(\varepsilon\eta)\sum_j W_j\chi_j \qquad (2\text{-}35b)$$

In the computations, C_0 is found in units of ε.

E. Microstrip Line with $\varepsilon_r\neq 1$

In the case where $\varepsilon_r\neq 1$, Eq. 2-20 must be solved. Let the first integral on the right hand side of Eq. 2-20 be designated by G_5

$$G_5=\int_{-1}^{1}\Phi(\zeta)/[(\zeta-\zeta_i)^2+(2/\eta)^2]\,d\zeta \qquad (2\text{-}36a)$$

Φ is known on the MIC and is equal to one volt. Thus, the portion of G_5 which is integrated over the MIC, G_6, can be easily found as

$$G_6\approx(\eta/2)\tan^{-1}[(1-\zeta_i)\eta/2]-(\eta/2)\tan^{-1}[(1+\zeta_i)\eta/2] \qquad (2\text{-}36b)$$

Using the quadrature formulae of integration [48], the portion of G_5 which is integrated over the DAI, G_7, can be approximated by

$$G_7=\sum_j \Phi_j\bar{W}_j\{1/[(\zeta_j-\zeta_i)^2+(2/\eta)^2]+1/[(\zeta_j+\zeta_i)^2(2/\eta)^2]\}, \qquad (2\text{-}36c)$$

where

$$\zeta_j=\bar{\nu}_j+1, \qquad (2\text{-}36d)$$

$\bar{W}_j$ and $\bar{\nu}_j$ are tabulated in [48]. G_5 is the sum of G_6 and G_7

$$G_5=G_6+G_7. \qquad (2\text{-}36e)$$

The results obtained for the case $\varepsilon_r=1$ can be used for the case $\varepsilon_r\neq 1$ when slightly modified. Considering Fig. 2-5,

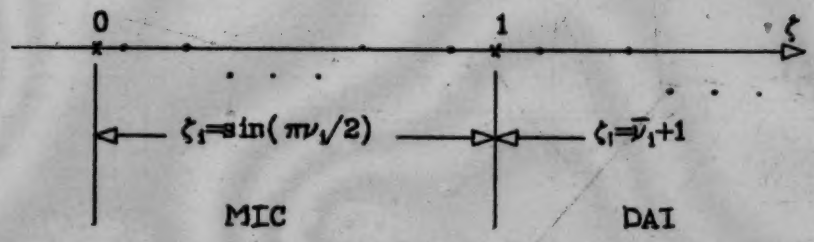

Fig. 2-5 Demonstration of ζ-axis divided into various segments using the data for numerical integration. (ζ-axis is the path defined by the y=h plane in a microstrip line cross-section).

ζ_i can be greater than unity for the case $\varepsilon_r \neq 1$; ζ_i can lie on the DAI, since the integrals on the DAI do not vanish (Eq. 2-20) for $\varepsilon_r \neq 1$. The matrices $[G_1]$ and $[G_2]$ should be modified to $[G_3]$ and $[G_4]$, respectively, when $\zeta_i > 1$.

The final matrix equation is

$$\{\bar{F}\} = \left[\begin{array}{c|c} [G_1]+[G_2] & \\ \hline & [\hat{G}_5] \\ \hline [G_3]+[G_4] & \end{array}\right] \left\{\begin{array}{c} \{\chi\} \\ \hline \{\Phi\} \end{array}\right\} \qquad (2\text{-}37)$$

where

$\{\Phi\}$ is a column matrix containing the unknown φ_i's on the DAI (Fig. 2-5).

$[G_1]$ and $[G_2]$ are the same as defined above, (Eqs. 2-33 to 34)

$[G_3]$ is a modification of $[G_1]$ when $\zeta_i > 1$,

$[G_4]$ is a modification of $[G_2]$ when $\zeta_i > 1$.

$[\hat{G}_5]$ is defined by Eqs. 2-36, and

$\{\hat{F}\}$ is a column matrix, the i' th element of which is $-2\pi(\varepsilon_r+1)\varphi_i$.

Eq. 2-37 should be further rearranged since φ_i is known only when ζ_i lies on the MIC. $\{\hat{F}\}$ contains some unknown φ_i and $\{\Phi\}$ contains some known φ_i; rearranging Eq. 2-37 results in

$$\{F\} = [G] \left\{\begin{array}{c} \{\chi\} \\ \hline \{\Phi\} \end{array}\right\} \qquad (2\text{-}38)$$

where $\{F\}$ is a column matrix all elements of which are equal to $-2\pi(\varepsilon_r+1)$. By solving Eq. 2-38, the charge distribution on the MIC, the potential distribution on the DAI,

and the capacitance per unit length, C, can be calculated. Having $\{\chi\}$, the charge distribution can be obtained from Eq. 2-18 and the capacitance per unit length, C, can be calculated from Eq. 2-35a. Moreover, $\{\Phi\}$ provides the potential distribution on the DAI.

Having C_0 and C, it is easy to determine ε_e and Z from Eqs. 1-4. Calculated results are presented in Figs. 2-6 and 7 for the case $\varepsilon_r = 9.9$ and $w/h = 1.0$, and for several values of ε_r in Figs. 2-8 and 9. The results coincide with the results obtained by Yamashita and Mittra [8], and Mittra and Itoh 12 . The overall matrix size is 15 x 15. The CPU time per run on the U. of A. AMDAHL 47/V6 computer is 0.08 sec. The computer programs, together with an illustrative example are presented in App. A.

As Figs. 2-6 through 9 show, the obtained results are identical to those obtained in [8] and [12]. However, the present method is easier to formulate, is more economical, and provides more information than other methods. Specifically, the variational method [8] provides ε_e and Z only; the computer time is 10 secs. on an IBM 7094. The integral equation method [11] provides $\rho(x)$, ε_e, and Z and the typical computer time is 30 secs. with a final matrix size of 30x30. The Wiener-Hopf method [12] provides $\rho(x)$, $\varphi(x,h)$, ε_e, and Z; the final matrix size is less than 10x10, but it is essentially an analytical method which seems impossible to generalize to coupled lines.

F. Coupled Microstrip Lines

Eq. 2-17 can easily be generalized to the case of

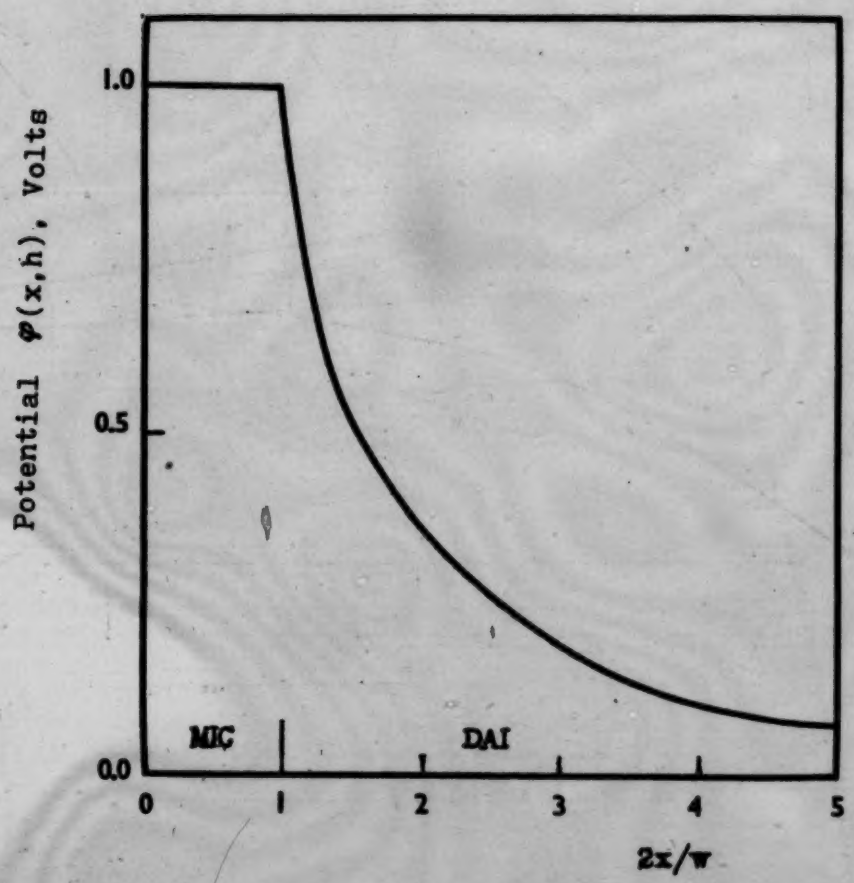

Fig. 2-6 Potential distribution of a microstrip line on the DAI vs. normalized distance with ϵ_r=9.9 and w/h=1.0; results coincide with those of [12].

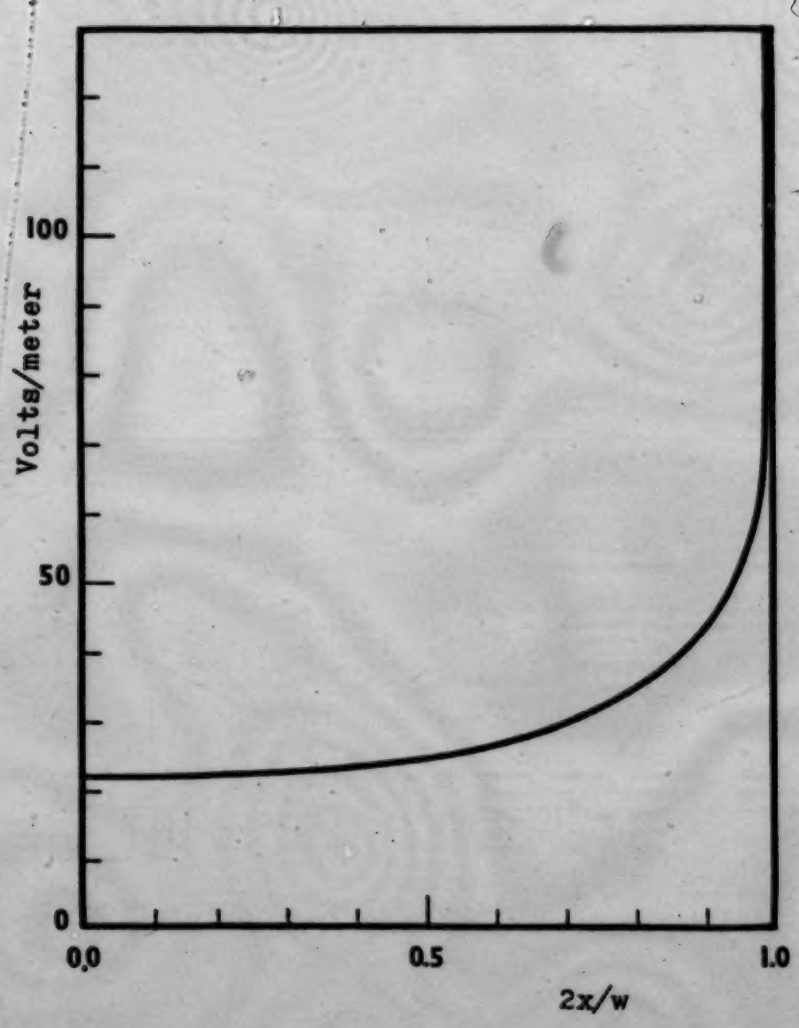

Fig. 2-7 Surface charge of a microstrip line vs. normalized distance on the MIC with ϵ_r= 9.9 and w/h=1.0; results coincide with those of [12].

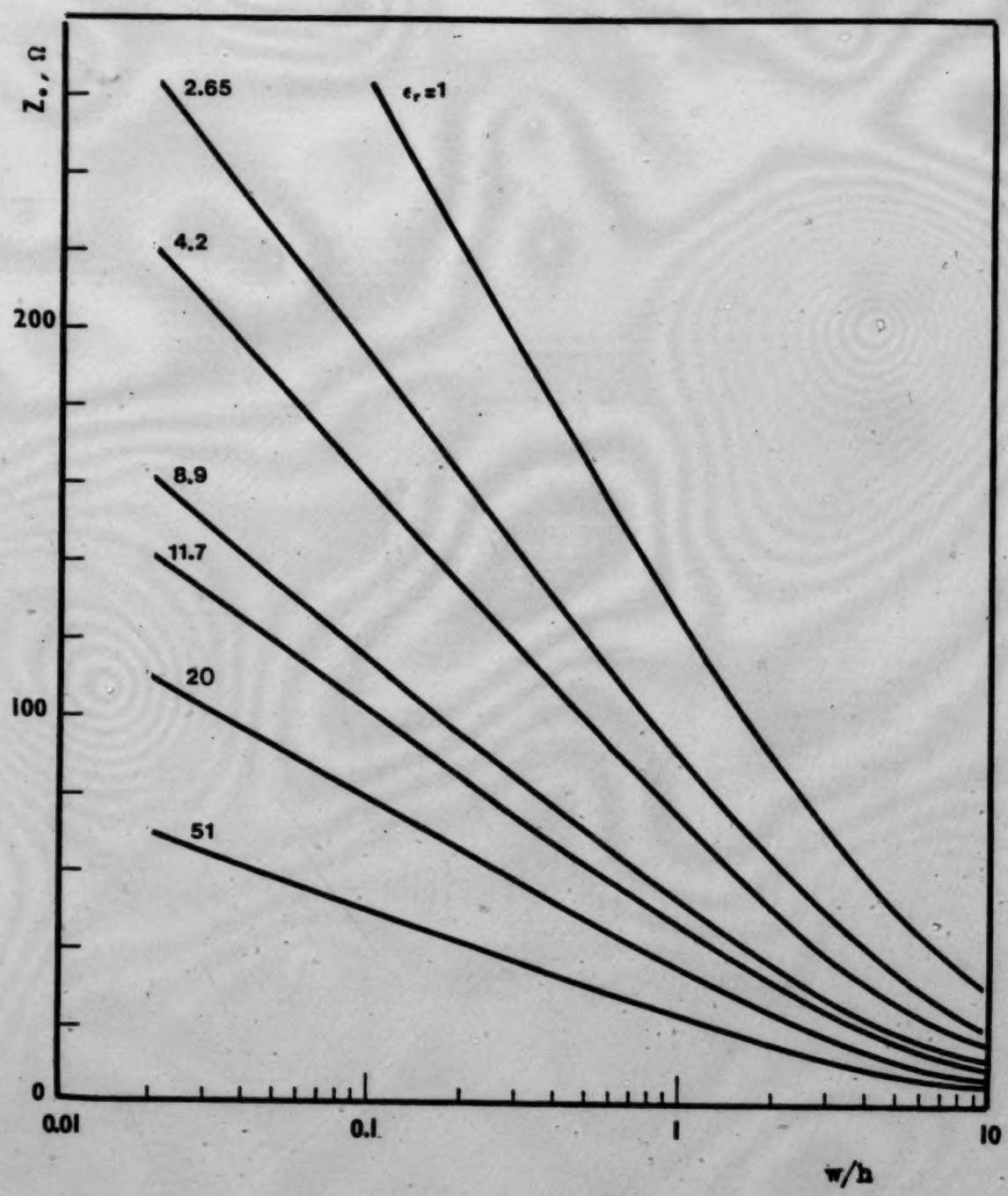

Fig. 2-8 Characteristic impedance of a microstrip line vs. w/h for various ε_r; results coincide with those of [8].

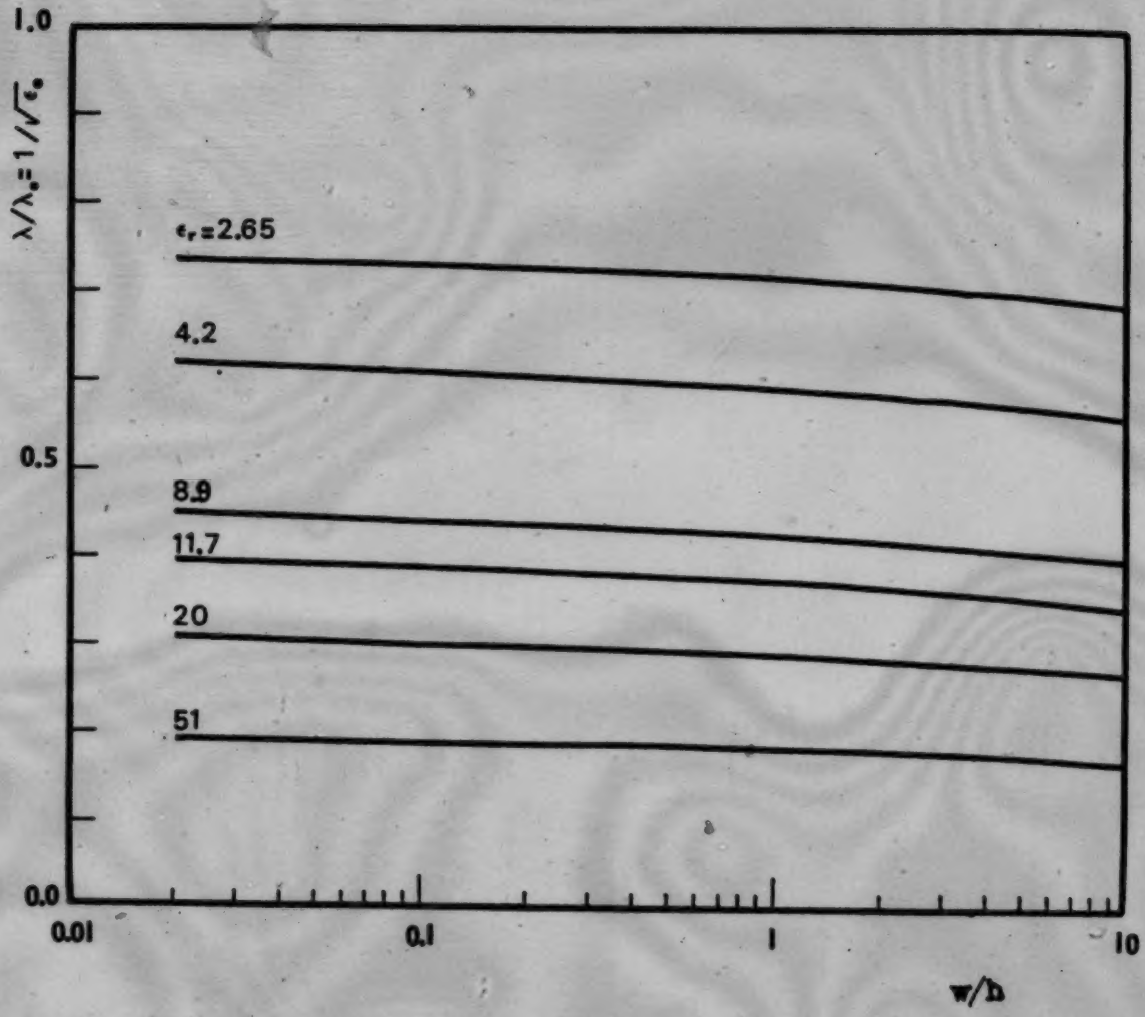

Fig. 2-9 Normalized wavelength of a microstrip line vs. w/h for various ϵ_r ; results coincide with those of [8].,

coupled microstrip lines. The integration domain of the second integral on the right hand side of Eq. 2-17 should be modified to include both strips. The formulation details are given only for the case $\epsilon_r=1$ since the procedure for $\epsilon_r\neq 1$ closely follows that of the single microstrip line.

For coupled microstrip lines with $\epsilon_r=1$, Eq. 2-17 reduces to

$$4\pi\Phi_i=\int_{MIC}[\rho(x)/\varepsilon]\ln\{(x-x_i)^2/[(x-x_i)^2+(2h)^2]\}\,dx. \qquad (2\text{-}39)$$

Let

$$\xi=x/h; \qquad (2\text{-}40a)$$

define (Fig. 2-10)

$$\sigma=(s+w)/(2h), \qquad (2\text{-}40b)$$

and

$$\eta=w/(2h). \qquad (2\text{-}40c)$$

Then Eq. 2-39 can be rewritten as

$$4\pi\Phi_i=\int_{\sigma-\eta}^{\sigma+\eta}[\rho_p(\xi)/\varepsilon]\ln\{(\xi-\xi_i)^2/[(\xi-\xi_i)^2+(2/\eta)^2]\}\,d\xi$$
$$+\int_{-\sigma-\eta}^{-\sigma+\eta}[\rho_n(-\xi)/\varepsilon]\ln\{(\xi-\xi_i)^2/[(\xi-\xi_i)^2+(2/\eta)^2]\}\,d\xi, \qquad (2\text{-}41)$$

where ρ_p and ρ_n are the charge distributions on the MIC on the positive and on the negative ξ-axis. For the even modes

$$\rho_p(\xi)=\rho_n(-\xi); \qquad (2\text{-}42a)$$

For the odd modes

$$\rho_p(\xi)=-\rho_n(-\xi). \qquad (2\text{-}42b)$$

Considering the singularity of the charge at the MIC edges $\rho_p(\xi)$ can be written as

$$\rho_p=\varepsilon\bar{\chi}(\sigma-\xi)/\sqrt{1-[(\sigma-\xi)/\eta]^2}, \qquad (2\text{-}43)$$

where $\bar{\chi}$ is a slowly varying function of ξ.

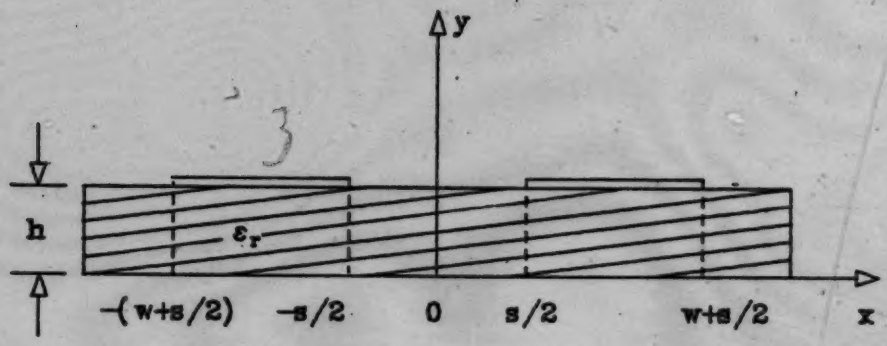

(a)

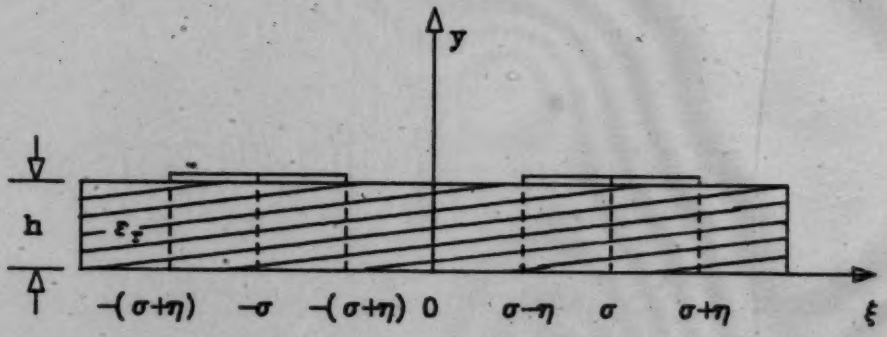

(b)

Fig. 2-10 (a) Coupled microstrip lines;
(b) coupled microstrip lines with normalized x-axis.

For the even modes it is assumed that the voltages on both strips are +1 volt and that the voltage is zero on the ground plane. For the odd modes, it is assumed that the voltages are +1 volt on the right strip, -1 on the left strip, and zero on the ground plane.

The point ξ_i is chosen to lie on the right strip; thus

$$\Phi_i = 1. \tag{2-44}$$

Combining Eqs. 2-41, 43, and 44 results in

$$4\pi = \int_{\sigma-\eta}^{\sigma+\eta} \{\chi[(\sigma-\xi)/\sqrt{1-((\sigma-\xi)/\eta)^2}]\cdot$$
$$\{\ln[(\xi-\xi_j)^2/((\xi-\xi_j)^2+(2/\eta)^2)] \pm \ln[(\xi+\xi_j)^2/((\xi+\xi_j)^2+(2/\eta)^2)]\}\, d\xi, \tag{2-45}$$

where the plus sign holds for the even modes and the minus sign for the odd modes.

The transformation

$$\zeta = (\sigma-\xi)/\eta \tag{2-46}$$

simplifies Eq. 2-45 to

$$4\pi = \eta \int_{-1}^{+1} [\chi(\zeta)/\sqrt{1-\zeta^2}]\{\ln[(\zeta_i-\zeta)^2/[(\zeta-\zeta_j)^2+(2/\eta)^2]]$$
$$\pm \ln[(\zeta_i'-\zeta)^2/((\zeta_i'-\zeta)^2+(2/\eta)^2)]\}\, d\zeta, \tag{2-47}$$

where

$$\zeta_i' = 2(\sigma/\eta) - \zeta_i. \tag{2-48}$$

Eq. 2-47 can be discretized as follows

$$4\pi = \eta \sum_j \chi_j (G_{1,ij} - G_{2,ij} \pm G_{3,ij} \pm G_{4,ij}), \tag{2-49}$$

where

$$G_{1,ij} = \int_{\zeta_{ij}}^{\zeta_{ij}} \ln(\zeta_i-\zeta)^2/\sqrt{1-\zeta^2}\, d\zeta. \tag{2-50a}$$
$$G_{2,ij} = \int_{\zeta_{ij}}^{\zeta_{ij}} \ln(\zeta_i'-\zeta)^2/\sqrt{1-\zeta^2}\, d\zeta. \tag{2-50b}$$
$$G_{3,ij} = -W_j \ln[(\zeta_i-\zeta_j)^2+(2/\eta)^2]. \tag{2-50c}$$
$$G_{4,ij} = -W_j \ln[(\zeta_i'-\zeta_j)^2+(2/\eta)^2]. \tag{2-50d}$$

χ_j was defined in Eq. 2-25b, W_j and ζ_j are the parameters

of formulae for quadrature integration available in [48].

Eq. 2-49 can be written in matrix form as

$$\{U\} = ([G_1] \pm [G_2])\{\chi\} + ([G_3] \pm [G_4])\{\chi\}. \qquad (2\text{-}51)$$

where $\{U\}$ is a column matrix, all elements of which are equal to 4π, and $\{\chi\}$ is a column matrix with elements χ_j. The plus and minus signs refer to the even and the odd modes, respectively. To evaluate $G_{1,ij}$, let

$$\zeta = \sin\theta, \qquad (2\text{-}52)$$

Then, it can be shown that

$$G_{1,ij} = \int_{\theta_1}^{\theta_2} \ln\{[\sin((\theta-\theta_j)/2)/((\theta-\theta_j)/2)]^2 \cdot [\pi\cos((\theta+\theta_j)/2)]^2/[((\pi/2)-((\theta+\theta_j)/2))((\pi/2)+((\theta+\theta_j)/2))]^2\}\, d\theta$$
$$-2(\theta_2-\theta_1)\ln(2\pi) + 2\int_{\theta_1}^{\theta_2} \ln(\theta-\theta_j)\, d\theta$$
$$+2\int_{\theta_1}^{\theta_2} \ln[\pi-(\theta+\theta_j)]\, d\theta + 2\int_{\theta_1}^{\theta_2} \ln(\pi+\theta+\theta_j)\, d\theta. \qquad (2\text{-}53)$$

$G_{2,ij}$ can be found similarly.

Coupled Lines with $\epsilon_r \neq 1$

For coupled lines with $\epsilon_r \neq 1$ Eq. 2-17 should be modified as

$$-2\pi(\epsilon_r+1)\Phi_i = 2(\epsilon_r-1)\int_{-\eta}^{\eta} \bar{\Phi}(\xi)/[(\xi-\xi_i)^2+4]\, d\xi$$
$$+\int_{\sigma-\eta}^{\sigma+\eta} [\bar{\chi}(\sigma-\xi)/\sqrt{1-((\sigma-\xi)/\eta)^2}]\{\ln(\xi-\xi_i)^2/[(\xi-\xi_i)^2+(2/\eta)^2] \pm \ln(\xi+\xi_i)^2/[(\xi+\xi_i)^2+(2/\eta)^2]\}\, d\xi, \qquad (2\text{-}54)$$

where

$$\bar{\Phi}(\xi) = \Phi(\eta\xi) = \Phi(x).$$

The + and - signs in the right hand side of Eq. 2-54 refer to the even and odd modes, respectively. To simplify the integrations we introduce the following change of variables

$$\zeta = (\sigma - \xi)/\eta, \qquad (2\text{-}55a)$$
$$\sigma' = \sigma/\eta, \qquad (2\text{-}55b)$$
$$\zeta_i' = 2\sigma' - \zeta_i. \qquad (2\text{-}55c)$$

Consider the integrals of Eq. 2-54. The potential is unknown on the DAI and the charge is unknown on the MIC. Thus, the integration domain is divided into three regions (i.e., the DAI in between the two strips, the strips and the DAI outside the strips) to make the numerical integration possible:

$$\zeta = \begin{cases} (\sigma'-1)\bar{\nu}/2+(\sigma'+1)/2; & 1<\zeta<\sigma' \\ \sin 0.5\pi\bar{\nu}; & -1<\zeta<1 \\ -(1+\bar{\nu}); & -\infty<\zeta<-1 \end{cases} \qquad (2\text{-}55d)$$

Substituting the change of variables for Eqs. 2-55 into 54 and following the same procedures as in the previous sections leads to

$$\{\bar{F}\} = ([E_1]\pm[E_2])\{\bar{\Phi}\}+([E_3]\pm[E_4])\{\bar{\bar{\Phi}}\} +([E_5]\pm[E_6])\{\chi\}+([E_7]\pm[E_8])\{\chi\} \qquad (2\text{-}56)$$

where $\{\bar{\Phi}\}$ is a column matrix which contains the unknown values of the potential on the DAI in between the strips. Similarly, $\{\bar{\bar{\Phi}}\}$ is a column matrix with the unknown potential values on the DAI outside the strips. $\{\chi\}$ is a column matrix representing the unknown charge distribution on the strips. $\{\hat{F}\}$ is a column matrix with elements $-2\pi(\varepsilon_r+1)\Phi_i$, if the point i lies on the DAI and

$$-2\pi(\varepsilon_r+1)\Phi_i - 2(\varepsilon_r-1)\int_{MIC}[(\xi-\xi_i)^2+4]^{-1}d\xi,$$

if the point i lies on the MIC (c.f. the first integral in the right hand side of Eq. 2-54).

$[E_1]$ through $[E_8]$ are defined as

$$E_{1,ij}\pm E_{2,ij} = [(\varepsilon_r-1)(\sigma'-1)/\eta]\bar{w}_j \{1/[(\zeta_i-\zeta_j)^2+(2/\eta)^2]\pm 1/[(\zeta_i'-\zeta_j)^2+(2/\eta)^2]\};$$
$$-\infty\le\zeta_i\le\sigma'; \quad 1\le\zeta_i\le\sigma'. \qquad (2\text{-}57a)$$

$$E_{3,ij} \pm E_{4,ij} = [2(\varepsilon_r - 1)/\eta]\,\bar{\bar{W}}_n \cdot$$

$$\{1/[(\zeta_i - \zeta_j)^2 + (2/\eta)^2] \pm 1/[(\zeta_i' - \zeta_j)^2 + (2/\eta)^2]\};$$

$$-\infty \le \zeta_j \le \sigma'; \quad -\infty \le \zeta_i \le -1; \tag{2-57b}$$

$$E_{5,ij} \pm E_{6,ij} = \pi\eta\,\bar{\bar{W}}_t/2 \cdot$$

$$\{\ln[(\zeta_i - \zeta_j)^2 + (2/\eta)^2] \pm \ln[(\zeta_i - \zeta_j)^2 + (2/\eta)^2]\};$$

$$-\infty \le \zeta_j \le \sigma'; \quad -\infty \le \zeta_i \le 1 \tag{2-57c}$$

$$E_{7,ij} \pm E_{8,ij} = \eta \int_{\zeta_{ij}}^{\sigma'} (1/\sqrt{1-\zeta^2}) \cdot$$

$$[\ln(\zeta_i - \zeta)^2 \pm \ln(\zeta_i' - \zeta)^2]\, d\zeta$$

$$-\infty \le \zeta_j \le \sigma'; \quad -1 \le \zeta_i \le 1 \tag{2-57d}$$

Moreover, different numerical procedures are required in evaluating $[E_7]$ and $[E_8]$ depending on which region the point ζ_i lies in; let

$$E_{7,ij} = \begin{cases} F_{1,ij} & \text{if } 1 \le \zeta_i \le \sigma' \\ G_{1,ij} & \text{if } -1 \le \zeta_i \le 1 \\ H_{1,ij} & \text{if } -\infty \le \zeta_i \le -1, \end{cases} \tag{2-58a}$$

Thus

$$[E_7] = \begin{bmatrix} [F_1] \\ \hdashline [G_1] \\ \hdashline [H_1] \end{bmatrix} \tag{2-58b}$$

Finally, considering Eq. 2-56, some of the Φ_i's appearing in $\{\hat{F}\}$ are unknown and should be transferred to the right hand side of the equation. Eq. 2-56 can thus be rearranged as

$$\{F_e\} = [G_e] \begin{Bmatrix} \{\bar{\Phi}\} \\ \hdashline \{\bar{\bar{\Phi}}\} \\ \hdashline \{\bar{X}\} \end{Bmatrix} \tag{2-59}$$

for the even modes. Similarly a matrix equation can be obtained for the odd modes.

By solving the final matrix equations the even- and odd-mode characteristic impedance and ε_e can be evaluated. The computer programs are presented in App. B. The results obtained by this method are

presented in Figs. 2-11 and 12, and coincide with the results in [4] and [26]. The charge and the potential distributions at the DAI are calculated and presented in Figs. 2-13 and 14.

Fig. 2-15 shows the ε_e vs. s/h obtained for the case

$$w/h=1.0, \text{ and } \varepsilon_r=9.0$$

The final matrix size is 35x35 and the CPU time on an AMDAHL 47/V6 per point per mode is 2.165 secs. For the sake of comparison, we note that with Green's functions [26], the required time on an IBM 360/67 is 22.12 secs., to obtain the same results with the same accuracy; the variational method [28] provides only ε_e and Z with a required time of 32 secs. on a Univac 1108, and is less accurate (within 2%) than [26].

G. Summary

In this chapter, microstrip lines and coupled lines in the quasi-TEM regime were analyzed by the BEM. Laplace's equation at the cross section of a microstrip line (Fig. 1-1a) should be solved for the potential distribution

$$\nabla^2\varphi=0. \tag{2-1}$$

The boundary and the continuity conditions at the y=h plane were

$$\varphi|_{y=h^-}=\varphi|_{y=h^+} \tag{2-2a}$$

On the DAI,

$$\varepsilon_r(\partial\varphi/\partial y|_{y=h^-})=(\partial\varphi/\partial y|_{y=h^+}) \tag{2-2b}$$

and on the MIC,

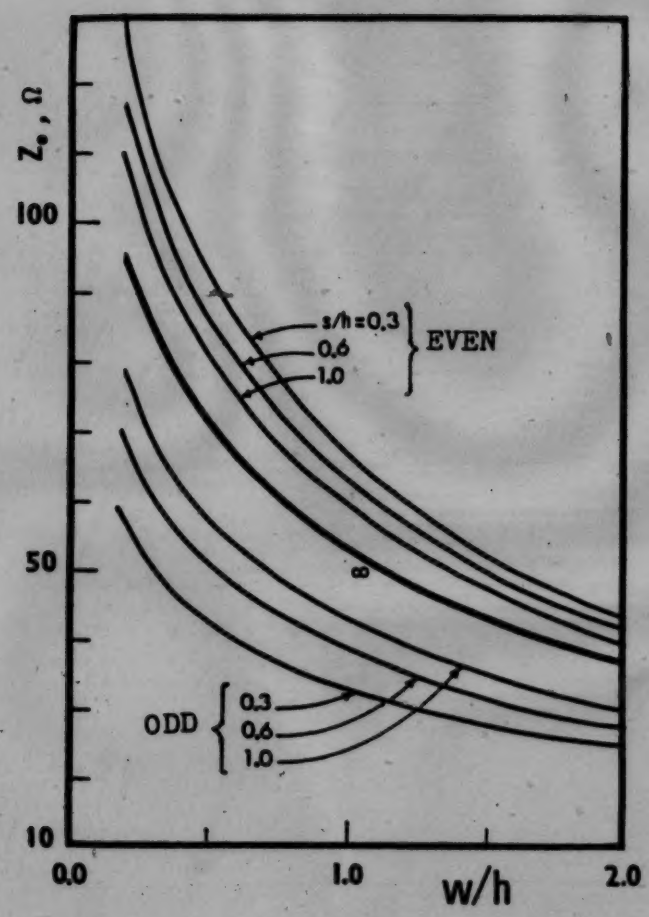

Fig. 2-11 Even- and odd-mode characteristic impedance of a coupled microstrip line vs. w/h for various values of s/h and ϵ_r=9.0; results coincide with [4] and [26].

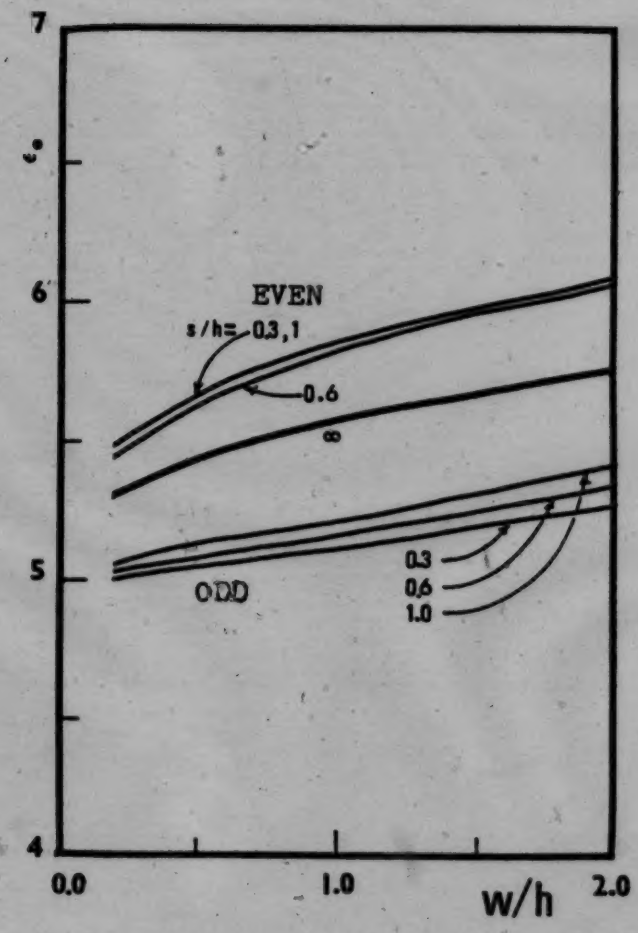

Fig. 2-12 Even- and odd-mode ε_e of coupled microstrip lines vs. w/h for various values of s/h and ε_r =9.0.

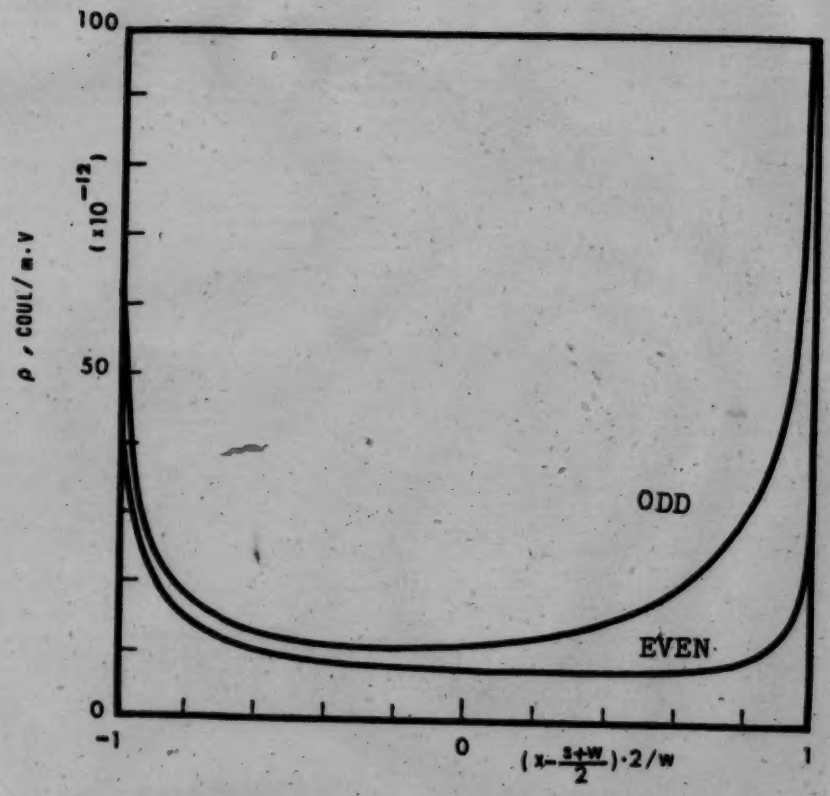

Fig. 2-13 Even- and odd-mode surface charge vs. normalized distance on coupled microstrip lines; ε_r =9.0, w/h=1.0 and s/h=0.3.

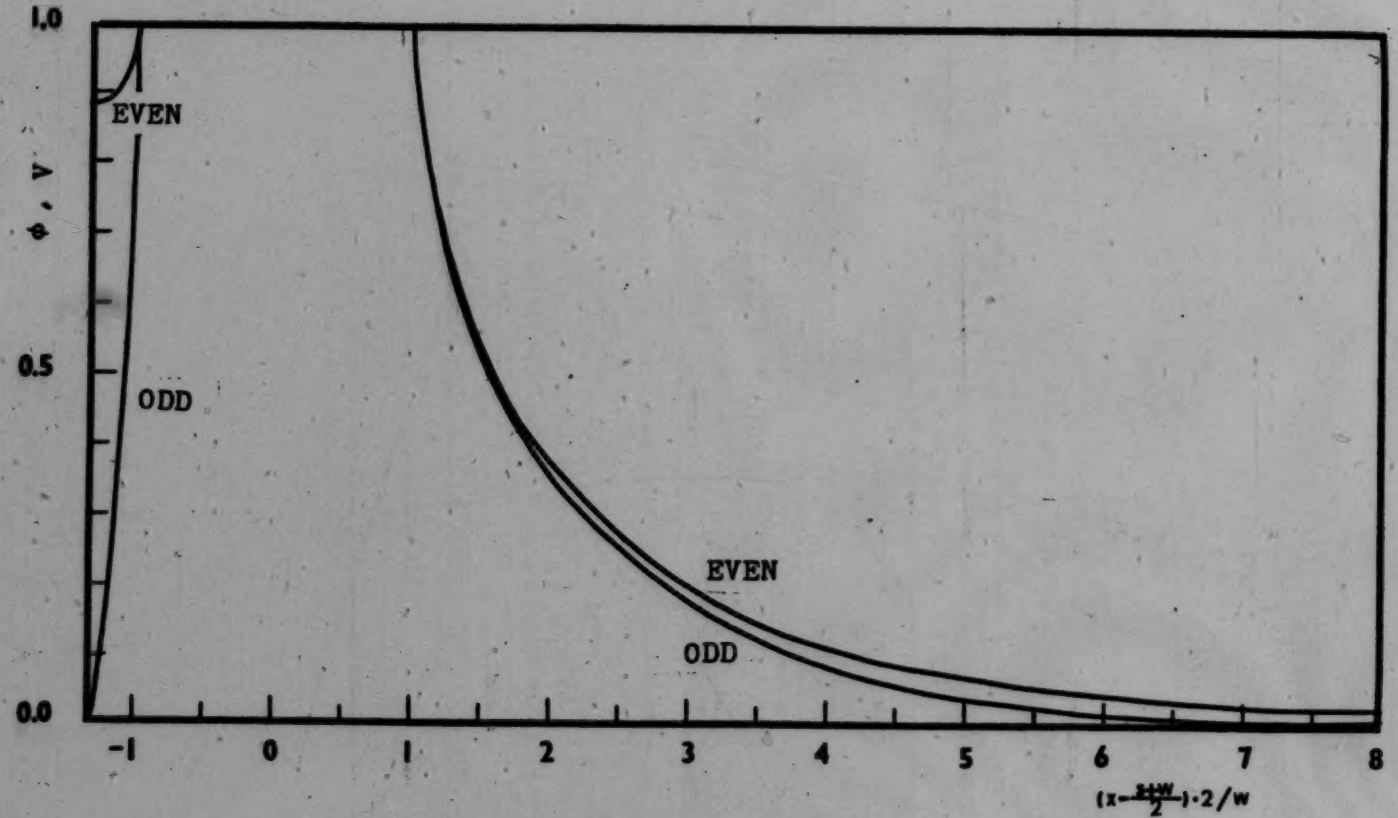

Fig. 2-14 Even- and odd-mode potential distribution of coupled microstrip lines on the DAI vs. normalized distance; ϵ_r=9.0, w/h=1.0 and s/h=0.3.

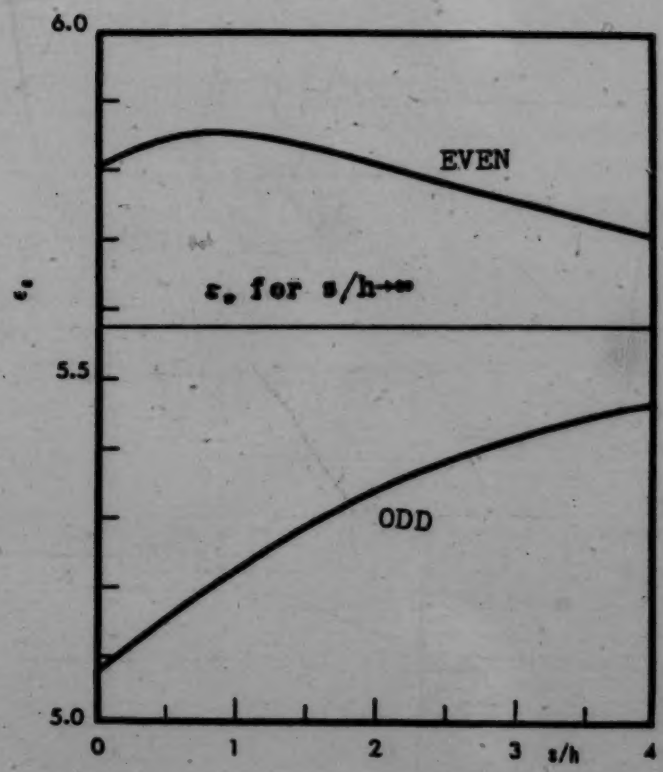

Fig. 2-15 Even- and odd-mode ε_e of coupled microstrip lines vs. s/h; w/h=1.0 and ε_r=9.0.

$$\varepsilon_r(\partial\varphi/\partial y|_{y=h^-}) - (\partial\varphi/\partial y|_{y=h^+}) = \rho(x)/\varepsilon \qquad (2\text{-}2c)$$

where $\rho(x)$ was the charge distribution on the MIC.

Green's second identity was used

$$\int_S(\varphi\nabla^2\psi - \psi\nabla^2\varphi)\,dS =$$

$$\int_C[\varphi(\partial\psi/\partial n) - \psi(\partial\varphi/\partial n)]\,dC \qquad (2\text{-}3)$$

where ψ was the free space Green's function. Using Eq. 2-3, both Laplace's equation and the boundary conditions were transformed into an integral equation on the y=h plane.

$$-(1/2)(\varepsilon_r+1)\varphi(x_i, h^+) =$$

$$(\varepsilon_r-1)\int_{-\infty}^{\infty}\varphi(x, h^+)(h/\pi)\{1/[(x-x_i)^2+(2h)^2]\}\,dx$$

$$-\int_{-w/2}^{w/2}[\rho(x)/(4\pi\varepsilon)]\ln\{(x-x_i)^2/[(x-x_i)^2+(2h)^2]\}\,dx \qquad (2\text{-}17)$$

The singularity in the charge distribution was inserted explicitly into Eq. 2-17

$$\rho(x) = \bar{\chi}(x)/\sqrt{1-(2x/w)^2}, \qquad (2\text{-}18)$$

where $\bar{\chi}(x)$ was a slowly varying function. This reduced the final matrix size and increased the accuracy [59].

The simple case of a microstrip with $\varepsilon_r=1$ was analyzed first. The singularities in the resulting equations were removed using appropriate transformations. The case $\varepsilon_r\neq1$ was then analyzed. The numerical results obtained for the single lines were shown in Figs. 2-6, 7, 8, and 9 and coincided with results obtained in [8] and [12].

The method was then applied to coupled microstrip lines. The results obtained by this method were presented in Figs. 2-11 and 12 and coincided with the results obtained in [4] and [26]. Additional original data were presented in Figs. 2-13, 14 and 15.

Conclusions

The BEM has been successfuly applied to microstrip lines and coupled lines in the quasi-TEM regime; the analysis is capable of evaluating the characteristic impedance, ε_e, the charge, and the potential distributions. The only other method yielding all of the above parameters and distributions is, to the author's knowledge, the Wiener-Hopf method [12]; however, it seems impossible to generalize the latter method to coupled lines and resonators.

The singularity in the charge distribution is included in the formulation. Moreover, the BEM has been modified by using the quadrature formulae for integration. This has resulted in increased accuracy and in a reduction of the size of the final set of equations. For microstrip lines, the final matrix size is 15x15 and for coupled lines, the final matrix size is 35x35.

The method is very efficient and accurate; the CPU time per run on the AMDAHL 74/V6 computer is 0.08 secs. for the analysis of microstrip lines and 2.165 secs. per run per mode for the analysis of the even- and odd-modes in coupled lines.

III. AN ALTERNATIVE INTEGRAL EQUATION METHOD

A. Introduction

In Chap. 2 the BEM was applied to microstrip lines in the quasi-TEM regime. It is possible to generalize this method to the wave analysis of microstrip lines, but the fundamental solution will be difficult to obtain.

To solve the Laplace equation, Green's functions are customarily defined so that they satisfy Poisson's equation; the forcing function is chosen to be a point charge. In this chapter, instead of Green's functions, a fundamental solution, ψ, is chosen so that it satisfies the Laplace equation. Moreover, the boundary conditions on ψ are defined such that the final integral equation is expressed in terms of the charge distribution alone. The method leads to expressions for the characteristic impedance and the effective dielectric constant for microstrip lines. The method is then applied to coupled microstrip lines, and in the following chapters it is generalized to the wave analysis of microstrips.

B. Formulation

For a microstrip line in the quasi-TEM regime, Laplace's equation for the potential function φ should be solved in the cross section of a microstrip line. The boundary conditions are given in Eq. 2-2 and are demonstrated in Fig. 3-1. The radius of the semicircle, R, in Fig. 3-1 is assumed to be infinite.

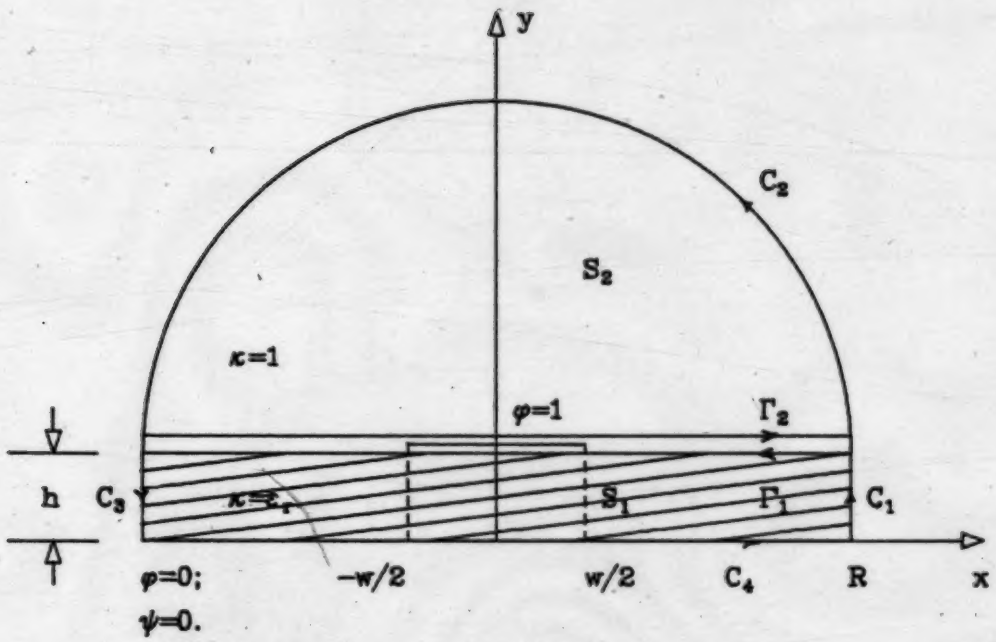

Fig. 3-1 Open microstrip line; R is assumed infinitely large.

Green's second identity can be applied to S_1 and S_2 of Fig. 3-1.

$$\int_{S_1}(\varphi\nabla_t^2\psi-\psi\nabla_t^2\varphi)\,dS=$$

$$\int_{C_1\cup\Gamma_1\cup C_3\cup C_4}[\varphi(\partial\psi/\partial n)-\psi(\partial\varphi/\partial n)]\,dC; \tag{3-1a}$$

$$\int_{S_2}(\varphi\nabla_t^2\psi-\psi\nabla_t^2\varphi)\,dS=$$

$$\int_{C_2\cup\Gamma_2}[\varphi(\partial\psi/\partial n)-\psi(\partial\varphi/\partial n)]\,dC. \tag{3-1b}$$

where, as shown in Fig. 3-1, the region S_1 is enclosed by paths C_1, Γ_1, C_3, and C_4; the region S_2 is enclosed by paths Γ_2 and C_2; φ is the desired potential distribution; ψ is an auxiliary function (fundamental solution), and $\partial/\partial n$ designates the normal derivative. Adding Eq. 3-1a to b results in

$$\int_{S_1\cup S_2}(\varphi\nabla_t^2\psi-\psi\nabla_t^2\varphi)\,dS=$$

$$\int_{C_1\cup\Gamma_1\cup C_3\cup C_4}[\varphi(\partial\psi/\partial n)-\psi(\partial\varphi/\partial n)]\,dC+\int_{C_2\cup\Gamma_2}[\varphi(\partial\psi/\partial n)-\psi(\partial\varphi/\partial n)]\,dC. \tag{3-2}$$

φ is zero on C_4 (Fig. 3-1). ψ is also defined to be zero on C_4. Moreover, φ and $\partial\varphi/\partial n$ tend to zero at infinity. Thus by letting R tend to infinity, Eq. 3-2 reduces to

$$\int_{S_1\cup S_2}(\varphi\nabla_t^2\psi-\psi\nabla_t^2\varphi)\,dS=$$

$$\int_{\Gamma_1}[\varphi(\partial\psi/\partial n)-\psi(\partial\varphi/\partial n)]\,dC+\int_{\Gamma_2}[\varphi(\partial\psi/\partial n)-\psi(\partial\varphi/\partial n)]\,dC, \tag{3-3}$$

where it is required that

$$\nabla_t^2\varphi=0. \tag{3-4}$$

Up to this point, the procedure is almost the same as that in Chap. 2. However, the auxiliary function ψ is assumed to satisfy Laplace's equation

$$\nabla_t^2\psi=0. \tag{3-5}$$

This choice makes the final equation much simpler and results in a very simple numerical procedure. Moreover, as will be explained in the next chapter, it is easier to

generalize this method, rather than the one in Chap. 2 to the wave analysis of microstrip lines.

Considering Eqs. 3-4 and 5, Eq. 3-3 can be written as

$$0=\int_{-\infty}^{\infty}[\varphi(\partial\psi/\partial y|_{y=h^-})-\psi(\partial\varphi/\partial y|_{y=h^-})](-dx)$$
$$+\int_{-\infty}^{\infty}[\varphi(-\partial\psi/\partial y|_{y=h^+})-\psi(-\partial\varphi/\partial y|_{y=h^+})]dx$$
$$=\int_{-\infty}^{\infty}[\varphi(\partial\psi/\partial y|_{y=h^-})-\varphi(\partial\psi/\partial y|_{y=h^+})]dx$$
$$-\int_{-\infty}^{\infty}[\psi(\partial\varphi/\partial y|_{y=h^-})-\psi(\partial\varphi/\partial y|_{y=h^+})]dx \qquad (3\text{-}6)$$

By properly imposing the boundary conditions on ψ, Eq. 3-6 can be reduced to a simple integral equation in terms of the charge distribution alone; let

$$(\psi|_{y=h^-})=\varepsilon_r(\psi|_{y=h^+}). \qquad (3\text{-}7a)$$

and

$$(\partial\psi/\partial y|_{y=h^-})-(\partial\psi/\partial y|_{y=h^+})=0.5[\delta(x-x_i)+\delta(x+x_i)]. \qquad (3\text{-}7b)$$

Substituting from Eqs. 3-7 into 6, and considering the boundary conditions on φ at y=h (Eqs. 2-2) the following integral equation is obtained

$$0=\varphi(x,h)-\int_{\text{metal}}(\rho/\varepsilon)(\psi|_{y=h^+})dx. \qquad (3\text{-}8)$$

To find the function ψ which satisfies Eqs. 3-7, let (considering an even symmetry in a microstrip line),

$$\psi=\begin{cases}\int_0^{\infty}A(\gamma)\cos(\gamma x)\sinh(\gamma y)\,d\gamma; & 0\le y<h\\ \int_0^{\infty}B(\gamma)\cos(\gamma x)\exp(-\gamma y)\,d\gamma. & h<y.\end{cases} \qquad (3\text{-}9a)$$

ψ as defined in Eq. 3-9a satisfies Laplace's equation. Imposing the boundary conditions of Eqs. 3-7 on ψ yields

$$A(\gamma)\sinh\gamma h=\varepsilon_r B(\gamma)\exp(-\gamma h), \qquad (3\text{-}9b)$$

and

$$B(\gamma)=(2/\pi)\exp(\gamma h)\cos(\gamma x_i)/\{\gamma[1+\varepsilon_r/\tanh(\gamma h)]\}. \qquad (3\text{-}9c)$$

Substituting ψ from Eqs. 3-9 into 8 results in

$$\int_0^\infty \int_{MIC} [\rho(x)/\varepsilon] \cos(\gamma x) \cos(\gamma x_i) / \{\gamma[1+\varepsilon_r/\tanh(\gamma h)]\} dx d\gamma = \pi/2. \quad (3\text{-}10)$$

where x_i is chosen to lie on the MIC.

Eq. 3-10 is solved for the single microstrip line and coupled microstrip lines in the following sections.

C. Single Microstrip Line

As in Chap. 2, the singularity in the charge distribution is explicitly included in Eq. 3-10 for reducing the final matrix sizes

$$\rho(x) = e\bar{\chi}(x) / \sqrt{1-(2x/w)^2}, \quad (3\text{-}11)$$

Eq. 2-10 can be written as

$$\int_0^\infty \left\{ \int_{-w/2}^{w/2} \bar{\chi}(x) \cos(\gamma x) / \sqrt{1-(2x/w)^2} dx \right\} \cos(\gamma x_i) / \{\gamma[1+\varepsilon_r/\tanh(\gamma h)]\} d\gamma = \pi/2. \quad (3\text{-}12)$$

To solve Eq. 3-12, let

$$I = \int_{-w/2}^{w/2} \bar{\chi}(x) \cos(\gamma x) / \sqrt{1-(2x/w)^2} dx; \quad (3\text{-}13)$$

Considering the even symmetry of the quasi-TEM mode in a microstrip line, the slowly varying function $\bar{\chi}(x)$ can be expanded in a Taylor series as

$$\bar{\chi}(x) = \bar{K}_0 + \bar{K}_1 x^2 + \cdots, \quad (3\text{-}14)$$

Thus

$$I = \int_{-w/2}^{w/2} (\bar{K}_0 + \bar{K}_1 x^2 + \cdots) \cos(\gamma x) / \sqrt{1-(2x/w)^2} dx. \quad (3\text{-}15)$$

Applying the transformation

$$\sin\theta = 2x/w$$

to Eq. 3-15 and using the tabulated integrals of [49] yields

$$I = (\pi/2)[K_0 J_0(0.5\gamma w) + K_1 J_2(0.5\gamma w) + \cdots]. \quad (3\text{-}16)$$

Substituting from Eq. 3-16 into 12 yields

$$\sum_{n=0}^{\infty} K_n \int_0^\infty J_{2n}(0.5\gamma w) \cos(\gamma x_i) / \{\gamma[1+\varepsilon_r/\tanh(\gamma h)]\} d\gamma = 1. \quad (3\text{-}17)$$

The following transformations are further used to simplify Eq. 3-17

$$\alpha=\gamma h, \tag{3-18a}$$

$$\zeta_i=2x_i/w, \tag{3-18b}$$

and

$$\eta=w/(2h). \tag{3-18c}$$

Applying Eqs. 3-18 to 17 results in

$$\sum_{n=0}^{\infty} K_n \int_0^{\infty} J_{2n}(\eta\alpha)\cos(\alpha\eta\zeta_i)/[\alpha(1+\varepsilon_r/\tanh\alpha)]\,d\alpha=1. \tag{3-19}$$

Choosing N points for ζ_i and truncating the sum to N-1 results in an NxN matrix equation from which the charge distribution on the MIC can be found. However, for most practical values of η the only term of significant value is K_0; thus

$$K_0 \int_0^{\infty} J_0(\eta\alpha)\cos(\alpha\eta\zeta_i)/[\alpha(1+\varepsilon_r/\tanh\alpha)]\,d\alpha\simeq 1. \tag{3-20}$$

Only one ζ_i is needed in order to obtain K_0 in Eq. 3-20, so let

$$\zeta_i=0, \tag{3-21}$$

and hence

$$K_0 \int_0^{\infty} J_0(\eta\alpha)/[\alpha(1+\varepsilon_r/\tanh\alpha)]\,d\alpha\simeq 1. \tag{3-22}$$

A direct numerical integration of Eq. 3-22 leads to inaccurate results due to the oscillatory nature of $J_0(\eta\alpha)$; neither is the integral listed in available handbooks of integrals or Hankel transforms [49] and [50]. Thus, the fraction in the integrand of Eq. 3-22 is expanded as

$$1/(1+\varepsilon_r/\tanh\alpha)=[1/(\varepsilon_r+1)](1-e^{-2\alpha})\sum_{n=0}^{\infty}(-\tau)^n e^{-2n\alpha} \tag{3-23a}$$

where

$$\tau=(\varepsilon_r-1)/(\varepsilon_r+1). \tag{3-23b}$$

Substituting from Eq. 2-23a into 22 yields

$$K_o\sum_{n=0}^{\infty}(-\tau)^n\int_0^{\infty}J_o(\eta\alpha)\left[e^{-2n\alpha}-e^{-2(n+1)\alpha}\right]/\alpha\ d\alpha=(\varepsilon_r+1). \qquad (3\text{-}24)$$

Using the tabulated integrals of [49] and manipulating, Eq. 3-24 results in

$$K_o\sum_{n=0}^{\infty}(-\tau)^n\ln\left\{\left[2(n+1)+\sqrt{4(n+1)^2+\eta^2}\right]/\left(2n+\sqrt{4n^2+\eta^2}\right)\right\}=(\varepsilon_r+1). \qquad (3\text{-}25)$$

The capacitance per unit length can be readily found from Eq. 3-25. For $\varepsilon_r=1$

$$C_o=2/\left\{\varepsilon\ln\left[\left(2+\sqrt{4+\eta^2}\right)/\eta\right]\right\}, \qquad (3\text{-}26)$$

and for $\varepsilon_r\neq 1$

$$C=(\varepsilon_r+1)/\left\{\varepsilon\sum_{n=0}^{\infty}(-\tau)^n\ln\left[\left[2(n+1)+\sqrt{4(n+1)^2+\eta^2}\right]/\left(2n+\sqrt{4n^2+\eta^2}\right)\right]\right\}. \qquad (3\text{-}27)$$

Considering Eqs. 3-26 and 27, ε_e is given by

$$\varepsilon_e=\left[(\varepsilon_r+1)/2\right]\ln\left[\left(2+\sqrt{4+\eta^2}\right)/\eta\right]/$$
$$\left\{\sum_{n=0}^{\infty}(-\tau)^n\ln\left[\left[2(n+1)+\sqrt{4(n+1)^2+\eta^2}\right]/\left(2n+\sqrt{4n^2+\eta^2}\right)\right]\right\}, \qquad (3\text{-}28)$$

and the characteristic impedance is given by

$$Z=\left[120/\sqrt{2(\varepsilon_r+1)}\right]\left\{\ln\left[\left(2+\sqrt{4+\eta^2}\right)/\eta\right]\right\}^{1/2}$$
$$\left\{\sum_{n=0}^{\infty}(-\tau)^n\ln\left[\left[2(n+1)+\sqrt{4(n+1)^2+\eta^2}\right]/\left(2n+\sqrt{4n^2+\eta^2}\right)\right]\right\}^{1/2}. \qquad (3\text{-}29)$$

The results obtained by this method are compared to the results obtained in [8], as shown in Figs. 3-2 and 3.

The method is efficient and the accuracy is reasonable. As evident from Fig. 3-2 for $\varepsilon_r\leq 20$ the largest error is in the order of 5%. The accuracy reduces for $\varepsilon_r=51$ to approximately 10%, as is evident from Fig. 3-2. For practical values of η , the results obtained by Eqs. 3-28 and 29 are acceptable. For increased accuracy, more terms in the Taylor series expansion of Eq. 3-14 can be included; this procedure will be carried out for coupled microstrip lines in the

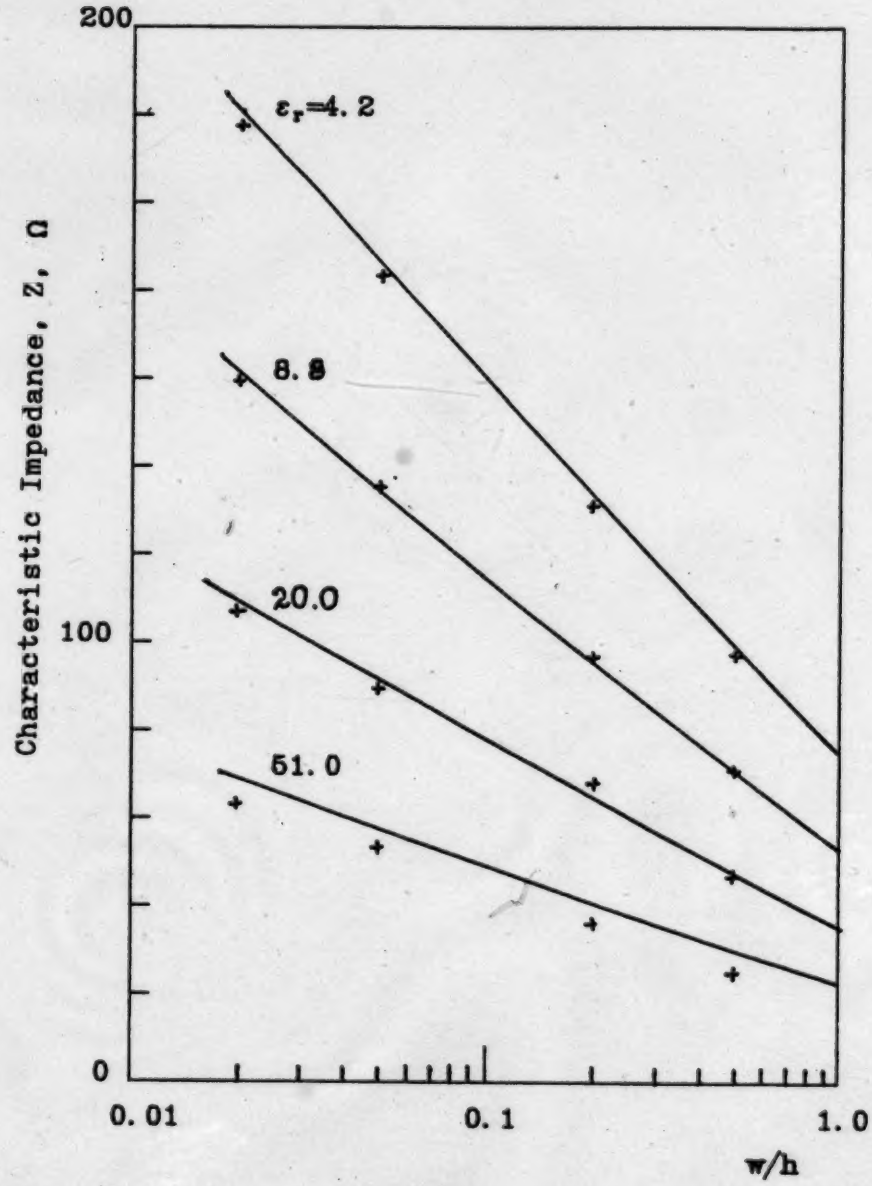

Fig. 3-2 Characteristic impedance of a microstrip line vs. w/h. Solid curves: [8], +: present method

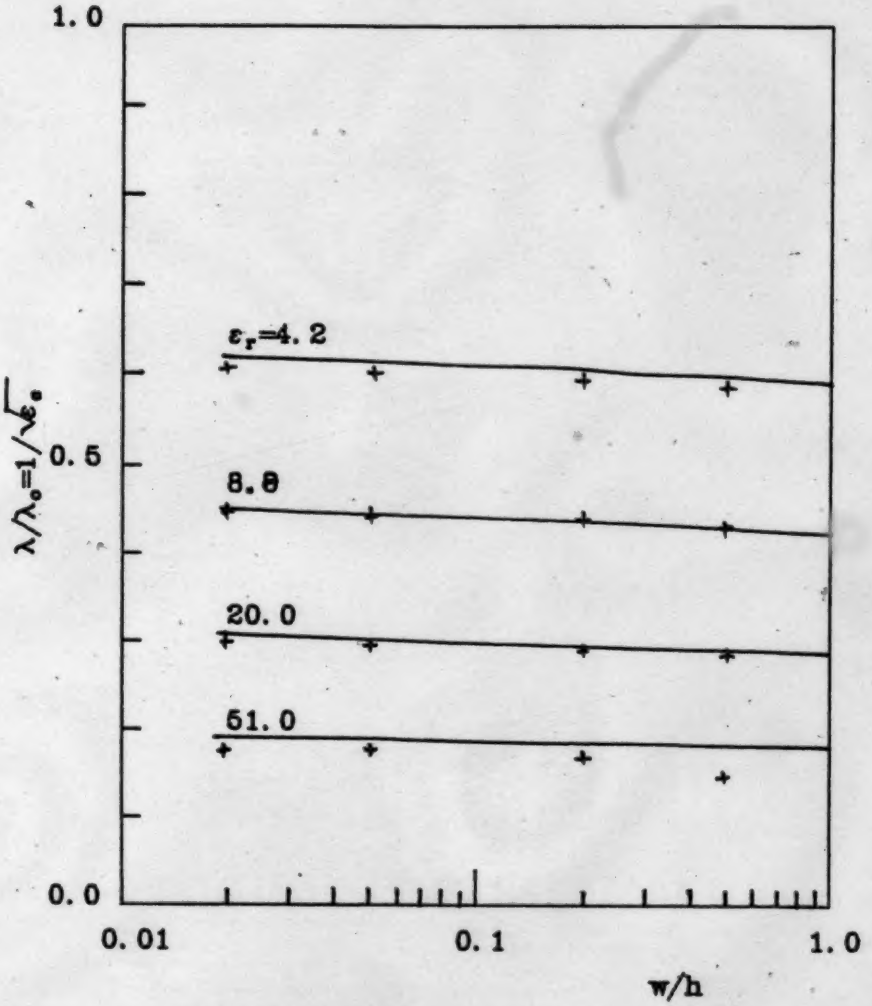

Fig. 3-3 Normalized wavelength of a microstrip line vs. w/h. Solid curves: [8], +: present method.

following sections. For the sake of comparison, note that experimental results obtained by Pucel, et. al. [51] indicate 5 to 10% error for the value of Z over 1 to 6 GHz in the widely used Wheeler's formulae [1].

D. Coupled Microstrip Lines

For coupled microstrip lines, Eq. 3-12 and 13 should be modified so that the domain of integration includes both strips in the coupled lines. Considering Fig. 2-10a let

$$s'=s+(w/2) \tag{3-30a}$$

$$\eta=w/(2h), \tag{3-30b}$$

and

$$\sigma=s'/h. \tag{3-30c}$$

Eq. 3-12 can in general be written as

$$\int_0^\infty I(\gamma)/\{\gamma[1+\varepsilon_r/\tanh(\gamma h)]\}\,d\gamma=\pi/2, \tag{3-31a}$$

where I is different for the even and odd modes. The details are explained for the even modes. The results for the odd modes are then summarized.

For the even modes,

$$I=I_x\cos(\gamma x_i), \tag{3-31b}$$

where

$$I_x=(1/\varepsilon)\int_{s'-w/2}^{s'+w/2}\rho_x(s'+x)\cos(\gamma x)\,dx + (1/\varepsilon)\int_{s'-w/2}^{s'+w/2}\rho_x(s'-x)\cos(\gamma x)\,dx, \tag{3-31c}$$

and $\rho_x(x)$ is the even-mode charge distribution. The charge distribution can be expressed as

$$\rho_x(s'-x)/\varepsilon=\chi(s'-x)/\sqrt{1-[2(s'-x)/w]^2}. \tag{3-32}$$

Substituting ρ_x from Eq. 3-32 into 31c and introducing the

change of variable

$$\sin\theta = 2(s'-x)/w \tag{3-33}$$

to remove the singularities at $x=s'\pm w/2$ results in

$$I_x = 2(w/2)\int_{-\pi/2}^{\pi/2} \chi_x(0.5w\sin\theta)\cos[\gamma(s'-0.5w\sin\theta)]\,d\theta, \tag{3-34}$$

The slowly varying function χ_x can be expanded in powers of $(s'-x)$ as follows

$$\begin{aligned}(w/2)\chi(s'-x) &= \bar{K}_0+\bar{K}_1(s'-x)+\bar{K}_2(s'-x)^2+\cdots \\ &= K_0+K_1\sin\theta+K_2\cos 2\theta+K_3\sin 3\theta+\cdots.\end{aligned} \tag{3-35}$$

Substituting from Eq. 3-35 into 34 and utilizing the tabulated integrals of [49] results in

$$\begin{aligned}I_x = {} & 2\pi\cos(\gamma s')\sum_0^{\infty} K_{2n}J_{2n}(0.5\gamma w) \\ & +2\pi\sin(\gamma s')\sum_0^{\infty} K_{2n+1}J_{2n+1}(0.5\gamma w).\end{aligned} \tag{3-36}$$

Substituting from Eqs. 3-23 and 36 into 31a, and introducing the change of variable

$$\gamma h = \alpha,$$

results in

$$\begin{aligned}(\varepsilon_r+1)/2 = {} & \sum_{n=0}^{\infty}\sum_0^{\infty}(-\tau)^n \\ & \{K_{2n}\,\mathrm{Re}\int_0^{\infty}[e^{-2n\alpha}-e^{-2(n+1)\alpha}]/\alpha\}\cdot \\ & \{\pm\exp[-j(\xi_1+\sigma)\alpha]+\exp[-j(\xi_1-\sigma)\alpha]\}J_{2n}(\eta\alpha)\,d\alpha \\ & +K_{2n+1}^{*}\,\mathrm{Im}\int_0^{\infty}[e^{-2n\alpha}-e^{-2(n+1)\alpha}]/\alpha\} \\ & \{\exp[-j(\xi_1+\sigma)\alpha]-\exp[\pm j(\xi_1-\sigma)\alpha]\}J_{2n+1}(\eta\alpha)\,d\alpha\}\end{aligned} \tag{3-37}$$

where the plus signs hold for the even modes and the negative signs for the odd modes. The integral which is essential for solving Eq. 3-37 is

$$W_\nu(n,\zeta) = \int_0^{\infty} J_\nu(\eta\alpha)\exp[-(2n+j\zeta)\alpha]\,d\alpha.$$

The integral can be found in [49] and [50]. For $n\neq 0$ and $\nu\neq 0$

the result is

$$W_\nu(n,\zeta) = \exp[-j\nu\Phi(n,\zeta)]/\{\nu[R(n,\zeta)]^\eta\}. \qquad (3\text{-}38a)$$

R and Φ are defined as follows; let

$$P(n,\zeta) = (2n+j\zeta) + \sqrt{(2n+j\zeta)^2+\eta^2}, \qquad (3\text{-}38b)$$

then $P(n,\zeta)$ can be written in polar form as

$$P(n,\zeta) = \eta R(n,\zeta)\exp[j\Phi(n,\zeta)]. \qquad (3\text{-}38c)$$

Thus, $\eta \cdot R(n,\zeta)$ is the modulus of P, and Φ is the phase of P. Similar expressions can be obtained for the special cases where n=0 or ν=0. Eq. 3-37 thus yields a matrix equation in the terms of unknown K_ν. From K_ν the charge distribution and thus the parameters of the coupled lines can be evaluated.

E. Numerical Results

The results obtained by this method for coupled microstrip lines are presented in Fig. 3-4 and are compared with the results obtained in [4]. As in the case of single lines, the results are more accurate for small values of w/h (less than unity). The charge distribution on the two strips are perturbed less for larger values of s/h than in the case of single lines. Therefore, the results are more accurate for larger values of s/h. A complete error analysis is presented below.

There are two infinite sums which are truncated in the numerical solution, namely,

1. the infinite sum of Eq. 3-24 is truncated to N_m terms, and

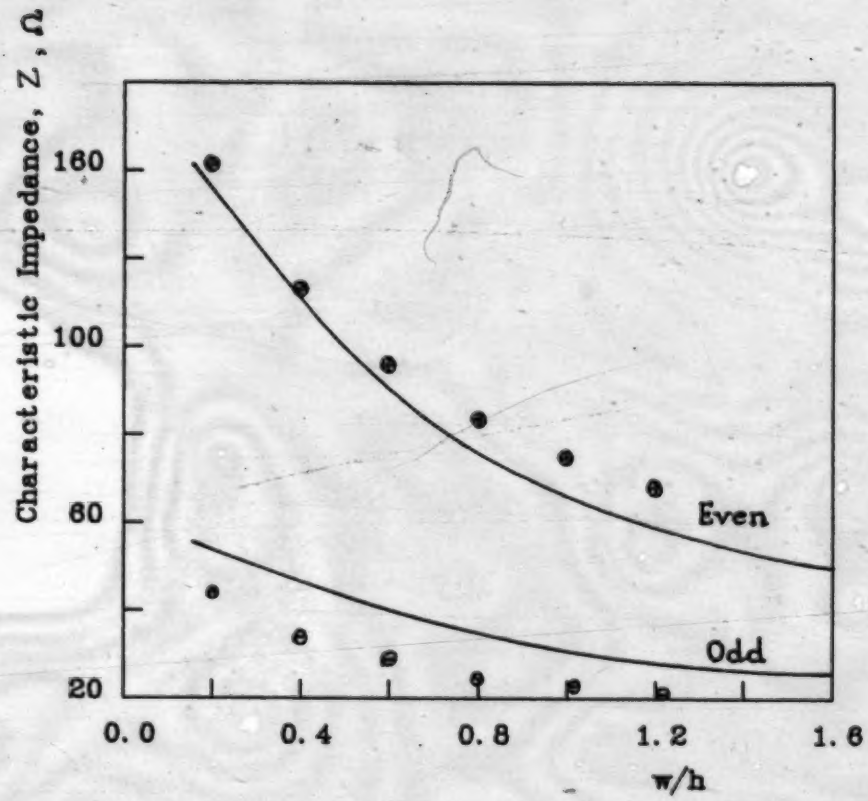

Fig. 3-4 Even- and odd-mode characteristic impedance vs. w/h for s/h=0.2; coupled microstrip lines with ϵ_r=9.0; Solid curves: [4],

●: present method, even mode,

⊖: present method, odd mode.

2. the infinite sum of Eq. 3-35 is truncated to L_m terms; L_m is the final matrix size.

The effect of each truncation is considered separately.

The Effect of N_m

To assess the effect of N_m on the numerical results, L_m is assigned the fixed value of 5, and N_m is increased until the values of the calculated parameters are no longer influenced by N_m. The results of one typical analysis are presented in Fig. 3-5 below. A value of N_m=50 is seen to be sufficiently large to produce negligible truncation error; in fact, such a value is large enough for all cases of interest.

The Effect of L_m

To assess the effect of L_m on the numerical results, N_m is assigned the fixed value of 50, and L_m is varied. The percentage error in each case can be obtained and plotted versus L_m. A typical result is shown in Fig. 3-6. Unfortunately, as L_m increases, some of the intermediate numbers become excessively large, causing an overflow in the computer (specifically R^{ν} in Eq. 3-38a). Thus, a further increase in the final matrix size is not useful. However, for values of η less than unity this overflow does not occur.

An example of typical values of the different parameters in this error analysis is as follows: For w/h=1.5 and s/h=0.3, N_m=30 and L_m=9 (the final matrix size) will result in 5% error for the values of the characteristic impedance. The results will be more accurate for smaller values of w/h and larger values of s/h. In general, the

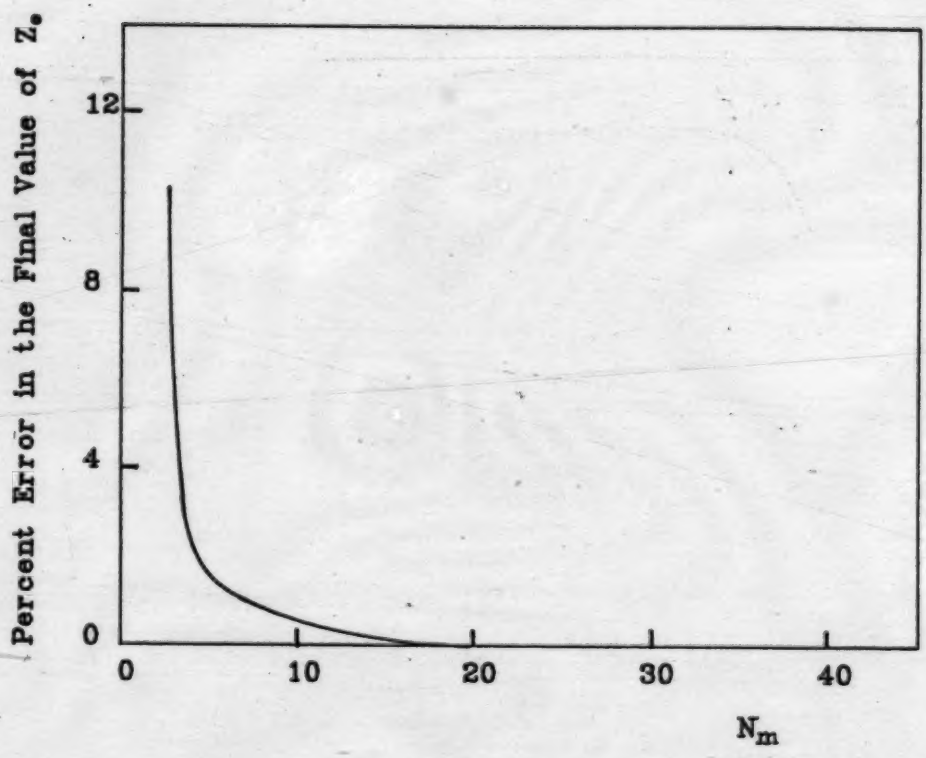

Fig. 3-5 Percent error in final value of Z_e vs. N_m; (N_m is the number of terms to which the sum of Eq. 3-24 is truncated).

w/h=1.5, s/h=0.3, ϵ_r=9.0, and L_m=5 (L_m is the final matrix size).

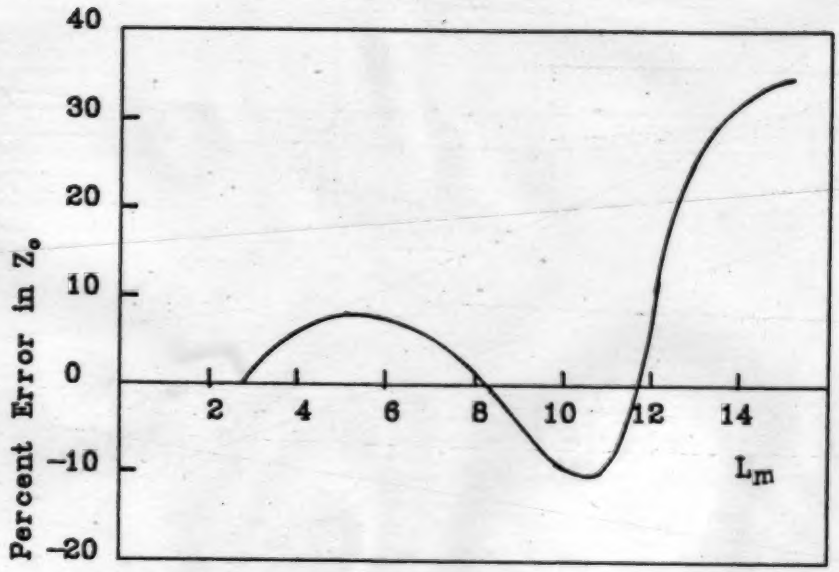

Fig. 3-6 Percent error in Z_o vs. L_m; (L_m is the final matrix size).

$w/h=1.5$, $s/h=1.0$, $\epsilon_r=9.0$ and $N_m=40$. (N_m is the number of terms to which the sum of Eq. 3-24 is truncated).

recommended value for L_m is 9 to obtain results with reasonable accuracy. The method developed in this chapter is quite efficient and the computer time and memory space required is minimal, since the resulting matrix sizes are small (of the order of 8x8). For the sake of comparison, the final matrix size obtained by the mode matching method is 40x40 as explained in Chap. 1, [3].

F. Summary

In this chapter, an integral equation method was developed in order to obtain the potential distribution, φ, at the cross section of microstrip lines in the quasi-TEM regime. Green's second identity was considered

$$\int_S (\varphi\nabla_t^2\psi - \psi\nabla_t^2\varphi)\,dS = \int_C [\varphi(\partial\psi/\partial n) - \psi(\partial\varphi/\partial n)]\,dC; \qquad (2\text{-}3)$$

where φ satisfied Laplace's equation. Unlike Green's functions, we also required that

$$\nabla_t^2\psi = 0. \qquad (3\text{-}5)$$

This reduced the left hand side of Eq. 2-3 to zero. By properly choosing the boundary conditions on ψ it was possible to reduce the right hand side of Eq. 2-3 to

$$\int_{-\infty}^{\infty}\int_{m\in C}[\rho(x)/\varepsilon]\cos(\gamma x)\cos(\gamma x_i)/\{\gamma[1+\varepsilon_r/\tanh(\gamma h)]\}\,dx\,d\gamma = \pi/2. \qquad (3\text{-}10)$$

The singularity in the charge distribution was included in Eq. 3-10;

$$\rho(x) = \varepsilon\bar{\chi}(x)/\sqrt{1-(2x/w)^2}. \qquad (3\text{-}11)$$

$\rho(x)$ was in turn expanded in terms of a Taylor series with unknown coefficients. Thus, the integral on the left hand side of Eq. 3-10 could be evaluated. For microstrip lines, the following expressions were obtained for ε_e and Z.

$$\varepsilon_e = [(\varepsilon_r+1)/2]\ln[(2+\sqrt{4+\eta^2})/\eta] / \{\sum_{n=0}^{\infty}(-\tau)^n \ln[[2(n+1)+\sqrt{4(n+1)^2+\eta^2}]/(2n+\sqrt{4n^2+\eta^2})]\}. \quad (3\text{-}28)$$

$$Z = [120/\sqrt{2(\varepsilon_r+1)}]\{\ln[(2+\sqrt{4+\eta^2})/\eta]\}^{1/2} \{\sum_{n=0}^{\infty}(-\tau)^n \ln[[2(n+1)+\sqrt{4(n+1)^2+\eta^2}]/(2n+\sqrt{4n^2+\eta^2})]\}^{1/2}. \quad (3\text{-}29)$$

where

$$\tau = (\varepsilon_r-1)/(\varepsilon_r+1). \quad (3\text{-}23b)$$

The numerical results obtained using the above expressions were shown in Figs. 3-3 and 4 and were compared to the results of Ref. [8]. The accuracy was better than 5% for $\varepsilon_r \leq 20$ and $w/h \leq 1$.

For coupled lines, the method led to a matrix equation from which Z and ε_e could be obtained. The results obtained by this method were presented in Fig. 3-4 and were compared to the results of Ref. [4].

G. Conclusions

The method developed in this chapter makes the use of Green's functions more flexible. Green's functions are obtained by placing a point charge in the geometry of interest. The final solution is then obtained by the superposition principle. In the method developed in this chapter no point charge is needed in obtaining a fundamental solution by which the actual solution can be obtained. The boundary conditions on the fundamental solution can be arbitrarily chosen to simplify the final integral equation. The inaccuracy in the obtained results is caused by the approximations which are introduced in solving the obtained integral equations (specifically, truncating the infinite sums of Eqs. 3-24 and 35). Chap. 3 can be viewed as a

building block for the wave analysis of microstrips. The theory developed for solving Laplace's equation is applied to Helmholtz's equation in the following chapters.

IV. WAVE ANALYSIS OF MICROSTRIP LINES

A. Introduction

The wave analysis of microstrip lines is presented in this chapter. The theory developed in Chap. 3 is applied to Helmholtz's equation for the wave analysis of microstrip lines. Furthermore, rather than using the two customary potential functions $\psi^{(e)}$ and $\psi^{(h)}$ which were introduced in Chap. 1, this chapter uses one function only; it is shown that the boundary conditions for E_y are separable from the other components of $\vec{E}$ and $\vec{H}$. The choice of E_y as the unknown function greatly reduces the numerical effort of analyzing a microstrip line.

B. Formulation

The boundaries and the interfaces of microstrips are along or perpendicular to the coordinate axes. Therefore, the boundary conditions for the electric field, $\vec{E}$, and the magnetic field, $\vec{H}$, are greatly simplified. On the conductors

$$E_{tan}=0, \tag{4-1a}$$

$$H_{nor}=0, \tag{4-1b}$$

$$\partial E_{nor}/\partial n=0, \tag{4-1c}$$

$$\partial H_{tan}/\partial n=0, \tag{4-1d}$$

where the subscript "tan" denotes the tangential component, and "nor" denotes the normal component.

The continuity of the normal component of the displacement vector at the DAI implies that

$$\varepsilon_r(E_y|_{y=b^-})=(E_y|_{y=b^+}). \tag{4-2a}$$

On the MIC

$$\varepsilon_r(E_y|_{y=h^-}) - (E_y|_{y=h^+}) = \rho/\varepsilon_0 \qquad (4\text{-}2b)$$

In the absence of charge

$$\nabla \cdot \vec{E} = 0, \qquad (4\text{-}3)$$

Thus,

$$(\partial E_y/\partial y|_{y=h^-}) = -[\partial E_x/\partial x + \partial E_z/\partial z]_{y=h^-}. \qquad (4\text{-}4a)$$

$$(\partial E_y/\partial y|_{y=h^+}) = -[\partial E_x/\partial x + \partial E_z/\partial z]_{y=h^+}. \qquad (4\text{-}4b)$$

Subtracting Eq. 4-4b from 4a results in

$$(\partial E_y/\partial y|_{y=h^-}) - (\partial E_y/\partial y|_{y=h^+}) =$$

$$(\partial/\partial x)[(E_x|_{y=h^+}) - (E_x|_{y=h^-})] + (\partial/\partial z)[(E_z|_{y=h^+}) - (E_z|_{y=h^-})]. \qquad (4\text{-}5)$$

E_x and E_z are continuous across the DAI, so Eq. 4-5 leads to

$$(\partial E_y/\partial y|_{y=h^-}) = (\partial E_y/\partial y|_{y=h^+}) \quad \text{on the DAI.} \qquad (4\text{-}6)$$

According to Eq. 4-1c

$$(\partial E_y/\partial y|_{y=h^-}) = (\partial E_y/\partial y|_{y=h^+}) = 0 \quad \text{on the MIC.} \qquad (4\text{-}7)$$

Eqs. 4-2, 6, and 7 indicate that the boundary conditions for E_y are separable from the other components of $\vec{E}$ and $\vec{H}$. Similarly, it can be proven that

$$(H_y|_{y=h^-}) = (H_y|_{y=h^+}) \quad \text{on the DAI,} \qquad (4\text{-}8a)$$

$$(H_y|_{y=h^-}) = (H_y|_{y=h^+}) = 0 \quad \text{on the MIC,} \qquad (4\text{-}8b)$$

$$(\partial H_y/\partial y|_{y=h^-}) = (\partial H_y/\partial y|_{y=h^+}) \quad \text{on the DAI.} \qquad (4\text{-}8c)$$

Eqs. 4-2, 6, 7, and 8 do not prove that pure LSE or LSM (Longitudinal Section Magnetic) modes can exist in microstrips. Rather, they indicate that microstrips can be analyzed by considering E_y and H_y separately. For the determination of the fields, both E_y and H_y should be found. However, the quantities of interest, such as ε_e of microstrip lines or the resonant frequencies of resonators can be found

from either E_y or H_y and the boundary conditions. The above conclusions are based on the assumptions that the dielectric and the conductors are lossless, and that a microstrip line is infinitely thin.

For the case of microstrip lines, the variation of the fields along the z-axis is as $\exp(-j\beta z)$. Thus, E_y should satisfy

$$\nabla_t^2 E_y + (\kappa k^2 - \beta^2) E_y = 0. \tag{4-9}$$

In the following sections, the theory developed in Chap. 3 is applied to solving Eq. 4-9.

C. An Integral Equation Formulation

Green's second identity can be rearranged as

$$\int_S \{\psi[\nabla_t^2\varphi + (\kappa k^2 - \beta^2)\varphi] - \varphi[\nabla_t^2\psi + (\kappa k^2 - \beta^2)\psi]\}\, dS =$$
$$\int_C [\psi(\partial\varphi/\partial n) - \varphi(\partial\psi/\partial n)]\, dC. \tag{4-10}$$

where S is the area enclosed by the curve C. Let

$$\varphi = E_y, \tag{4-11}$$

and let ψ be an auxiliary function such that

$$\nabla_t^2\psi + (\kappa k^2 - \beta^2)\psi = 0. \tag{4-12}$$

The boundary conditions for ψ will be described below.

Considering Eqs. 4-9, 11, and 12, Eq. 4-10 reduces to

$$\int_C [\psi(\partial\varphi/\partial n) - \varphi(\partial\psi/\partial n)]\, dC = 0. \tag{4-13}$$

The line is assumed to be shielded by a metallic plane at y=h+d (Fig. 4-1). In the x-direction, the line is assumed to extend to infinity.

Eq. 4-13 applied to S_1 and S_2 in Fig. 4-1 results in

$$\int_{C_1 \cup C_2} [\psi(\partial\varphi/\partial n) - \varphi(\partial\psi/\partial n)]\, dC = 0, \tag{4-14a}$$

$$\int_{C_3 \cup C_4} [\psi(\partial\varphi/\partial n) - \varphi(\partial\psi/\partial n)]\, dC = 0. \tag{4-14b}$$

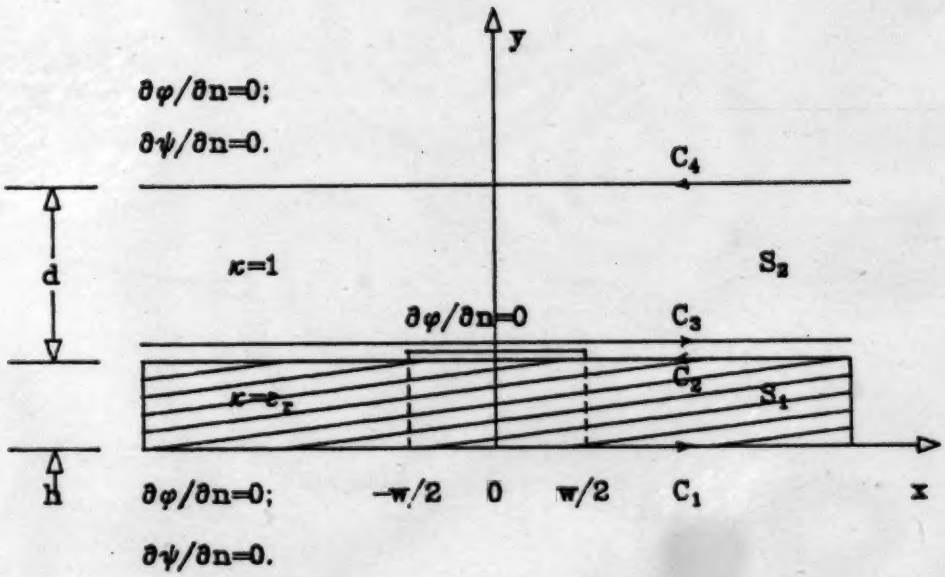

Fig. 4-1 A single microstrip line shielded on top by a metallic plane.

where it is assumed that φ and $\partial\varphi/\partial n$ tend to zero for large x. To simplify the present problem, the boundary conditions on ψ are defined as follows:

$$\partial\psi/\partial n=0 \text{ at } y=0 \text{ and } y=h+d, \tag{4-15a}$$

and

$$(\partial\psi/\partial y|_{y=h^-})=\varepsilon_r(\partial\psi/\partial y|_{y=h^+}). \tag{4-15b}$$

Imposing the boundary conditions of Eqs. 4-15 on 14 and manipulating yields

$$\int_{DAI}[(\psi|_{y=h^-})-(\psi|_{y=h^+})](\partial\varphi/\partial y|_{y=h})\,dx=(1/\varepsilon)\int_{MEC}\rho(x)(\partial\psi/\partial y|_{y=h^+})\,dx. \tag{4-16}$$

It is necessary to find ψ such that Eqs. 4-12 and 15 are satisfied. Thus let

$$\psi=\begin{cases}\varepsilon_r\cos(\alpha x)\cosh(\gamma' y)/[\gamma'\sinh(\gamma' h)]; & 0\le y<h,\\ \cos(\alpha x)\cosh[\gamma(y-h-d)]/[\gamma\sinh(\gamma d)]; & h<y\le h+d.\end{cases} \tag{4-17a}$$

where

$$\varepsilon_r k^2-\beta^2+\gamma'^2-\alpha^2=0, \tag{4-17b}$$

and

$$k^2-\beta^2+\gamma^2-\alpha^2=0. \tag{4-17c}$$

Substituting ψ from Eq. 4-17a into 16 results in

$$\int_{DAI}\bar{G}(\alpha)\cos(\alpha x)(\partial\varphi/\partial y|_{y=h})\,dx=(1/\varepsilon)\int_{MEC}\rho(x)\cos(\alpha x)\,dx, \tag{4-18a}$$

where

$$\bar{G}(\alpha)=\{\varepsilon_r/[\gamma'\tanh(\gamma' h)]\}+\{1/[\gamma\tanh(\gamma d)]\} \tag{4-18b}$$

Multiplying both sides of Eq. 4-18a by $\cos(\alpha x_i)$ and integrating over α from zero to infinity results in

$$\int_{DAI}\bar{\bar{K}}(x, x_i)(\partial\varphi/\partial y|_{y=h})\,dx=0, \tag{4-19a}$$

where x_i is assumed to lie on the MIC and

$$\bar{K}(x,x_i)=2\pi\int_{-\infty}^{\infty}\bar{G}(\alpha)\,[\exp(j\alpha|x+x_i|)+\exp(j\alpha|x-x_i|)]\,d\alpha \qquad (4\text{-}19b)$$

Let

$$\bar{K}(x')=2\pi\int_{-\infty}^{\infty}\bar{G}(\alpha)\exp(j\alpha|x'|)\,d\alpha, \qquad (4\text{-}20a)$$

then

$$\bar{K}(x,x_i)=\bar{K}(x+x_i)+\bar{K}(x-x_i). \qquad (4\text{-}20b)$$

For a single microstrip line, Eq. 4-19a can be written as

$$\int_{w/2}^{\infty}\bar{a}(x-w/2)\,[\bar{K}(x+x_i)+\bar{K}(x-x_i)]\,dx=0, \qquad (4\text{-}21a)$$

where

$$\bar{a}(x-w/2)=(\partial\varphi/\partial y|_{y=0}). \qquad (4\text{-}21b)$$

The following changes of variables simplify the above equations.

$$\nu=\alpha h, \qquad (4\text{-}22a)$$

$$\xi=x/h, \qquad (4\text{-}22b)$$

$$\eta=w/(2h), \qquad (4\text{-}22c)$$

$$K(\xi)=\bar{K}(h\xi), \qquad (4\text{-}22d)$$

$$a(\xi)=\bar{a}(h\xi), \qquad (4\text{-}22e)$$

$$G(\nu)=\bar{G}(\nu/h)/h, \qquad (4\text{-}22f)$$

$$\delta=d/h. \qquad (4\text{-}22g)$$

Considering Eqs. 4-22, Eq. 4-21a can be written as

$$\int_{0}^{\infty}a(\xi)\,[K(\xi+\xi_i+2\eta)+K(\xi-\xi_i)]\,d\xi=0; \quad \xi_i>\eta. \qquad (4\text{-}23a)$$

where (Eq. 4-20a)

$$K(\xi)=(2\pi)\int_{-\infty}^{\infty}G(\nu)\ \exp(j\nu|\xi|)\,d\nu. \qquad (4\text{-}23b)$$

and (Eqs. 4-17 and 18b)

$$G(\nu)=\{\varepsilon_r/[\sqrt{\nu^2-C^2}\,\tanh(\sqrt{\nu^2-C^2})]\}+1/[\sqrt{\nu^2+B^2}\,\tanh(\delta\sqrt{\nu^2+B^2})]. \qquad (4\text{-}23c)$$

with

$$B^2=(\varepsilon_r-1)(hk)^2, \qquad (4\text{-}23d)$$

and

$$C^2=(\varepsilon_r-\varepsilon_e)(hk)^2. \tag{4-23e}$$

D. Evaluation of the Kernel $K(\xi)$

$K(\xi)$ of Eq. 4-23b can be evaluated by complex integration. Assume that ν is a complex variable, and integrate $G(\nu)\exp(j\nu|\xi|)$ along the infinite semicircular path, Γ, shown in Fig. 4-2; it can be shown that the integrand vanishes over γ_1 ; therefore

$$K(\xi)=2\pi\int_{\Gamma}G(\nu)\ \exp(j\nu|\xi|)\,d\nu=$$

$$-j[(\Sigma 0.5\ \text{Res. of poles on the real axis})+(\Sigma\text{Res. of poles inside }\Gamma)]. \tag{4-24}$$

The poles of $G(\nu)$ are located at (Eq. 4-23c)

$$\rho_0^+=C, \tag{4-25a}$$

$$\rho_0^-=-C, \tag{4-25b}$$

$$j\rho_n=j\sqrt{(n\pi)^2-C^2};\quad n=1, 2, 3, \cdots, \tag{4-25c}$$

$$j\sigma_n=j\sqrt{(n\pi/\delta)^2+B^2};\quad n=0, 1, 2, \cdots. \tag{4-25d}$$

Eq. 4-24 leads to

$$K(\xi)=\{\varepsilon_r[\sin(C|\xi|)]/(2C)\}$$

$$-\{\varepsilon_r\sum_{n=1}^{\infty}[\exp(-\rho_n|\xi|)]/\rho_n\}-\{\sum_{n=0}^{\infty}[\exp(-\sigma_n|\xi|)]/(\delta\sigma_n)\}. \tag{4-26}$$

The kernel of Eq. 4-26 is not sufficient for solving the integral equation. This is evident by considering the limiting case k=0, which implies (Eq. 4-23e) that

$$C|_{k=0}=\sqrt{\varepsilon_r-\varepsilon_e}(hk)|_{k=0}=0. \tag{4-27}$$

For the quasi-TEM mode in a microstrip line, ε_e remains finite for k=0. Thus, from Eq. 4-23d

$$B|_{k=0}=\sqrt{\varepsilon_e-1}(hk)|_{k=0}=0. \tag{4-28}$$

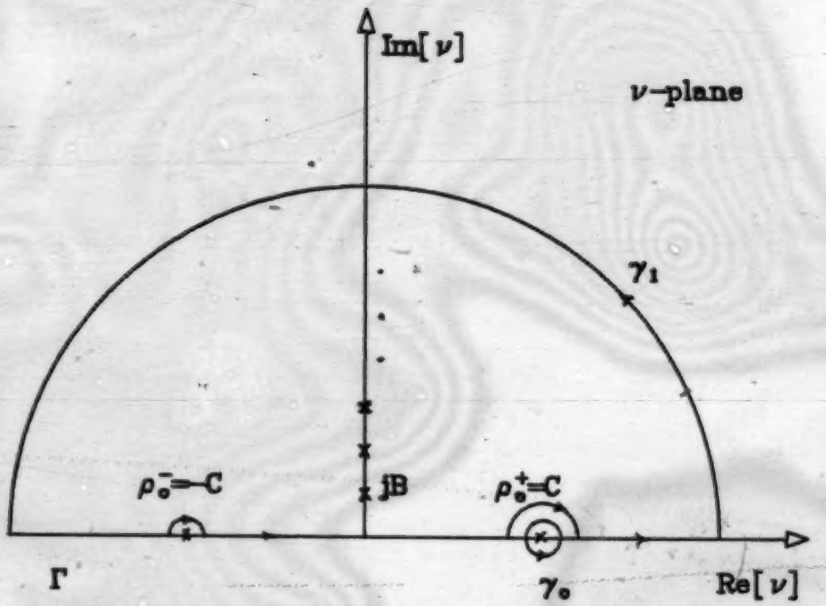

Fig. 4-2 Contour for the complex integration of Eq. 4-23b; γ_0' is used to find a complementary kernel.

Since (from Eq. 4-25d)

$$\sigma_e \to B \to 0 \text{ as } k \to 0,$$

the first term in the second summation of Eq. 4-26 tends to infinity and $K(\xi)$ becomes independent of C. It is therefore necessary to find a complementary kernel which is dependent on C for small C.

Both sides of Eq. 4-18 can be multiplied by $\cos(\nu\xi_i)$ and integrated along the small circle around $\nu=C$, namely γ_0 in Fig. 4-2. ν and ξ are defined in Eqs. 4-22. Thus, Eq. 4-18a becomes

$$\int_\eta^\infty \left[\oint_{\gamma_0} G(\nu)\cos(\nu\xi)\cos(\nu\xi_i)\,d\nu\right] a(\xi-\eta)\,d\xi$$

$$= (1/\varepsilon)\int_{\text{arc}} \rho(h\xi)\left[\oint_{\gamma_0}\cos(\nu\xi)\cos(\nu\xi_i)\,d\nu\right] d\xi$$

$$= 0; \quad \text{regardless of } \xi_i. \tag{4-29}$$

The right hand side of Eq. 4-29 is identically zero since none of the functions in the integrand have a pole at $\nu=C$. Considering Eq. 4-23c $G(\nu)$ has a pole at $\nu=C$, therefore the left hand side of Eq. 4-29 leads to

$$\int_0^\infty \cos[C(\xi+\eta)]\cdot a(\xi)\,d\xi = 0. \tag{4-30}$$

For the quasi-TEM mode, Eqs. 4-23a, 27, 28, and 30, prove that ε_e should remain finite at zero frequency. Consider Eqs. 4-23d and 23e. As k tends to zero, both B and C tend to zero. The kernels of Eqs. 4-23a and 30 both become constant for B=C=0; in this limiting case, Eq. 4-23a tends to

$$\int_0^\infty a(\xi)\,d\xi = 0,$$

and Eq. 4-30 tends to

$$\int_0^\infty a(\xi)\,d\xi = 0.$$

Thus, regardless of the method used to solve Eqs. 4-23a and

30, B=C=0 is a solution. This verifies that ε_e remains finite as the frequency tends to zero (from Eqs. 4-23d and 23e).

E. Numerical Solution

In order to solve the above equations numerically, $f(\xi)$ is defined with respect to $a(\xi)$ of Eq. 4-22e;

$$a(\xi)=\exp(-\xi L)f(\xi). \tag{4-31}$$

where L is an arbitrary number. This definition is based on the fact that the fields decay rapidly away from the MIC edges. L can be varied arbitrarily to obtain the most accurate numerical results; the obtained numerical results are nearly independent of L. Then Eq. 4-30 can be approximated by

$$\sum_{j=1}^{M} f_j \int_{\xi_{1j}}^{\xi_{uj}} \exp(-\xi L)\cos[C(\xi+\eta)]\,d\xi=0, \tag{4-32a}$$

where M determines the final matrix size, and

$$f_j=f(\xi_j). \tag{4-32b}$$

Eq. 4-23a can similarly be approximated by

$$\sum_{j=1}^{M} f_j \int_{\xi_{1j}}^{\xi_{uj}} [K(\xi+\xi_i+2\eta)+K(\xi-\xi_i)]\exp(-\xi L)\,d\xi=0. \tag{4-32c}$$

The relationship between W_j, ξ_{1j}, ξ_{uj}, and ξ_j is shown in Fig. 4-3; the ξ axis is divided into segments of width W_j about the point ξ_j, ranging from the lower edge ξ_{1j} to the upper edge ξ_{uj}. W_j and ξ_j are the parameters for the quadrature integration [48]. This choice of parameters reduces the integration errors.

The following definitions will simplify the procedure for evaluating the integrals of Eqs. 4-32a and 32c.

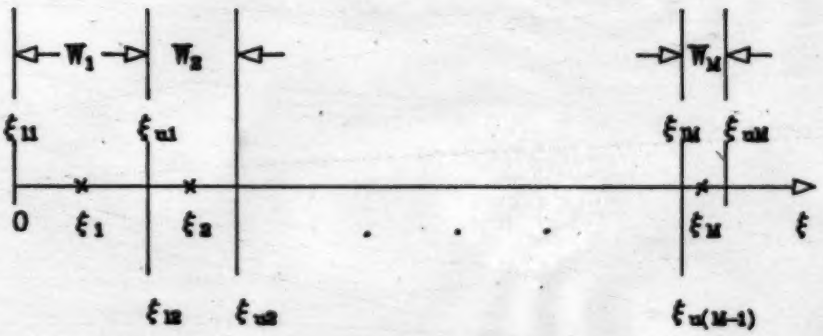

Fig. 4-3 ξ -axis divided into various segments for the numerical integration of Eqs. 4-23a and 30.

$$G_{1,ij}=[1/(2C)]\int_{\xi_{ij}}^{\xi_{ij}} \sin[C(\xi+\xi_i+2\eta)]\exp(-\xi L)\,d\xi, \qquad (4\text{-}33a)$$

$$G_{2,ij}=[1/(2c)]\int_{\xi_{ij}}^{\xi_{ij}} \sin[C|\xi-\xi_i|]\exp(-\xi L)\,d\xi, \qquad (4\text{-}33b)$$

$$G_{3m,ij}=(1/\rho_m)\int_{\xi_{ij}}^{\xi_{ij}} \exp[(\xi+\xi_i+2\eta)]\exp(-\xi L)\,d\xi, \qquad (4\text{-}33c)$$

$$G_{4m,ij}=(1/\rho_m)\int_{\xi_{ij}}^{\xi_{ij}} \exp[-\rho_m|\xi-\xi_i|]\exp(-\xi L)\,d\xi, \qquad (4\text{-}33d)$$

$$G_{5,j}=\int_{\xi_{ij}}^{\xi_{ij}} \cos[C(\xi+\eta)]\exp(-\xi L)\,d\xi, \qquad (4\text{-}33e)$$

$$G_{6m,ij}=(B/\sigma_m)\int_{\xi_{ij}}^{\xi_{ij}} \exp[-\sigma_m(\xi+\xi_i+2\eta)]\exp(-\xi L)\,d\xi, \qquad (4\text{-}33f)$$

$$G_{7m,ij}=(B/\sigma_m)\int_{\xi_{ij}}^{\xi_{ij}} \exp[-\sigma_m|\xi-\xi_i|]\exp(-\xi L)\,d\xi, \qquad (4\text{-}33g)$$

The integrals of Eqs. 4-33 can be easily evaluated. Considering Eqs. 4-33 we can now rewrite Eq. 4-32a as

$$\sum_{j=1}^{N} f_j G_{5,j}=0 \qquad (4\text{-}34a)$$

and Eq. 4-32c can be expressed as

$$\sum_{j=1}^{N} f_{ji}\{\varepsilon_r\delta B[G_{1,ij}+G_{2,ij}-\sum_{m=1}^{M}(G_{3m,ij}+G_{4m,ij})]-\sum_{m=0}^{M}(G_{6m,ij}+G_{7m,ij})\}=0. \qquad (4\text{-}34b)$$

In matrix form Eqs. 4-34 can be represented as

$$[G]\{f\}=0. \qquad (4\text{-}34)$$

where the first row of $[G]$ is $G_{5,j}$ of Eq. 4-33e. The matrix $[G]$ is a function of B and C of Eqs. 4-23d and 23e, which are both directly proportional to hk or hf; this signifies the fact that, for microstrip lines, the normalized frequency fh can be used (i.e., the dispersion relation can be plotted vs. fh rather than f). In a similar fashion, the strip width can be normalized to w/h as in the quasi-TEM regime.

The numerical results obtained by this method for different representative cases are shown in Figs. 4-4 and 5 and are compared to the results of [15], [23] and [52]. The results obtained by this method are in good agreement with other methods for high frequencies. For low frequencies, ε_e converges smoothly to the zero frequency limit of the

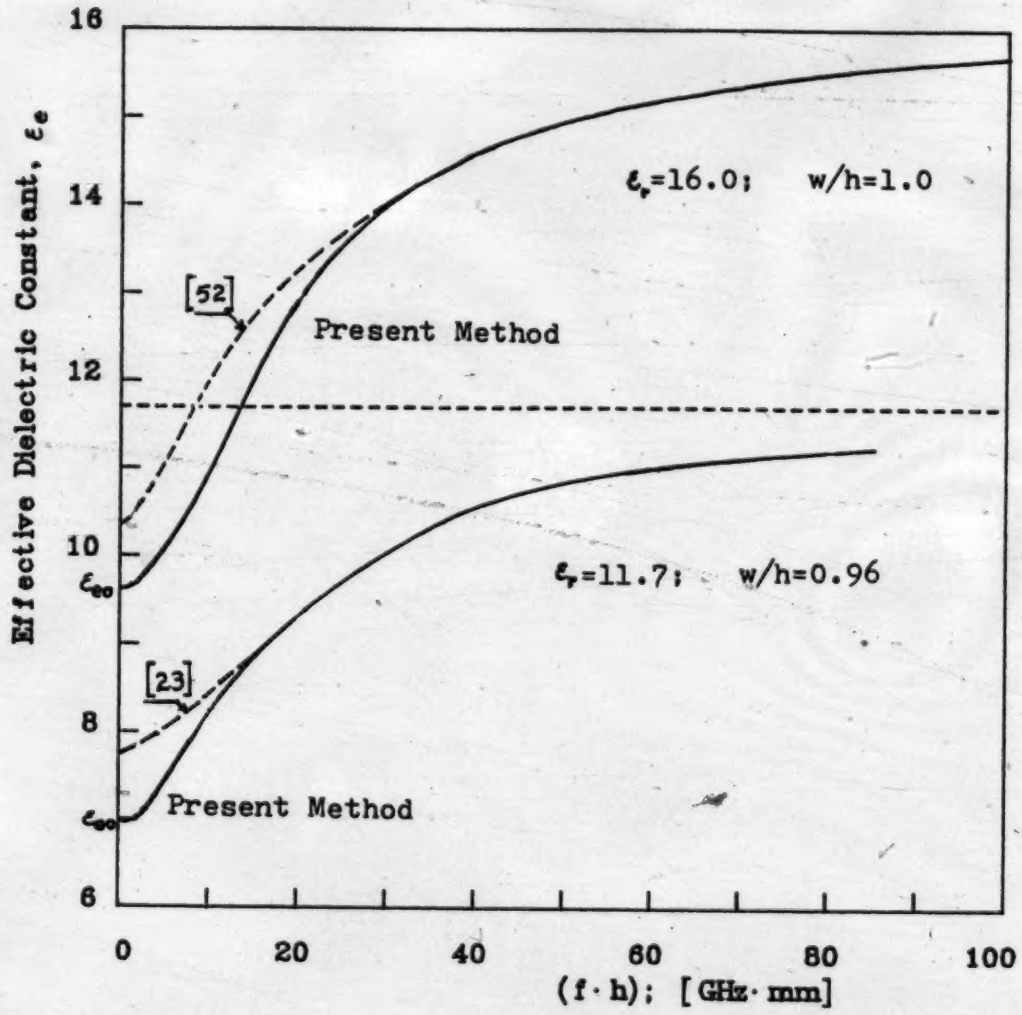

Fig. 4-4 ε_e of a single microstrip line vs. normalized frequency;
ε_{oo} is obtained from quasi-TEM methods ([8] and the method of Chap. 2).
As the frequency tends to zero, the results obtained by the present method smoothly converge to ε_{eo}.

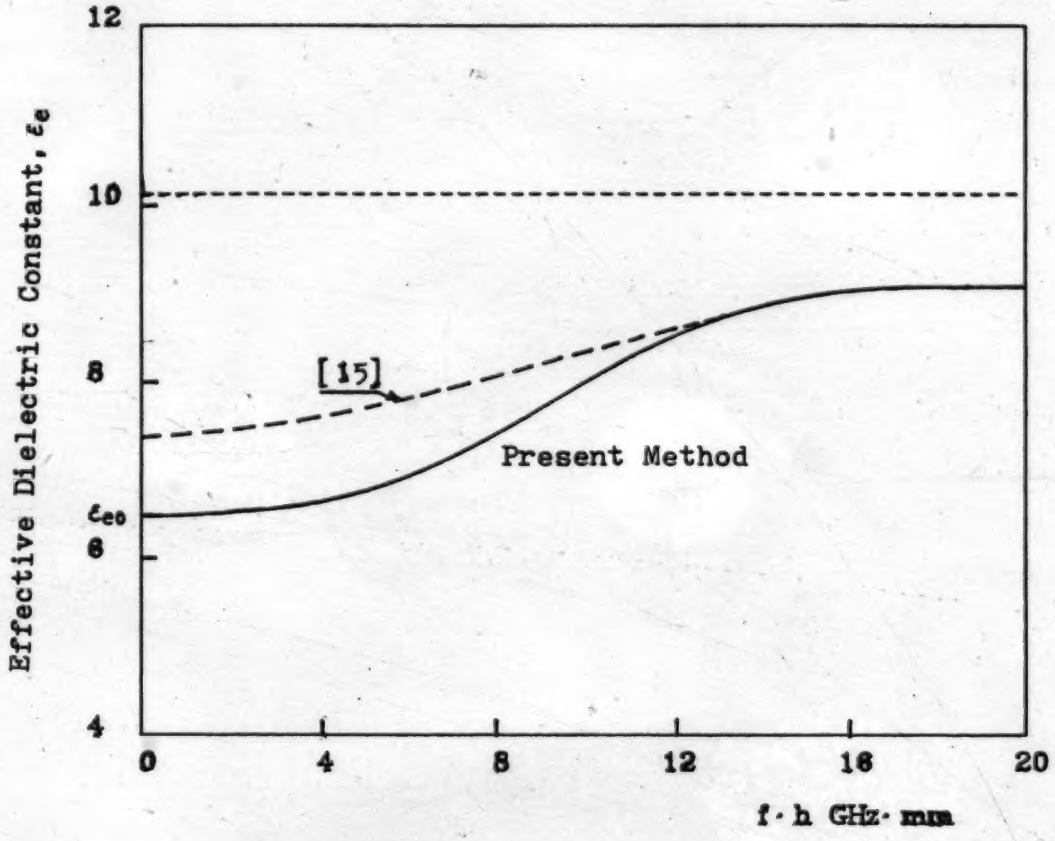

Fig. 4-5 ε_e of a single microstrip line vs. normalized frequency; ε_r=10.1 and w/h=2.5; ε_{eo} is obtained from quasi-TEM methods ([8] and the method of Chap. 2). As the frequency tends to zero, the results obtained by the present method smoothly converge to ε_{eo}.

effective dielectric constant, ϵ_{eo} , obtained by the quasi-TEM methods. The results of [15], [23] and [52] do not converge to ϵ_{eo} at zero frequency.

Considering the numerical efficiency of the present method the size of the final eigenvalue matrix used was 14x14 and fifty terms were needed in Eq. 4-26. The final matrix size in the TLM method [22] is 270x270, in the finite difference method [19] it is 100x100, and for the finite element method 21 it is 126x126. The computer programs are presented in App. C. The results of Figs. 4-4 and 5 have been obtained by finding the values of ϵ_e at which the determinant of $[G]$ in Eq. 4-34 vanishes.

F. Summary

In this chapter, it was shown that, for microstrips, the boundary conditions for E_y could be separated from the other components of $\vec{E}$ and $\vec{H}$. E_y satisfied Helmholtz's equation

$$\nabla_t^2 E_y + (\kappa k^2 - \beta^2) E_y = 0. \qquad (4-9)$$

with the boundary conditions

$$\epsilon_r (E_y|_{y=h^-}) = (E_y|_{y=h^+}). \qquad (4-2a)$$

on the DAI, and

$$\epsilon_r (E_y|_{y=h^-}) - (E_y|_{y=h^+}) = \rho/\epsilon \qquad (4-2b)$$

on the MIC. Moreover,

$$(\partial E_y/\partial y|_{y=h^-}) = (\partial E_y/\partial y|_{y=h^+}) \quad \text{on the DAI.} \qquad (4-6)$$

and

$$(\partial E_y/\partial y|_{y=h^-}) = (\partial E_y/\partial y|_{y=h^+}) = 0 \text{ on the MIC.} \qquad (4-7)$$

Green's second identity was rearranged as

$$\int_S \{\psi[\nabla_t^2\varphi+(\kappa k^2-\beta^2)\varphi]-\varphi[\nabla_t^2\psi+(\kappa k^2-\beta^2)\psi]\}\,dS=$$
$$(\int_C[\psi(\partial\varphi/\partial n)-\varphi(\partial\psi/\partial n)]\,dC. \qquad (4\text{-}10)$$

where

$$\varphi=E_y. \qquad (4\text{-}11)$$

The method developed in Chap. 3 was applied to this case; it was assumed that

$$\nabla_t^2\psi+(\kappa k^2-\beta^2)\psi=0. \qquad (4\text{-}12)$$

Considering Eqs. 4-9, 10 and 12, the left hand side of Eq. 4-10 could be set equal to zero. By properly choosing the boundary conditions on ψ, Eq. 4-10 resulted in

$$\int_{DAI}\bar{G}(\alpha)\cos(\alpha x)(\partial\varphi/\partial y|_{y=h})\,dx=(1/\varepsilon)\int_{MC}\rho(x)\cos(\alpha x)\,dx; \qquad (4\text{-}18a)$$

$$\bar{G}(\alpha)=\varepsilon_r/[\gamma'\tanh(\gamma' h)]+1/[\gamma\tanh(\gamma d)]; \qquad (4\text{-}18b)$$

where

$$\varepsilon_r k^2-\beta^2+\gamma'^2-\alpha^2=0; \qquad (4\text{-}17a)$$

$$k^2-\beta^2+\gamma^2-\alpha^2=0. \qquad (4\text{-}17b)$$

Eq. 4-18a multiplied by $\cos(\alpha\cdot x_i)$ and integrated over α in the complex α-domain resulted in

$$\int_0^\infty a(\xi)\cos[C(\xi+\eta)]\,d\xi=0. \qquad (4\text{-}30)$$

and

$$\int_0^\infty a(\xi)[K(\xi+\xi_1+2\eta)+K(\xi-\xi_1)]\,d\xi=0. \qquad (4\text{-}23a)$$

where $a(\xi)$ was defined by $\partial\varphi(x,y)/\partial y$ on the DAI, where

$$\xi=x/h, \qquad (4\text{-}22b)$$

and the kernel was given by

$$K(\xi)=\varepsilon_r\sin(C|\xi|)/(2C)$$
$$-\varepsilon_r\sum_{n=1}^{\infty}\exp(-\rho_n|\xi|)/\rho_n-\sum_{n=0}^{\infty}\exp(-\sigma_n|\xi|)/(\delta\sigma_n). \qquad (4\text{-}26)$$

with

$$B=\sqrt{\varepsilon_r-1}(hk), \tag{4-23d}$$

$$C=\sqrt{\varepsilon_r-\varepsilon_e}(hk). \tag{4-23e}$$

$$\rho_n=\sqrt{(n\pi)^2-C^2}, \quad n=1, 2, 3, \cdots, \tag{4-25c}$$

$$\sigma_n=\sqrt{(n\pi/\delta)^2+B^2}, \quad n=0, 1, 2, \cdots. \tag{4-25d}$$

Eqs. 4-23a and 30 yielded an eigenvalue matrix equation when discretized. The numerical results obtained by this method were presented in Figs. 4-4 and 5 and were compared to the results of [15], [23] and [52].

G. Conclusions

It has been shown that the wave analysis of microstrips can be performed using only E_y. In contrast to the customary two potential functions $\psi^{(e)}$ and $\psi^{(h)}$, the use of only one function greatly reduces the effort for analyzing microstrips. In order to solve Helmholtz's equation for E_y, the theory developed in Chap. 3 was used. The results obtained for microstrip lines show good agreement with other methods (Figs. 4-4 and 5). As the frequency tends to zero, the results converge smoothly to the values obtained by quasi-TEM methods. The method is economical (final matrix size of 14x14). However, it is not readily apparent how this method can be generalized to microstrip resonators. Therefore, in Chap. 5 the method of this chapter is modified so that it can be generalized more easily to microstrip resonators.

V. AN ALTERNATIVE INTEGRAL EQUATION METHOD FOR THE WAVE ANALYSIS OF MICROSTRIPS

A. Introduction

It seems difficult to generalize the integral equation method of Chap. 4 to microstrip resonators of arbitrary shapes. Considering Eq. 4-19a, the domain of integration of this integral equation is the DAI. The resulting matrix equations would be smaller if an integral equation could be found whose domain of integration is the MIC alone. The generalization of such an integral equation to microstrip resonators would then be simpler. The development and solution of an integral equation for microstrip lines with only the MIC as the domain of integration is discussed in this chapter. This solution is then generalized to a rectangular resonator, resonating in the even mode.

B. Formulation

Eq. 4-18b can be inverted to result in

$$1/\bar{G}(\alpha) = \gamma \cdot \sinh(\gamma d)\,\gamma' \cdot \sinh(\gamma' h) / [\varepsilon_r \gamma \cdot \sinh(\gamma d)\cosh(\gamma' h) + \gamma' \cdot \sinh(\gamma' h)\cosh(\gamma d)], \quad (5\text{-}1a)$$

where

$$\gamma^2 = \alpha^2 + \beta^2 - k^2, \quad (5\text{-}1b)$$

$$\gamma'^2 = \alpha^2 + \beta^2 - \varepsilon_r k^2, \quad (5\text{-}1c)$$

Multiplying Eq. 4-18a by Eq. 5-1a results in

$$\int_{DAI} \cos(\alpha x)\,(\partial\varphi/\partial y|_{y=h})\,dx = (1/\varepsilon)\int_{MIC} [\cos(\alpha x)/\bar{G}(\alpha)]\,\rho(x)\,dx. \quad (5\text{-}2)$$

where $\varphi = E_y$. Eq. 5-2 cannot be integrated over α from zero to infinity, since

$$1/\bar{G}(\alpha) \sim \alpha \text{ for large } \alpha.$$

However, both sides of Eq. 5-2 can be multiplied by

$$\cos(\alpha x_i) \cdot \sin^2(\alpha d_i'/2)/\alpha^2,$$

and integrated over α from 0 to ∞.

Thus, the left hand side of Eq. 5-2 results in

$$\int_{DAI} f(x)(\partial\varphi/\partial y|_{y=h})\,dx \tag{5-3a}$$

where

$$f(x) = \int_0^\infty \cos(\alpha x)\cos(\alpha x_i)\sin^2(\alpha d'/2)/\alpha^2 d\alpha \tag{5-3b}$$

f(x) of Eq. 5-3b is nonzero only on the regions

$$x_i - d_i' < x < x_i + d_i', \text{ and}$$
$$-(x_i + d_i') < x < -(x_i - d_i'),$$

shown in Fig. 5-1. Thus, f(x)=0 on the DAI if

$$|x_i \pm d_i'| \leq w/2 \quad \forall\ i. \tag{5-4a}$$

With the condition of inequality 5-4a, the integrand of Eq. 5-3a is identically zero. Thus, the right hand side of Eq. 5-2 results in

$$\int_{MC} K(x, x_i)\rho(x)\,dx = 0; \tag{5-4b}$$

where

$$K(x, x_i) = \int_0^\infty [\sin^2(\alpha d'/2)/\alpha^2]\cos(\alpha x_i)\cos(\alpha x)/\bar{G}(\alpha)\,d\alpha; \tag{5-4c}$$

The integral which is needed for evaluating $K(x, x_i)$ of Eq. 5-3b is

$$K_i(\zeta) = \int_0^\infty \exp(j\nu\zeta)/[\nu^2 G(\nu)]\,d\nu, \tag{5-5a}$$

where

$$\nu = \alpha h; \tag{5-5b}$$

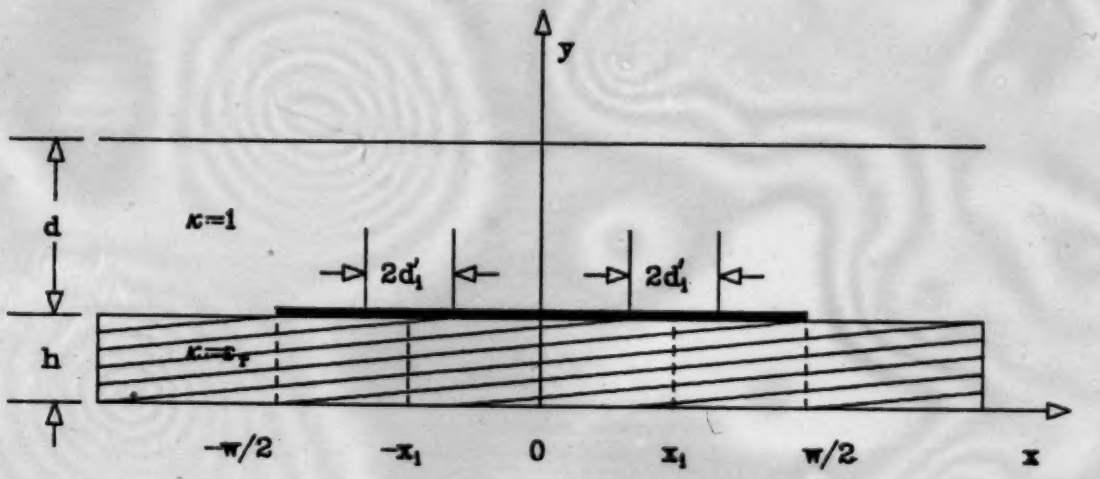

Fig. 5-1 Microstrip line shielded on top by a metallic plane; f(x) of Eq. 5-4 is nonzero on $-(x_i+d'_i)$ to $-(x_i-d'_i)$, and $(x_i-d'_i)$ to $(x_i+d'_i)$.

$$\xi = x/h; \tag{5-5c}$$

In other words,

$$K(x, x_i) = \sum_{q=1}^{6} a_q K_1(x_{qi}/h), \tag{5-5d}$$

where the coefficients a_q and x_{qi} can be found easily from Eq. 5-3b. Moreover

$$G(\nu) = \bar{G}(\nu/h)/h. \tag{5-5e}$$

$G(\nu)$ can be rewritten as

$$G(\nu) = P_2(\rho)/P_1(\rho), \tag{5-6a}$$

where, from Eq. 5-1a,

$$P_1(\rho) = -\rho \sin(\rho)\sqrt{A^2-\rho^2}\sinh(\delta\sqrt{A^2-\rho^2}); \tag{5-6b}$$

$$P_2(\rho) = \varepsilon_r\sqrt{A^2-\rho^2}\sinh(\delta\sqrt{A^2-\rho^2})\cos(\rho) - \rho\sin(\rho)\cosh(\delta\sqrt{A^2-\rho^2}) \tag{5-6c}$$

with

$$\delta = d/h, \tag{5-7a}$$

$$\rho^2 = (\gamma' h)^2 \tag{5-7b}$$

$$A^2 = (\varepsilon_r - 1)(hk)^2. \tag{5-7c}$$

$$\nu^2 = C^2 - \rho^2. \tag{5-7d}$$

$$C^2 = (\varepsilon_r - \varepsilon_e)(hk)^2, \tag{5-7e}$$

To evaluate K_1 of Eq. 5-5a, it is assumed that ν is a complex variable and the integrand of Eq. 5-5a is integrated over the contour shown in Fig. 5-2. The integral vanishes over the semicircle, C_L, when the radius of the semicircle becomes infinitely large. Then

$$K_1(\xi) = \pi j \Sigma[(\text{Res. on the real axis}) + (\text{Res. on the imaginary axis})]. \tag{5-8}$$

The real poles in Eq. 5-8 are treated differently from those in Eq. 4-24 of the previous chapter. The reason for

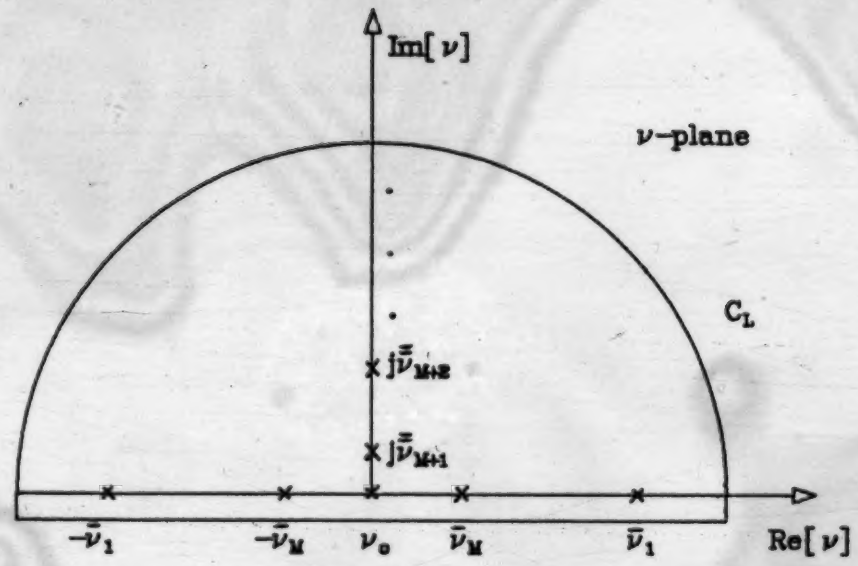

Fig. 5-2 Contour for the integral of Eq. 5-5a.

including the real poles inside the contour of integration in Fig. 5-2 is that f(x) of Eq. 5-4 is defined on the basis of step functions; in defining the step functions by Fourier transform methods the contour of integration approaches the real axis from below and includes any pole on the real axis.

It is then necessary to find the poles of the integrand in Eq. 5-5a; they can be obtained from the roots of $P_2(\rho)$ of Eq. 5-6c. It can be shown that all the roots of Eq. 5-6c are real. Let the m-th positive root of $P_2(\rho)$ be denoted by ρ_m. The poles, ν_m, can be found from ρ_m via Eq. 5-7d.

The poles of the integrand of Eq. 5-5a are located at

$$\nu_o=0, \text{ double pole; and} \tag{5-9a}$$

$$\nu_m=\sqrt{C^2-\rho_m^2}, \tag{5-9b}$$

or

$$\nu_m=\begin{cases}\pm\bar{\nu}_m=\pm\sqrt{C^2-\rho_m^2} \text{ for } \rho_m<C; \quad m=1,\cdots,M,\\ \\ \pm\bar{\nu}_m=\pm j\sqrt{\rho_m^2-C^2} \text{ for } \rho_m>C; \quad m=M+1,\cdots.\end{cases} \tag{5-9c}$$

Eq. 5-8 leads to

$$K_1(\xi)=Q_o\xi+\sum_{m=1}^{M}2\bar{Q}_m\sin(\bar{\nu}_m\xi)+\sum_{m=M+1}^{\infty}\bar{Q}_m\exp(-\bar{\nu}_m\xi). \tag{5-10a}$$

where

$$Q_o=(-\pi/2)P_1(C)/P_2(C). \tag{5-10b}$$

$$\bar{Q}_m=-\pi P_1(\rho_m)/[\bar{\nu}_m^2P_3(\rho_m)]. \tag{5-10c}$$

$$\bar{Q}_m=-\pi\bar{P}_1(\rho_m)/[\bar{\nu}_m^2P_3(\rho_m)]. \tag{5-10d}$$

and

$$P_3(\rho)=-(1/\rho)P_2'(\rho) \tag{5-10e}$$

C. Single Microstrip Lines

Due to the even symmetry of the quasi-TEM mode in microstrip lines, Eq. 5-3a can be rewritten as

$$\int_0^{w/2} \rho(x)\, K(x, x_i)\, dx = 0; \qquad 0 \le x_i \pm d_i' \le w/2. \tag{5-11}$$

where $K(x,x_i)$ is a linear combination of forms like $K_1(\xi)$. As evident from Eq. 5-10a

$$K_1(\xi) \sim \ln(\xi) \text{ for small } \xi;$$

$K(x,x_i)$ behaves logarithmically as x approaches

$$(x_i - d_i'),\ x_i,\ \text{or}\ (x_i + d_i').$$

Moreover, as discussed in the previous chapters, $\rho(x)$ is singular for $x=w/2$.

By devising a numerical method which includes both the singularities in the kernel and the charge distribution of Eq. 5-11, accurate results could be obtained. However, generalizing such a method to microstrip resonators of arbitrary shapes seems very difficult. Two approximate methods for solving Eq. 5-11 can be devised. The singularity in the charge distribution can be included in the kernel of Eq. 5-11 and the logarithmic singularities of $K(x,x_i)$ can be "avoided" by dividing the domain of integration into intervals which have

$$(x_i - d_i'),\ x_i,\ \text{or}\ (x_i + d_i')$$

as their end points.

Alternatively, the singularity in the charge distribution can be implicitly included in the integration procedure by choosing finer intervals near the singular point, $x=w/2$.

The two methods yielded very similar numerical results and the computational efficiencies were also comparable. However, for reasons of conciseness, only the former method will be explained.

As in the previous chapters, let

$$\rho(x)=\chi(x)/\sqrt{1-(2x/w)^2}. \tag{5-12}$$

Substituting Eq. 5-12, together with the change of variable

$$\sin\theta=2x/w, \tag{5-13}$$

into Eq. 5-11, results in

$$\int_0^{\pi/2}\chi(0.5w\sin\theta)\,K(0.5w\sin\theta,\,0.5w\sin\theta_i)\,d\theta=0. \tag{5-14}$$

The change of variable of Eq. 5-13 removes the singularity at x=w/2.

Eq. 5-14 can be approximated by

$$\sum_{r=1}^{R}\chi_r\int_{\theta_{lr}}^{\theta_{ur}}K(0.5w\sin\theta,\,0.5w\sin\theta_i)\,d\theta\sim 0, \tag{5-15a}$$

where

$$\chi_r=\chi(0.5w\sin\theta_r); \tag{5-15b}$$

$$\sin\theta_{lr}=2(x_r-d_r')/w; \tag{5-15c}$$

$$\sin\theta_r=2x_r/w; \tag{5-15d}$$

$$\sin\theta_{ur}=2(x_r+d_r')/w. \tag{5-15e}$$

Eqs. 5-15c, d, and e are graphically represented in Fig. 5-3.

Eq. 5-15a can be written in matrix form as

$$[H]\{\chi\}=0, \tag{5-16}$$

where [H] is a square matrix, with elements

$$H_{ir}=\int_{\theta_{lr}}^{\theta_{ur}}K(0.5w\sin\theta,\,x_i)\,d\theta, \tag{5-17}$$

and $\{\chi\}$ is a column matrix with χ_r as its elements. Substituting from Eq. 5-5d into 17 results in

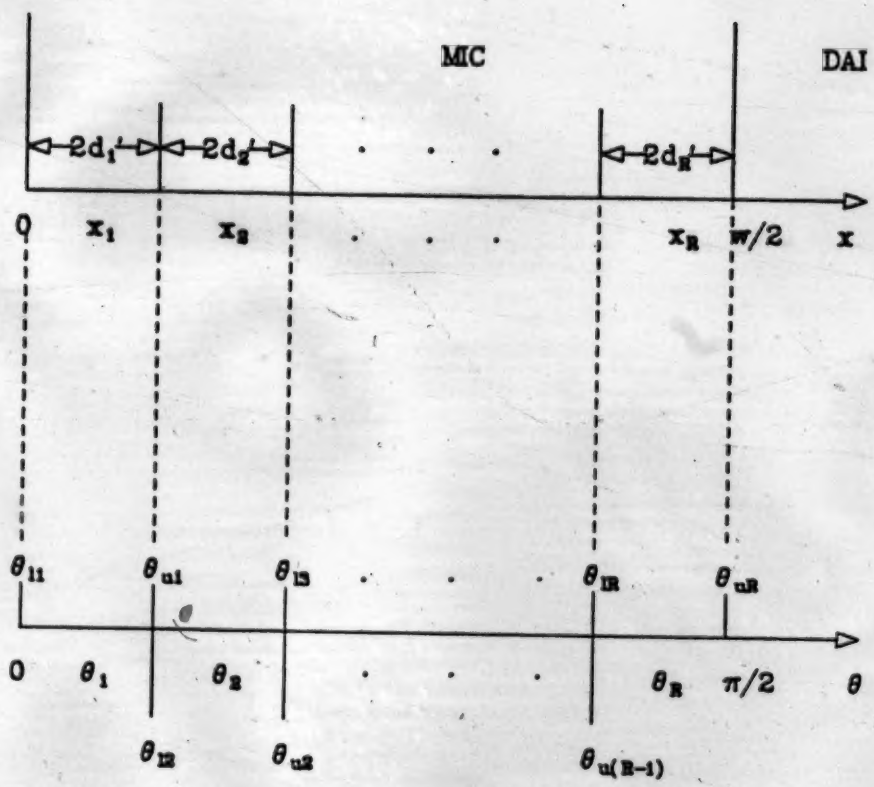

Fig. 5-3 MIC divided into several intervals for the numerical integration of Eq. 5-15.

$$H_{ir}=\sum_{q=1}^{8} a_q \int_{\theta_{ir}}^{\theta_{ir}+w} K_2(\zeta_{qi})\, d\theta \qquad (5\text{-}18)$$

From Eqs. 5-3b, 5d, and 13 x_{qi}; can be found as

$$x_{11}/(w/2)=|\sin\theta-\sin\theta_{11}|; \qquad (5\text{-}19a)$$

$$x_{21}/(w/2)=|\sin\theta-\sin\theta_{21}|; \qquad (5\text{-}19b)$$

$$x_{31}/(w/2)=|\sin\theta-\sin\theta_{31}|; \qquad (5\text{-}19c)$$

$$x_{41}/(w/2)=|\sin\theta-\sin\theta_{41}|; \qquad (5\text{-}19d)$$

$$x_{51}/(w/2)=|\sin\theta-\sin\theta_{51}|; \qquad (5\text{-}19e)$$

$$x_{61}/(w/2)=|\sin\theta-\sin\theta_{61}|; \qquad (5\text{-}19f)$$

Finally $K_1(\zeta)$ must be evaluated from Eq. 5-10a. To simplify the evaluation procedure, the following definitions are introduced.

$$f_{1,m}(s,s')=\begin{cases}\eta|s+s'| & \text{for } m=0,\\ 2\sin(\eta\bar{\nu}_m|s+s'|) & \text{for } 1\le m\le M,\\ \exp(-\eta\bar{\nu}_m|s+s'|) & \text{for } m>M;\end{cases} \qquad (5\text{-}20a)$$

$$f_{2,m}(s,s')=f_{1,m}(s,-s')+f_{1,m}(s,s'); \qquad (5\text{-}20b)$$

$$f_{3,m}(\sin\theta)=f_{2,m}(\sin\theta,\sin\theta_{11})-2f_{2,m}(\sin\theta,\sin\theta_1)+f_{2,m}(\sin\theta,\sin\theta_{61}); \qquad (5\text{-}20c)$$

Substituting from Eqs. 5-10a and 20 into 18 results in

$$H_{ir}=\sum_{m=0}^{M} Q_m\cdot\left[\int_{\theta_{ir}}^{\theta_{ir}+w} f_{2,m}(\sin\theta)\,d\theta+\int_{\theta_{ir}}^{\theta_{ir}+w} f_{3,m}(\sin\theta)\;d\theta\right]. \qquad (5\text{-}21)$$

The integration domain of Eq. 5-21 is divided into two regions to avoid the logarithmic singularity in $K_1(\zeta)$, as discussed above. The integrals of Eq. 5-21 can be carried out numerically using the Gauss quadrature formulae. The programming details are presented in App. D. The dispersion relation is obtained by the determinant search of [H] in the eigenvalue Eq. 5-16.

Having formulated the above modified method for analyzing microstrip lines, we now generalize it to microstrip resonators. The numerical results for both cases are subsequently presented.

D. Microstrip Resonators

In this section, an example is given of how the general problem of microstrip resonators can be analyzed. The case of a rectangular resonator (Fig. 5-4) with the even mode of resonance is studied since, for it, the results of the previous section can be more easily generalized. Eq. 5-3a can be generalized to

$$\int_{\text{strip}} K(x, z; x_i, z_i)\, \rho(x, z)\, dx dz = 0 \qquad (5\text{-}22)$$

where $\rho(x,z)$ is now the two-dimensional charge distribution on the MIC and

$$K(x, z; x_i, z_i) = \int_0^\infty \int_0^\infty (P_1/P_2)\,(\sin\alpha d_1'/\alpha)^2 (\sin\beta d_1''/\beta)^2 \cdot \cos(\alpha x)\cos(\alpha x_i)\cos(\beta z)\cos(\beta z_i)\, d\alpha d\beta. \qquad (5\text{-}23)$$

$P_1(\rho)$ and $P_2(\rho)$ are defined in Eqs. 5-6b and 6c. From Eqs. 5-1c and 5-7b

$$\rho^2 = D^2 - (\alpha h)^2 - (\beta h)^2, \qquad (5\text{-}24a)$$

where

$$D^2 = \epsilon_r (hk)^2, \qquad (5\text{-}24b)$$

K of Eq. 5-23 is a linear combination of terms like

$$K_2(\xi, \zeta) = \int_{-\infty}^{\infty} \int_{-\infty}^{\infty} (P_1/P_2) \exp[j(\nu\xi + \nu'\zeta)]/(\nu\nu')^2 d\nu d\nu', \qquad (5\text{-}25a)$$

where

$$\xi = x/h; \qquad (5\text{-}25b)$$

$$\zeta = z/h; \qquad (5\text{-}25c)$$

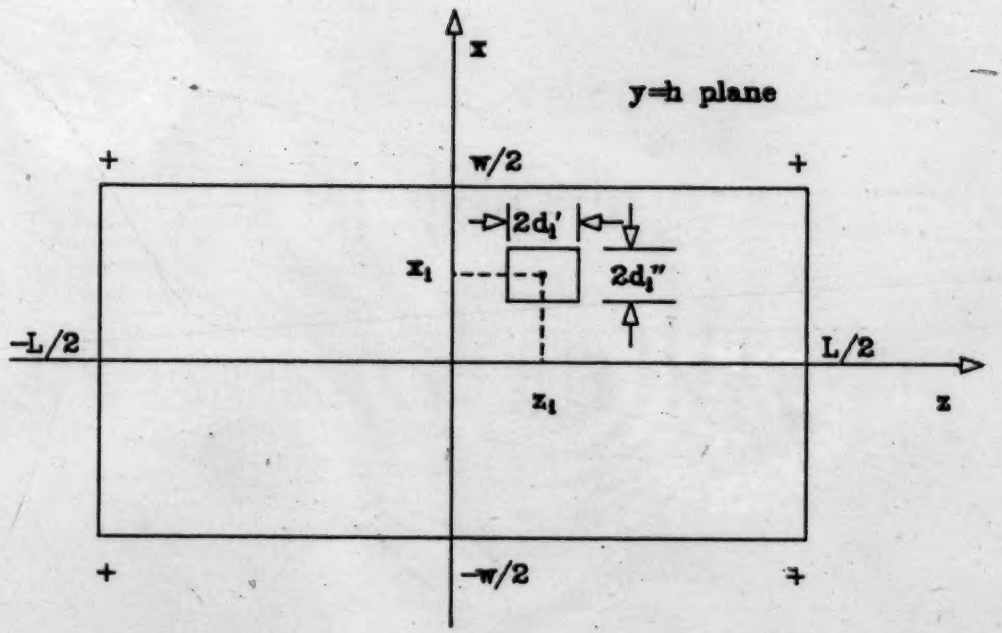

Fig. 5-4 Rectangular microstrip resonator with even mode of resonance; + indicates the charge polarity.

$$\nu=\alpha h, \tag{5-25d}$$

$$\nu'=\beta h, \tag{5-25e}$$

To integrate K_2, the following transformations are introduced

$$\nu=\sigma\cos\theta, \tag{5-26a}$$

$$\nu'=\sigma\sin\theta, \tag{5-26b}$$

Substituting from Eqs. 5-26 into 25a results in

$$K_2=\int_{-\infty}^{\infty}(P_1/P_2)(I(\theta)/\sigma^3)\,d\sigma. \tag{5-27a}$$

where

$$I(\theta')=2\int_0^{\infty}\exp(j\sigma E)/[(1-\cos\theta')(1+\cos\theta')]\cdot d\theta', \tag{5-27b}$$

with

$$\theta'=2\theta, \tag{5-27c}$$

and

$$E=\xi\cos(\theta'/2)+\zeta\sin(\theta'/2). \tag{5-27d}$$

Eq. 5-27b can be evaluated by complex integration methods. Let

$$\bar{Z}=\exp(j\theta'), \tag{5-28}$$

then

$$d\bar{Z}/(j\bar{Z})=d\theta', \tag{5-29}$$

and

$$I=(-8/j)\oint_C\bar{Z}\cdot\exp(j\sigma E)/[(\bar{Z}-1)(\bar{Z}+1)]^2 d\bar{Z}, \tag{5-30}$$

where C is the contour shown in Fig. 5-5. There are two double poles at

$$\bar{Z}=1 \text{ and } \bar{Z}=-1.$$

Whether these poles should be fully enclosed within C of Fig. 5-5 or not is a valid question. However, in either case, the solutions to Eq. 5-3a will be the same, since the right hand side of Eq. 5-3a is zero and multiplying both sides by a constant will not affect the solutions.

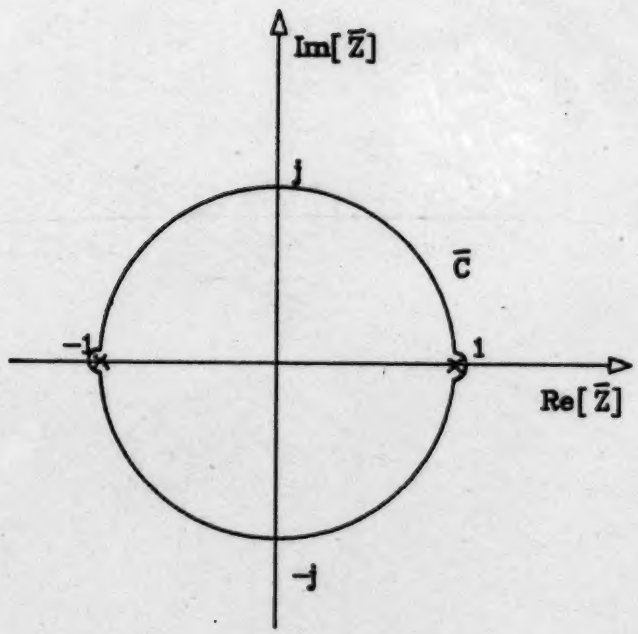

Fig. 5-5 Contour for the integration of Eq. 5-30.

To evaluate I of Eq. 5-30, the residues of the integrand at the right hand side of Eq. 5-30 should be found: Let

$$R_1=(d/d\bar{Z})[\bar{Z}\cdot\exp(j\sigma E)/(\bar{Z}+1)^2]_{\bar{Z}=-1}$$

$$=\{[\exp(j\sigma E)+j\sigma(dE/d\theta')(d\theta'/d\bar{Z})\bar{Z}\cdot\exp(j\sigma E)](\bar{Z}+1)^2$$

$$-2(\bar{Z}+1)\bar{Z}\cdot\exp(j\sigma E)\}/(\bar{Z}+1)^4|_{\bar{Z}=-1}. \qquad (5\text{-}31)$$

From Eq. 5-28

$$\theta'|_{\bar{Z}=-1}=0. \qquad (5\text{-}32)$$

Substituting from Eq. 5-32 into 27 results in

$$E|_{\bar{Z}=-1}=0.5\xi, \qquad (5\text{-}33a)$$

and

$$dE/d\theta'|_{\bar{Z}=-1}=0.5\zeta. \qquad (5\text{-}33b)$$

Substituting from Eqs. 5-33 into 31 results in

$$R_1=(1/8)\sigma\zeta\ \exp(j\sigma\xi). \qquad (5\text{-}34)$$

Similarly,

$$R_2=(d/d\bar{Z})[\bar{Z}\cdot\exp(j\sigma E)/(\bar{Z}-1)^2]_{\bar{Z}=-1}=(-1/8)\sigma\xi\ \exp(j\sigma\zeta). \qquad (5\text{-}35)$$

The addition of the two residues yields

$$I=(-8/j)(2\pi j)(R_1+R_2)$$

$$=-16\pi\sigma[\zeta\ \exp(j\sigma\xi)+\xi\ \exp(j\sigma\zeta)]. \qquad (5\text{-}36)$$

Substituting this result into Eq. 5-27a, we obtain

$$K_2=\zeta M(\xi)-\xi M(\zeta) \qquad (5\text{-}37a)$$

where

$$M(\xi)=\int_{-\infty}^{\infty}(P_1/P_2)[\exp(j\sigma\xi)/\sigma^2]\,d\sigma, \qquad (5\text{-}37b)$$

The evaluation of $M(\xi)$ is similar to the evaluation of $K_1(\zeta)$ in Eq. 5-5a, above. The results are similar to Eq. 5-10. In this way, K_2 of Eq. 5-37a is found.

The kernel of Eq. 5-23 is a linear combination of terms like K_2 of Eq. 5-37a. Having found the kernel, Eq. 5-23 can be discretized. The resulting eigenvalue matrix equation

yields the resonant frequency of the resonator. The procedure for finding and solving this matrix equation closely parallels that in the previous section. The numerical results obtained by this method are presented below.

E. Numerical Results

The numerical results obtained by this method for single microstrip lines are shown in Fig. 5-6 and are compared to results obtained in [24]. The results show good agreement with [24] for higher frequencies. This method is less accurate for lower frequencies. At f.h=20 GHz·mm, for example, the error is 10.7%.

A numerical error analysis is performed as follows. The effect of truncating the infinite sum of Eq. 5-10a to N_x terms is demonstrated in Fig. 5-7. The final matrix size, M_R, is assigned the constant value of 4. The curve shows the change in the calculated value of ε_e vs. N_x; the kernel of Eq. 5-11 converges very slowly. Fig. 5-8 shows the effect of increasing the final matrix size, M_R. N_x is assigned the fixed value of 500. It is seen that an increase in the matrix size from 4x4 to 8x8 has little effect upon the obtained results.

Unfortunately, the rate of convergence varies for different frequencies. For frequencies below the inflection point in the dispersion curve, even values of N_x=1000 provide poor results. Furthermore, the cost of running the computer programs becomes prohibitive as N_x becomes very large, even though the matrix size is as small as 4x4.

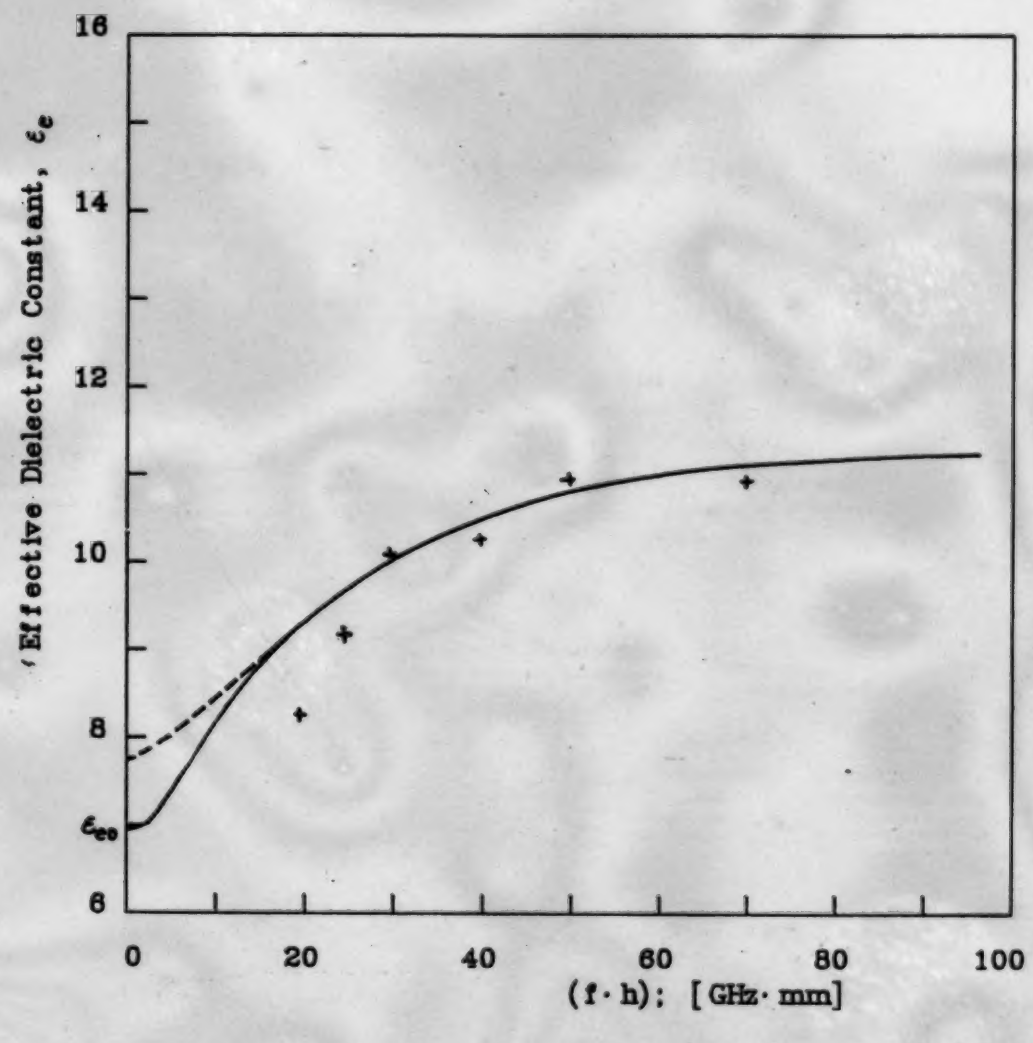

Fig. 5-6 Effective dielectric constant of a microstrip line vs. normalized frequency; ε_r=11.7 and w/h=0.96
Solid curve: method of Chap. 4,
Dashed curve: Ref. [24],
Plus signs: present method.

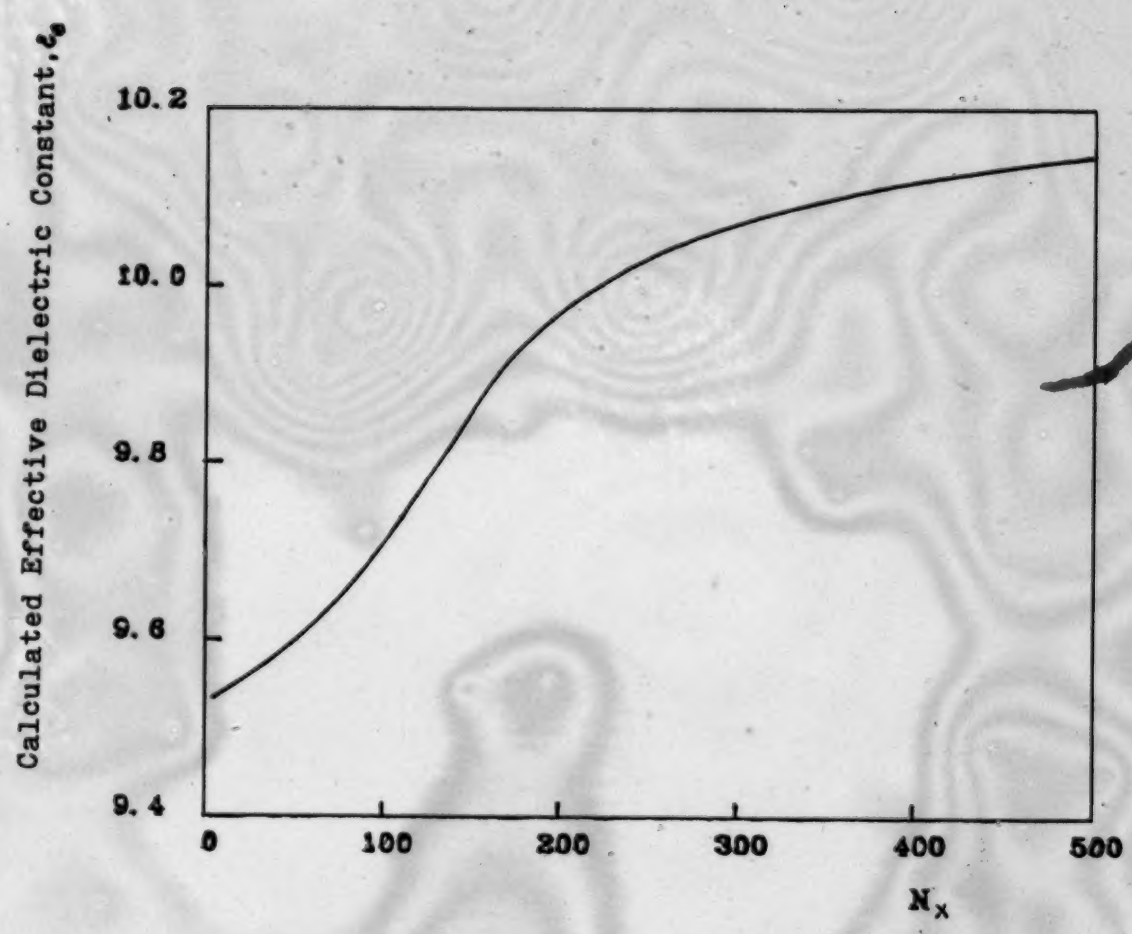

Fig. 5-7 Calculated effective dielectric constant vs. N_x (N_x is the number of terms to which Eq. 5-10a is truncated).
fh=40.0 GHz mm, w/h=0.96, ε_r=11.7 and M_R=4 (M_R is the final matrix size).
The actual value of ε_e is 10.5.

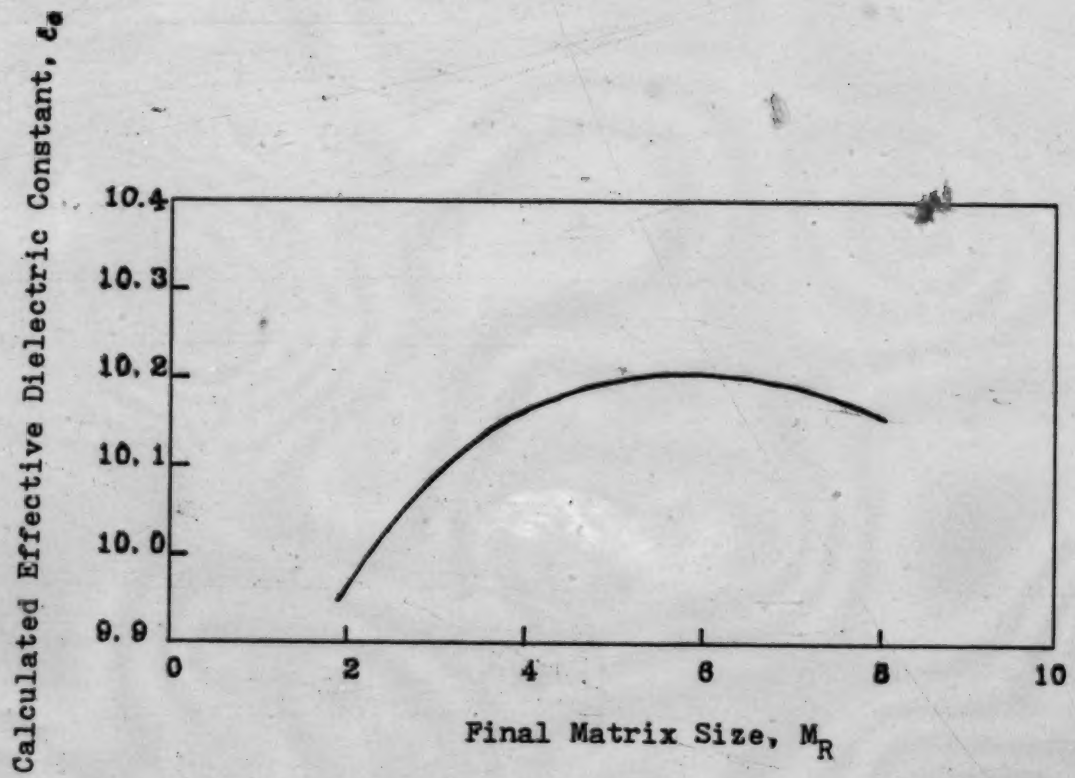

Fig. 5-8 Calculated effective dielectric constant vs. final matrix size, M_R; fh=40.0 GHz·mm, w/h=0.96, ϵ_r=11.7 and N_x=500. (N_x is the number of terms to which Eq. 5-10a is truncated).

Thus, the approximate range of usefulness of this method is the frequency range above the inflection point in the dispersion curve (Fig. 5-6). In order to obtain accurate results with this method, the dimensions of a rectangular resonator should be chosen such that the resonant frequency remains within this range. In other words, the product of the resonator's expected resonant frequency and substrate height should be above the inflection point in the corresponding dispersion curve (i.e., the dispersion curve for the line which results from extending the resonator length to infinity).

Thus, a resonator with the following specifications is analyzed (Fig. 5-4):

ε_r=11.7,

h=3.17 mm,

w/h=0.96, and

L/h=3.253.

According to the transmission line model described in Chap. 1, where dispersion in the line is included and fringing at the ends neglected, the resonant frequency should be 9.2 GHz. With the method developed in Chap. 5, the calculated resonant length for this resonant frequency is L/h=3.248. This indicates an error of 0.15% from the specification. However, the transmission line model by itself may be in error by a few percent [32] and [35].

F. Summary

In this chapter, the integral equation method of Chap. 4 was modified such that the domain of integration of the integral equation was the MIC. In this way, the method could be more easily applied to the rectangular resonator. Eq. 4-25b was rearranged as

$$\int_{\Delta M} \cos(\alpha x)\,(\partial\varphi/\partial y|_{y=h})\,dx = (1/\varepsilon)\int_{MC}[\cos(\alpha x)/\bar{G}(\alpha)]\,\rho(x)\,dx. \quad (5\text{-}2)$$

where $\varphi = E_y$ and

$$1/\bar{G}(\alpha) = \gamma\cdot\sinh(\gamma d)\,\gamma'\cdot\sinh(\gamma' h)\,/$$
$$[\varepsilon_r\gamma\cdot\sinh(\gamma d)\cosh(\gamma' h)+\gamma'\cdot\sinh(\gamma' h)\cosh(\gamma d)], \quad (5\text{-}1a)$$

with

$$\gamma^2 = \alpha^2+\beta^2-k^2, \quad (5\text{-}1b)$$

$$\gamma'^2 = \alpha^2+\beta^2-\varepsilon_r k^2, \quad (5\text{-}1c)$$

Both sides of Eq. 5-2 were multiplied by

$$\cos(\alpha x_i)\cdot\sin^2(\alpha d_i'/2)/\alpha^2,$$

and integrated over α from zero to infinity to result in

$$\int_{MC} K(x, x_i)\,\rho(x)\,dx = 0; \quad (5\text{-}3a)$$

$K(x, x_i)$ was a linear combination of forms like

$$K_1(\zeta) = \int_0^\infty \exp(j\nu\zeta)/[\nu^2 G(\nu)]\,d\nu, \quad (5\text{-}5a)$$

where

$$\nu = \alpha h; \quad (5\text{-}5b)$$

$$\zeta = x/h; \quad (5\text{-}5c)$$

$$G(\nu) = \bar{G}(\nu/h)/h. \quad (5\text{-}5d)$$

$K_1(\zeta)$ could be found by complex integration techniques.

Eq. 5-3a was further developed for the case of the rectangular resonator in the even mode of resonance.

The numerical results for microstrip lines obtained by

this method were presented in Fig. 5-6 and showed good agreement with the results of [24] at higher frequencies. The method failed to be accurate at lower frequencies. The range of usefulness of this method was for frequencies higher than the inflection point in the dispersion curve. Using this range of usefulness, the method was then applied to the rectangular resonator and a numerical example was provided, which showed good agreement with transmission line model methods.

G. Conclusions

The method developed in this chapter reduces the problem of analyzing microstrips to an integral equation with only the MIC as the domain of integration. The method for solving the final integral equation has been presented. This method gave results which are in good agreement with those of other methods for high frequencies, but is less accurate for low frequencies (e.g., the error at f·h=20 GHz. mm is 10.7% for the dispersion curve shown in Fig. 5-6).

$K_1(\zeta)$ of Eq. 5-10a converges very slowly and becomes logarithmically singular for small arguments. The numerical analysis indicates that a better accuracy can be achieved for lower frequencies if more terms are included in Eq. 5-10a. However, this causes a large increase in computational costs even when the final matrix size is as small as 4x4. For frequencies above the inflection point in the dispersion curve, the method is quite useful and can be generalized to microstrip resonators, as indicated by the example given in this chapter.

VI. CONCLUSIONS

In the previous chapters, various integral equation methods were applied to the analysis of microstrips. The BEM was applied to single and coupled microstrip lines in the quasi-TEM regime. The analysis was capable of evaluating the characteristic impedance, Z, the effective dielectric constant, ϵ_e, as well as the charge density, $\rho(x)$, and the potential distribution, φ. The inclusion of the singularity of the charge distribution in the formulation resulted in increased efficiency, increased accuracy, and reduced final matrix sizes.

However, complications were evident for generalizing the BEM to the wave analysis of microstrips, since it was difficult to obtain the "fundamental solution" (see p. 45). It was easier to obtain the results by modifying the classical integral equation solution of Chap. 2. Thus, in Chap. 3, the quasi-TEM microstrip line was analyzed by a novel method which can be considered as a generalization of Green's functions.

Green's functions are customarily defined so that they satisfy a nonhomogeneous differential equation. For example, the forcing function can be chosen to be a point charge. In Chap. 3, it was shown that instead of Green's functions, a fundamental solution could be chosen which satisfies a homogeneous differential equation. The boundary conditions on this fundamental solution could be arbitrarily chosen in such a manner that the final integral equation was simplified.

This method resulted in reasonably accurate expressions for the characteristic impedance and ϵ_e of microstrip lines.

This method was then generalized in Chap. 4 to the wave analysis of microstrip lines. The problem of analyzing microstrip lines reduced to solving an integral equation with the DAI as the domain of integration. Moreover, unlike the customary employment of two potential functions for the wave analysis of microstrip lines, it was shown that only one properly chosen function, namely E_y, was sufficient for obtaining the parameters of the microstrips. This approach reduced the effort for analyzing microstrips.

The obtained results exhibited good agreement with other methods and converged smoothly to the quasi-TEM results. Furthermore, there were two conclusions of interest regarding the wave analysis of microstrips:

1. as in the quasi-TEM regime, the dimensions of microstrips could be normalized to the substrate height, h, and
2. the frequency, f, could be normalized to f·h.

In order to generalize the formulation to resonators, an alternative integral equation method was developed in Chap. 5 with the MIC as the domain of integration. This method was more elaborate, but could be more easily generalized to microstrip resonators. The obtained results were accurate for higher frequencies but the accuracy was reduced for lower frequencies (i.e., below the inflection point in the dispersion curve).

The rectangular microstrip resonator with an even mode

of resonance was then analyzed using this method. This analysis indicated how the method could be generalized to microstrip resonators in order to provide a basis for the computer-aided design of microstrips. For the further development of the above methods, the following recommendations can be employed:

The general problem of analyzing microstrip resonators can be approached in a way similar to the analysis of the rectangular resonator. The MIC area of an arbitrarily shaped resonator can be subdivided into a mesh of rectangles; in this way, the obtained integral equations can be discretized. Due to the singularity in the charge distribution, smaller rectangles can be chosen near the MIC edges. Furthermore, the numerical errors caused by the slow convergence of the obtained functions could perhaps be reduced by expressing these functions in terms of more rapidly convergent functions (e.g., a logarithmic function added to a Taylor series).

The methods developed in this thesis can also be used for analyzing coplanar microwave integrated circuits (i.e. circuits in which the dielectric substrate is metalized on one side only). Another possible field of application can be the analysis of the higher order modes in microstrips.

This thesis can therefore be viewed as a stepping stone toward the eventual analysis of arbitrarily shaped resonators. In addition, the methods proposed for the analysis of microstrip lines and coupled lines can be applied directly to engineering designs.

REFERENCES

1. Wheeler, H.A., "Transmission-line properties of parallel strips separated by a dielectric sheet". IEEE Trans Microwave Theory Tech. Vol. 13, pp. 172-185 (1965)
2. Mittra, R. and Itoh, T., "Analysis of microstrip transmission lines." Advances in Microwaves, Vol. 8, pp. 67-141, Academic Press (1974)
3. Judd, S.V., Whitely, I., Clowed, R.J., and Richard, D.C. "An analytical method for calculating microstrip transmission line parameters." IEEE Trans Microwave Theory Tech. Vol. 18, pp. 78-87 (1970)
4. Weiss, J.A., "Microwave propagation on coupled pairs of microstrip transmission lines." Advances in Microwaves, Vol. 8, pp. 295-319, Academic Press (1974)
5. Eaves, R.E., and Bolle, D.M., "Guided waves in limit cases of microstrips." IEEE Trans Microwave Theory Tech. Vol. 18, pp. 231-232 (1970)
6. Green, H.E., "The numerical solution of some important transmission-line problems." IEEE Trans Microwave Theory Tech. Vol. 13, pp. 676-692 (1965)
7. Wexler, A., "Computation of electromagnetic fields." IEEE Trans Microwave Theory Tech. Vol. 17, pp. 416-439 (1969)
8. Yamashita, E. and Mittra, R., "Variational method for the analysis of microstrip lines." IEEE Trans Microwave Theory Tech. Vol. 16, pp. 251-256 (1968)

9. Yamashita, E. and Atuski, K., "Strip line with rectangular outer conductor and three dielectric layers." IEEE Trans Microwave Theory Tech. Vol. 18, pp. 234-238 (1970)

10. Yamashita, E. and Atuski, K., "Analysis of thick strip transmission lines." IEEE Trans Microwave Theory Tech. Vol. 19, pp. 120-122 (1971)

11. Farrar, A. and Adams, A.T., "Characteristic impedence of microstrip by the method of moments." IEEE Trans Microwave Theory Tech. Vol. 18, pp. 65-66 (1970)

12. Mittra, R. and Itoh, T., "Charge and potential distributions in shielded striplines." IEEE Trans Microwave Theory Tech. Vol. 18, pp. 149-156 (1970)

13. Mittra, R. and Lee, S.W., Analytical techniques in the theory of guided waves, Macmillan, New York, 1971

14. Harrington, R.F., Time-harmonic electromagnetic fields. McGraw-Hill, New York, 1961

15. Getsinger, W.J., "Microstrip dispersion model." IEEE Trans Microwave Theory Tech. Vol. 21, pp. 34-39 (1973)

16. Zysman, G.I. and Varon, D., "Wave and propagation in microstrip transmission lines." IEEE G-MTT Int. Symp. 1969 Digest, pp. 3-9 (1969)

17. Mittra, R., and Itoh, T., "A new technique for the analysis of the dispersion characteristics of microstrip lines." IEEE Trans Microwave Theory Tech. Vol. 19, pp. 47-56 (1971)

18. Hornsby, J.S., and Gopinath, A., "Fourier analysis of a dielectric-loaded waveguide with a microstrip line." Electron Lett. Vol. 5, pp. 265-267 (1969)

19. Hornsby, J.S. and Gopinath, A., "Numerical analysis of a dielectric-loaded waveguide with microstrip line - finite difference methods." IEEE Trans Microwave Theory Tech. Vol. 17, pp. 684-690 (1969)

20. Kowalski, G. and Pregla, R., "Dispersion characteristics of shielded microstrips with finite thickness." Arch Elektron Ubertragungstech. Vol. 25, pp. 193-196 (1971)

21. Daly, P., "Hybrid mode analysis of microstrip by finite-element method." IEEE Trans Microwave Theory Tech. Vol. 19, pp. 19-25 (1971)

22. Akhtarzad, S. and Johns, P.B.,"T.L.M. Analysis of the dispersion characteristics of microstrip lines on magnetic substrates using three dimensional resonators." Electron Lett. Vol. 11, No. 6, pp. 130-131 (1975)

23. Denlinger, E.J., "A frequency dependent solution for microstrip transmission lines." IEEE Trans Microwave Theory Tech. Vol. 19, pp. 30-39 (1971)

24. Itoh, T. and Mittra, R., "Dispersion characteristics of microstrip lines." Eur. Microwave Conf., Proc 1971, p. C4/3 (1971)

25. Weis, J.A., and Brayant, T.G., "Dielectric Green's function for parameters of microstrip." Electron Lett. Vol. 6, p. 462 (1970); see also Erratum, ibid. p. 560.

26. Brayant, T.G., and Weiss, J.A., "Parameters of microstrip transmission lines and of coupled pairs of microstrip lines." IEEE Trans Microwave Theory Tech. Vol. 16, pp. 1021-1027 (1968)

27. Krage, M.L. and Haddad, G.I., "Characteristics of coupled microstrip transmission lines-II: evaluation of coupled-line parameters." IEEE Trans Microwave Theory Tech. Vol. 18, pp. 222-228 (1970)

28. Chen, W.H., "Even and odd mode impedance of coupled pairs of microstrip lines." IEEE Trans Microwave Theory Tech. Vol. 18, pp. 55-57 (1970)

29. Maeda, M., "An analysis of gap in microstrip transmission lines." IEEE Trans Microwave Theory Tech. Vol. 20, pp. 390-396 (1972)

30. Benedek, P. and Silvester, P., "Equivalent capacitances for microstrip gaps and steps." IEEE Trans Microwave Theory Tech. Vol. 20, pp. 729-733 (1972)

31. de Ronde, F.C., Philips Nat Lab Patent Application, nr. 14.313 (Netherlands), May, 1973.

32. Shammas, S., "The effect of dispersion in microstrip on the resonant frequencies of an open-ring resonator." Philips Nat Lab Technical Note Nr. 230/73.

33. Wolf, I. and Knoppik, N., "The microstrip ring resonator and dispersion measurement on microstrip lines." Electron Lett. Vol. 7, pp. 779-781 (1971)

34. Wu, Y.S. and Rosenbaum, F.J., "Mode chart for microstrip ring resonators." IEEE Trans Microwave Theory Tech. Vol. 21, pp. 487-489 (1973)

35. Shammas, S., "Models for coupled open-ring resonators for filter designs. Philips International Institute Report Nr. 492 (Dec. 1973)

36. Wolf. I, and Knoppic, N., "Rectangular and circular microstrip disk capacitors and resonators." IEEE Trans Microwave Theory Tech. Vol. 22, pp. 857-864 (1974)

37. Krause, N., "Improved microstrip circulator design by modified resonance computations." Proceedings of the 8th EMC 1978 (Paris). pp. 216-220 (1978)

38. Pintzos, S.G. and Pregla, R., "A simple method for computing the resonant frequencies of microstrip ring resonators." IEEE Trans Microwave Theory Tech. Vol. 26, pp. 809-813 (1978)

39. Itoh, T., "Analysis of microstrip resonators." IEEE Trans Microwave Theory Tech. Vol. 22, pp. 946-951 (1974)

40. Akhtarzad, S. and Johns, P.B., "Three-dimensional transmission-line matrix computer analysis of microstrip resonators." IEEE Trans Microwave Theory Tech. Vol. 23, pp. 990-997 (1975)

41. Meixner, J., "The behavior of electromagnetic fields at edges." IEEE Trans on Antennas Prop. Vol. AP-20, pp. 442-446 (1972)

42. Brebbia, C.A., The boundary element method for engineers. Billing & Sons Ltd. (1978)

43. Brebbia, C.A., Recent advances in boundary element method. Penech Press (1978)

44. Kelly, D.W., Mustoe, G.G.W., and Zienkiewicz, O.C., Recent advances in boundary element method. Penech Press, pp. 359-373 (1978)

45. Beckenbach, E.F., Modern mathematics for the engineer. Royal Weller, New York, McGraw-Hill pp. 121-122 (1956)

46. Mittra, R. and Lee, S.W., Analytical techniques in the theory of guided waves. pp. 4-11, McMillan (1971)

47. Acton, S.A., Numerical methods that work. Harper and Row Publishers, pp. 410-430 (1970)

48. Abramowitz, M. and Stegun, I.A., Handbook of mathematical functions. Dover Publications Inc., New York, pp. 916-924 (1972)

49. Gradsteyn, I.S. and Rydzhik, I.M., Table of integrals, series, and products. Academic Press, pp. 712 and 952 (1965)

50. Bateman, H., Tables of integral transforms. Vol. 2, McGraw-Hill, New York (1954)

51. Pucel, R.A., Masse, D.J., and Hartwig, C.P., "Losses in microstrips" IEEE Trans Microwave Theory Tech. Vol. 16, pp. 342-350 (June 1968)

52. Yamashita, E., Atsuki, K., and Ueda, T., "An approximate formula of microstrip lines for computer-aided design of microwave integrated circuits."IEEE Trans Microwave Theory Tech. Vol. 27, pp. 1036-1038 (Dec. 1979)

APPENDICES

Appendix A

Computer Programs for Single MIC Lines

The programs are written in APL. The workspace is called SINGLE. The symbols used in the programs and their relation to the symbols in Chap. 2 is as follows:

CH: $\{\chi\}$ in Eqs 2-18 and 37

CO: C_o capacitance of the microstrip line for $\varepsilon_r=1$

C1: C capacitance of the microstrip line for $\varepsilon_r\neq 1$

ER: ε_r

ET: η Eq 2-21a

G1: $[G_1]$ Eqs 2-22b and 37

G2: $[G_2]$ Eqs 2-22b and 37

G3: $[G_3]$ Eq 2-37

G4: $[G_4]$ Eq 2-37

G5: $[\hat{G}_5]$ Eq 2-37

NJ: ν_j Eq 2-25a

NF: $\bar{\nu}_i$ Eq 2-36d

NM: Abscissa for Gaussian integration

THI: θ_i Eq 2-29c

TH1: θ_1 Eq 2-29a

TH2: θ_2 Eq 2-29b

WJ: W_j Eq 2-24

WF: $\bar{W}_j$ Eq 2-36c

WM: Weight factor for Gaussian integration

WOH: w/h

ZE: ζ_i with $0<\zeta<1$

ZF: ζ_i with $1<\zeta$

ZEF: ζ_i with $0<\zeta$

Program POINT

This program assigns the values to the parameters necessary for numerical integration; the data are obtained from Ref. [48].

```
      ▼ POINT
[1]   NJ← 0.07652652109999999 0.2277858511 0.3737060887 ,□
[2]   0.51086770019 0.6360536807
[3]   NJ←NJ, 0.7463319064 0.8391169718 0.9122344282 ,□
[4]   0.9639719272
[5]   NJ←NJ,0.9931285991
[6]   WJ← 0.1527533871 0.1491729864 0.1420961093 0.1316886384
[7]   WJ←WJ, 0.1181945319 0.1019301198 0.0832767415
[8]   WJ←WJ, 0.06267204830000001 0.0406014298 0.0176140071
[9]   TH1←○0.5×0,0.5×(¯1↓NJ)+1↓NJ
[10]  TH2←(1↓TH1),○0.5
[11]  THI←○0.5×NJ
[12]  ZE←1○THI
[13]  CF←6+⍳4
[14]  NF← 0.2635603197 1.4134030591 3.596425771 7.0858100058 ,□
[15]  12.6408008442
[16]  WF← 0.6790940422 1.6384878736 2.7694432424 4.3156569009 ,□
[17]  7.2191863544
[18]  ZF←NF+1
      ▼
```

Program INT

This program evaluates the elements of $[G_2]$ (Eq. 2-32).

```
      ▼ RR←INT
[1]   DTH←TH2[J]-TH1[J]
[2]   TH←0.5×(TH2[J]+TH1[J])+NM×DTH
[3]   A←TH-THI[I]
[4]   B←0.5×TH+THI[I]
[5]   C←B-○0.5
```

```
[6]   AR←*((10A)÷A)×((10B)÷B)×(10C)÷C
[7]   D1←DTH×+/WM×AR
[8]   A1←TH1[J]-THI[I]
[9]   A2←TH2[J]-THI[I]
[10]  B1←TH1[J]+THI[I]
[11]  B2←TH2[J]+THI[I]
[12]  C1←B1-01
[13]  C2←B2-01
[14]  D2←2×*((|A2)*A2)×((|B2)*B2)×((|C2)*C2)
[15]  D2←D2-2×*((|A1)*A1)×((|B1)*B1)×(|C1)*C1
[16]  RR←D1+D2-DTH×CF
      ▼
```

Program INT2

This program evaluates the elements of $[G_3]$ (Eq. 2-37).

```
      ▼ RS←INT2
[1]   DTH←TH2[J]-TH1[J]
[2]   TH←0.5×(TH2[J]+TH1[J])+NM×DTH
[3]   STH←10TH
[4]   R1←STH÷STH+ZF[I]
[5]   R2←((TH-00.5)×20TH)÷ZF[I]-STH
[6]   R3←2×DTH×+/WM×R1×R2
[7]   ZS←ZF[I]*2
[8]   R5←(ZS-(10TH1[J])*2)*TH1[J]-00.5
[9]   R6←(ZS-(10TH2[J])*2)*TH2[J]-00.5
[10]  R7←2×*R6÷R5
[11]  RS←R3+R7
      ▼
```

Program FIRST

This program forms the matrix $[G_1]$ (Eqs. 2-24, 22b).

```
      ▼FIRST[0]▼
      ▼ FIRST ET
[1]   CF1←(2÷ET)*2
[2]   JM←⍴WJ
[3]   AR1←CF1+(ZE∘.+ZE)*2
[4]   AR2←CF1+(ZE∘.-ZE)*2
[5]   AR3←*AR1×AR2
[6]   G1←-00.5×AR3×(JM,JM)⍴WJ
      ▼
```

Program SECOND

This program forms $|G_2|$ using INT2 (Eqs. 2-31, 22b).

```
      ▼ SCND
[1]   G2←(JM,JM)ρ0
[2]   I←1
[3]  L2:J←1
[4]  L3:G2[I;J]←INT
[5]   J←J+1
[6]   →(J≤JM)/L3
[7]   I←I+1
[8]   →(I≤JM)/L2
      ▼
```

Program THRD

This program forms $|G_3|$ using INT2 (Eqs. 2-37).

```
      ▼ THRD
[1]   JF←ρZF
[2]   G3←(JF,JM)ρ0
[3]   I←1
[4]  L4:J←1
[5]  L5:G3[I;J]←INT2
[6]   J←J+1
[7]   →(J≤JM)/L5
[8]   I←I+1
[9]   →(I≤JF)/L4
      ▼
```

Program FRTH

This program forms $|G_4|$ (Eqs. 2-24,37).

```
      ▼ FRTH ET
[1]   CF1←(2÷ET)*2
[2]   R1←CF1+(ZF∘.+ZE)*2
[3]   R2←CF1+(ZF∘.-ZE)*2
[4]   R3←⊛R1×R2
[5]   G4←-oo.5×R3×(JF,JM)ρWJ
      ▼
```

Program FFTH

This program forms $[\hat{G}_5]$ (Eqs. 2-36, 37).

```
      ▼ FFTH
[1]   ZEF←ZE,ZF
[2]   JN←⍴ZEF
[3]   R1←÷CF1+((-ZEF)∘.+ZF)*2
[4]   R2←÷CF1+(ZEF∘.+ZF)*2
[5]   R3←R1+R2
[6]   G5←(2×(ER-1)÷ET)×R3×(JN,JF)⍴WF
      ▼
```

Progran FNL

This program performs the final assembly for the case

$$\epsilon_r = 1$$

and solves the resulting equations to obtain $\{X\}$ and C_o (Eq. 2-34).

```
      ▼ FNL
[1]   GG←G1+G2
[2]   FF←JM⍴0 4
[3]   CH←FF⌹GG
[4]   CO←+/CH×WJ
      ▼
```

Program FNL2

This program performs the final assembly for the case

$$\epsilon_r \neq 1$$

and solves the resulting equations (Eqs. 2-37,38).

```
      ▼ FNL2 ER
[1]   CF3←0 2×ER+1
[2]   F←-CF3+(ER-1)×(¯3○ET×(1-ZEF)÷2)+¯3○ET×(1+ZEF)÷2
[3]   G←((G1+G2),[1] G3+G4),G5
[4]   I←JM+1
[5]  L6:G[I;I]←G[I;I]+CF3
[6]   F[I]←F[I]+CF3
[7]   I←I+1
[8]   →(I≤JN)/L6
[9]   CHP←F⌹G
[10]  C1←+/(JM↑CHP)×WJ
      ▼
```

Program TTL

This program produces the titles needed for the output in the main program IMPD.

```
     ▼ TTL
[1]  T1←'CHARACTERISTIC IMPEDANCE'
[2]  T2←'EFFECTIVE DIELECTRIC CONSTANT'
[3]  T3←'CHARGE DISTRIBUTION;CH VS. ZE'
[4]  T4←'POTENTIAL DISTRIBUTION ON THE DAI'
[5]  T5←'FIRST COLUMN: NORMALIZED DISTANCE'
[6]  T6←'SECOND COLUMN: POTENTIAL'
[7]  T7←''
[8]  T8←'SECOND COLUMN: CH'
     ▼
```

Program IMPD

This program is the main program; it executes the above programs and prints out ε_e, Z, charge distribution (X of Eqs. 2-18 and 21e), and the potential distribution on the DAI. The input to IMPD is w/h and ε_r.

```
     ▼ WOH IMPD ER
[1]  ET←WOH÷2
[2]  FIRST ET
[3]  FNL
[4]  FRTH ET
[5]  FFTH
[6]  FNL2 ER
[7]  T2
[8]  |C1÷C0
[9]  T7
[10] T7
[11] T1
[12] 120÷(|C0×C1)*0.5
[13] T7
[14] T7
[15] T3
[16] T5
[17] T8
[18] ⍉(2,JM)⍴ZE,(JM↑CHP)
[19] T7
```

```
[20]  T7
[21]  T4
[22]  T5
[23]  T6
[24]  ⍉(2,JF)⍴ZF,(JM↓CHP)
      ▼
```

Example

To analyze a microstrip line with w/h=1 and ε_r=9.9.

The workspace SINGLE is loaded first:

)LOAD SINGLE

IMPD is executed next .

```
      1 IMPD 9.9
EFFECTIVE DIELECTRIC CONSTANT
6.090198244


CHARACTERISTIC IMPEDANCE
51.26247005


CHARGE DISTRIBUTION;CH VS. ZE
FIRST COLUMN: NORMALIZED DISTANCE
SECOND COLUMN: CH
 0.1199182902 5.979617834
 0.3502192597 5.932851971
 0.5538791487 5.854585711
 0.7190733836 5.767108169
 0.8409902074 5.689695601
 0.9216592529 5.632856882
 0.9682372823 5.598098021
 0.9905120983 5.580976234
 0.9983990569 5.574818233
 0.99994175   5.573570186
```

POTENTIAL DISTRIBUTION ON THE DAI
FIRST COLUMN: NORMALIZED DISTANCE
SECOND COLUMN: POTENTIAL

1.26356032	0.641102785
2.413403059	0.2778148304
4.596425771	0.08741715987
8.085810006	0.02427627784
13.64080084	0.00750436892

Appendix B

Computer Programs for Coupled Microstrip Lines

The workspace is called COUPLED. The parameters for numerical integration are the same as in SINGLE (App. A) so they are copied into COUPLED. Besides the symbols defined in App. A, there are some symbols used in COUPLED which are defined below:

E1 through E8: $[E_1]$ through $[E_8]$. Eqs 2-56 and 57

FF1: $[F_1]$; Eq. 2-58

G1 through G4: $[G_1]$ through $[G_4]$; Eqs 2-50, 51

H1: $[H_1]$ Eq. 2-58

SIG: σ' Eq. 2-55b

ZD: $1 < \zeta_i < \sigma'$

ZE: $-1 < \zeta_i < 1$

ZF: $-\infty < \zeta_i < -1$

ZZ: $-\infty < \zeta_i < \sigma'$

ZPD: ζ_i' , $1 < \zeta_i < \sigma'$

ZPE: ζ_i' , $-1 < \zeta_i < 1$

ZPF: ζ_i' , $-\infty < \zeta_i < -1$

ZP: ζ_i' , $-\infty < \zeta_i < \sigma'$

Program PNT

This program evaluates the coefficients and vector sizes and forms matrices which are necessary for the numerical integrations.

```
      ▼ PNT
[1]   CF←6+2×⍳4
[2]   JD←⍴NM
[3]   JE←⍴ZE
[4]   JF←⍴ZF
[5]   JT←JD+JE+JF
[6]   WWD←(JT,JD)⍴WM
[7]   WWE←(JT,JE)⍴WJ
[8]   WWF←(JT,JF)⍴WF
      ▼
```

Program DATA

This program evaluates ζ_i and ζ_i' for a given σ.

```
      ▼ DATA SIG
[1]   ZD←0.5×(SIG+1)+(SIG-1)×NM
[2]   ZPD←(2×SIG)-ZD
[3]   ZPE←(2×SIG)-ZE
[4]   ZPF←(2×SIG)-ZF
[5]   ZP←ZPD,ZPE,ZPF
[6]   ZZ←ZD,ZE,ZF
      ▼
```

Program INT1

This program performs the integration of Eq. 2-53.

```
      ▼ RR←INT1
[1]   A1←TH1[J]-THI[I]
[2]   A2←TH2[J]-THI[I]
[3]   R1←((|A2)*A2)÷(|A1)*A1
[4]   B1←(○1)-TH1[J]+THI[I]
[5]   B2←(○1)-TH2[J]+THI[I]
[6]   R2←((|B1)*B1)÷(|B2)*B2
[7]   C1←(○1)+TH1[J]+THI[I]
[8]   C2←(○1)+TH2[J]+THI[I]
[9]   R3←((|C2)*C2)÷(|C1)*C1
[10]  R4←2×⍳R1×R2×R3
```

```
[11]  S1←0.5×TH[J;]-THI[I]
[12]  S2←0.5×TH[J;]+THI[I]
[13]  S3←(1○S1)÷S1
[14]  S4←●(0 2○S2)÷((○0.5)-S2)×(○0.5)+S2
[15]  R5←DTH[J]×+/WM×S4
[16]  RR←R4+R5-DTH[J]×CF
      ▼
```

Program INT2

Consider Eq. 2-50b

$$G_{2,ij}=\int_{\xi_{1j}}^{\xi_{uj}} \ln(\zeta_i'-\zeta)/\sqrt{1-\zeta^2}\,d\zeta. \qquad (2\text{-}50b)$$

Applying the transformation

$$\zeta=\sin\theta \qquad (2\text{-}32)$$

to Eq. 2-50b yields

$$G_{2,ij}=\int_{\theta_1}^{\theta_2}\ln(\zeta_i'-\sin\theta)\,d\theta. \qquad (B\text{-}1)$$

Applying the identity

$$(d/d\theta)[(\theta\pm\pi/2)\ln(\zeta_i'-\sin\theta)]=$$

$$\ln(\zeta_i'-\sin\theta)-(\theta\pm\pi/2)/(\zeta_i'-\sin\theta). \qquad (B\text{-}2)$$

to Eq. 2-50b results in

$$G_{2,ij}=2\ln(|\zeta_i'-\sin\theta_2|^{\theta_2-\pi/2}/|\zeta_i'-\sin\theta_1|^{\theta_1-\pi/2})$$

$$+2\int_{\theta_1}^{\theta_2}[(\theta-\pi/2)\cos\theta/(\zeta_i'-\sin\theta]\,d\theta, \qquad (B\text{-}3)$$

where the minus sign in Eq. B-2 is used. This choice of sign is used to remove the singularity occuring at $\zeta_i'=1$. Considering that

$$\zeta_i'=2(\sigma/\eta)-\zeta_i \qquad (2\text{-}48)$$

and the fact that ζ_i lies on the MIC for $\epsilon_r=1$, it is concluded that $\zeta_i'\geq 1$.

For coupled lines with $\epsilon_r\neq 1$ an integral similar to that of Eq. B-1 occurs in which ζ_i' is replaced by ζ_i and

can be less than or equal to minus one. Specifically, consider $H_{1,ij}$ of Eqs. 2-57d, 58a, and 58b

$$H_{1,ij} = -\eta \int_{\xi_{ij}}^{\xi_{ij}} \ln(\zeta_i - \zeta)^2 / \sqrt{1-\zeta^2}\, d\zeta . \qquad \text{(B-4)}$$

Applying the transformation of Eq. 2-32 followed by the identity of Eq. B-2 yields

$$H_{1,ij} = -2\eta \ln\left[|\zeta_i - \sin\theta_2|^{\theta_2 + \pi/2} / |\zeta_i - \sin\theta_1|^{\theta_1 + \pi/2} \right]$$
$$-2\eta \int_{\theta_1}^{\theta_2} (\theta + \pi/2) \cos\theta / (\zeta_i - \sin\theta)\, d\theta . \qquad \text{(B-5)}$$

where the plus sign of Eq. B-2 is used.

Program INT2 evaluates both Eqs. B-3 and B-5.

AZ can be ζ_i of Eq. B-3 in which the minus sign of Eq. B-3 is relevant, or AZ can be ζ_i, of Eq. B-5 in which case the positive sign applies. Correspondingly SGN can be -1 or +1.

```
      ▼ RS←SGN INT2 AZ
[1]   SP←○SGN×0.5
[2]   R2←(AZ[I]-1○TH2[J])*TH2[J]+SP
[3]   R1←(AZ[I]-1○TH1[J])*TH1[J]+SP
[4]   R3←2×⍟R2÷R1
[5]   R4←((TH[J;]+SP)×2○TH[J;])÷AZ[I]-1○TH[J;]
[6]   R5←DTH[J]×+/WM×R4
[7]   RS←R3+R5
      ▼
```

Program FIRST

This program forms the matrix $[G_1]$ (Eqs. 2-51 and 58b).

```
      ▼ FIRST
[1]   G1←(JE,JE)⍴0
[2]   I←1
[3]  L2:J←1
[4]  L3:G1[I;J]←INT1
[5]   J←J+1
[6]   →(J≤JE)/L3
[7]   I←I+1
[8]   →(I≤JE)/L2
      ▼
```

Program SCND

This program forms the matricies $[F_1]$, $[G_2]$, $[H_1]$, and $[E_8]$ (Eqs. 2-51, 56, and 58).

```
      ▼ RA←V SCND AZ
[1]   RA←(2↑V)⍴0
[2]   I←1
[3]  L4:J←1
[4]  L5:RA[I;J]←V[3] INT2 AZ
[5]   J←J+1
[6]   →(J≤V[2])/L5
[7]   I←I+1
[8]   →(I≤V[1])/L4
      ▼
```

Program THRD

This program assembles $[G_1]$ through $[G_4]$, $\{U\}$ of Eq. 2-51, $[E_1]$ through $[E_8]$ and $\{F\}$ of Eq. 2-56. The input to the program is VV, a vector which in this program contains ε_r , η , and σ' .

```
      ▼ THRD VV
[1]   ER←VV[1]
[2]   ET←VV[2]
[3]   SIG←VV[3]
[4]   DATA SIG
[5]   CF1←(2÷ET)*2
[6]   E1←((ER-1)×(SIG-1)÷ET)×WWD÷CF1+(ZZ∘.-ZD)*2
[7]   E2←((ER-1)×(SIG-1)÷ET)×WWD÷CF1+(ZP∘.-ZD)*2
[8]   E3←(2×(ER-1)÷ET)×WWF÷CF1+(ZZ∘.-ZF)*2
[9]   E4←(2×(ER-1)÷ET)×WWF÷CF1+(ZP∘.-ZF)*2
[10]  E5←00.5×WWE×∘CF1+(ZZ∘.-ZE)*2
[11]  E6←00.5×WWE×∘CF1+(ZP∘.-ZE)*2
[12]  FF1←(JD,JE,¯1) SCND ZD
[13]  H1←(JF,JE,1) SCND ZF
[14]  E7←(FF1,[1] G1),[1] H1
[15]  E8←(JT,JE,¯1) SCND ZP
[16]  U←JE⍴04
[17]  G2←(JE,JE,¯1) SCND ZPE
[18]  G3←-00.5×WW×∘CF1+(ZE∘.-ZE)*2
[19]  G4←-00.5×WW×∘CF1+(ZPE∘.-ZE)*2
[20]  GGE←G1+G2+G3+G4
[21]  GGO←G1+G3-G2+G4
      ▼
```

Program FNL

The final assembly and rearrangement of the equations are performed by this program.

$$\epsilon_r \neq 1$$

(i.e., to rearrange Eq. 2-56 into Eqs. 2-59).

```
      ▼ FNL
[1]   F1←¯300.5×ET×1-ZZ
[2]   F2←¯300.5×ET×1+ZZ
[3]   F3←¯300.5×ET×1-ZP
[4]   F4←¯300.5×ET×1+ZP
[5]   FE←(1-ER)×F1+F2+F3+F4
[6]   FO←(1-ER)×F1+F2-F3+F4
[7]   CF2←02×1+ER
[8]   V1←JD+⍳JE
[9]   FE[V1]←FE[V1]-CF2
[10]  FO[V1]←FO[V1]-CF2
[11]  GE←(E1+E2),(E7+E8-E5+E6),E3+E4
[12]  GO←(E1-E2),(E7-E8+E5-E6),E3-E4
[13]  I←1
[14] L6:GE[I;I]←GE[I;I]+CF2
[15]  GO[I;I]←GO[I;I]+CF2
[16]  I←I+1
[17]  →(I≤JD)/L6
[18]  I←I+JE
[19] L7:GE[I;I]←GE[I;I]+CF2
[20]  GO[I;I]←GO[I;I]+CF2
[21]  I←I+1
[22]  →(I≤JT)/L7
      ▼
```

Program FNL2

The final equations for both cases

$$\epsilon_r = 1 \text{ and } \epsilon_r \neq 1$$

are solved and the various coupled mic line parameters are evaluated by this program.

```
      ▼ FNL2
[1]   ABCE←FE⌹GE
[2]   AE←JD↑ABCE
[3]   BE←JD↓(-JF)↓ABCE
[4]   CE←(-JF)↑ABCE
[5]   ABCO←FO⌹GO
```

```
[6]    AD←JD↑ABCD
[7]    BD←JD↓(-JF)↓ABCD
[8]    CD←(-JF)↑ABCD
[9]    CE1←+/WJ×BE
[10]   CD1←+/WJ×BD
[11]   CE0←+/WJ×UBGGE
[12]   CD0←+/WJ×UBGGD
[13]   T12
[14]   T12
[15]   T1
[16]   240÷(|CE0×CE1)*0.5
[17]   T12
[18]   T12
[19]   T2
[20]   240÷(|CD0×CD1)*0.5
[21]   T12
[22]   T12
[23]   T2P
[24]   |CE1÷CE0
[25]   T12
[26]   T12
[27]   T3P
[28]   |CD1÷CD0
[29]   T12
[30]   T12
[31]   T3
[32]   T4
[33]   T5
[34]   T6
[35]   ⍉(3,JE)⍴ZE,BE,BD
[36]   T12
[37]   T12
[38]   T7
[39]   T8
[40]   T9
[41]   T10
[42]   ⍉(3,JD)⍴ZD,AE,AD
[43]   T12
[44]   T12
[45]   T11
[46]   T8
[47]   T9
[48]   T10
[49]   ⍉(3,JF)⍴ZF,CE,CD
       ∇
```

IMPD

This is the main program. The input to this program is VV. In this program VV is a vector with the following elements:

VV[1]=ε_r,

VV[2]=w/h (Fig 2-10a) and

VV[3]=s/h (Fig 2-10a).

VV is modified by IMPD to contain ε_r, η , and σ needed as the input to THRD.

```
      ▼ IMPD VV
[1]   VV[3]←1+VV[3]÷VV[2]
[2]   VV[2]←VV[2]÷2
[3]   THRD VV
[4]   FNL
[5]   FNL2
      ▼
```

Program TTL

This program produces the titles and comments necessary for the output in FNL2.

```
      ▼ TTL
[1]   T1←'EVEN-MODE CHARACTERISTIC IMPEDANCE'
[2]   T2←'ODD-MODE CHARACTERISTIC IMPEDANCE'
[3]   T2P←'EVEN-MODE EFFECTIVE DIELECTRIC CONSTANT'
[4]   T3P←'ODD-MODE EFFECTIVE DIELECTRIC CONSTANT'
[5]   T3←'CHARGE DISTRIBUTION:'
[6]   T4←'FIRST COLUMN: NORMALIZED DISTANCE ON THE MIC'
[7]   T5←'SECOND COLUMN: EVEN-MODE CH'
[8]   T6←'THIRD COLUMN: ODD-MODE CH'
[9]   T7←'POTENTIAL DISTRIBUTION ON DAI BETWEEN MICS'
[10]  T8←'FIRST COLUMN: NORMALIZED DISTANCE'
[11]  T9←'SECOND COLUMN: EVEN-MODE PPOTENTIAL'
[12]  T10←'THIRD COLUMN: ODD MODE POTENTIAL'
[13]  T11←'POTENTIAL DISTRIBUTION ON DAI OUTSIDE MICS'
[14]  T12←''
      ▼
```

Example

To analyze coupled mic lines with

$\varepsilon_r = 9.9$,
$w/h = 1.0$, and
$s/h = 1.0$

the workspace COUPLED is loaded first. The response to

```
IMPD 9 1 1
```

is

```
EVEN-MODE CHARACTERISTIC IMPEDANCE
59.70066832

ODD-MODE CHARACTERISTIC IMPEDANCE
43.22294308

EVEN-MODE EFFECTIVE DIELECTRIC CONSTANT
5.856033191

ODD-MODE EFFECTIVE DIELECTRIC CONSTANT
5.225940583

CHARGE DISTRIBUTION:
FIRST COLUMN: NORMALIZED DISTANCE ON THE MIC
SECOND COLUMN: EVEN-MODE CH
THIRD COLUMN: ODD-MODE CH
 -0.99994175     6.754553263    7.964977794
 -0.9983990569   5.955192724    6.8120589
 -0.9905120983   5.623564688    6.335101657
 -0.9682372823   5.390650995    6.003415031
 -0.9216592529   5.235309422    5.789411168
 -0.8409902074   5.138075753    5.67031868
 -0.7190733836   5.084286331    5.634514068
 -0.5538791487   5.054407753    5.669359218
 -0.3502192597   5.022212962    5.758712778
 -0.1199182902   4.959754888    5.886318488
  0.1199182902   4.848171275    6.042027748
  0.3502192597   4.688702156    6.224333422
  0.5538791487   4.506285863    6.435227221
  0.7190733836   4.342177833    6.672403318
  0.8409902074   4.239352342    6.928322168
  0.9216592529   4.229350085    7.198439857
  0.9682372823   4.328538908    7.491717851
  0.9905120983   4.549176108    7.840944982
  0.9983990569   4.900981007    8.289778812
  0.99994175     5.777186024    9.335118178
```

POTENTIAL DISTRIBUTION ON DAI OUTSIDE MICS
FIRST COLUMN: NORMALIZED DISTANCE
SECOND COLUMN: EVEN-MODE PPOTENTIAL
THIRD COLUMN: ODD MODE POTENTIAL

-1.26356032	0.6779665161	0.6687968417
-2.413403059	0.3032838761	0.2755921618
-4.596425771	0.101707095	0.07841470369
-8.085810006	0.03033464862	0.01752825718
-13.64080084	0.008757300631	0.003875702662

POTENTIAL DISTRIBUTION ON DAI BETWEEN MICS
FIRST COLUMN: NORMALIZED DISTANCE
SECOND COLUMN: EVEN-MODE PPOTENTIAL
THIRD COLUMN: ODD MODE POTENTIAL

1.013046736	0.9955866221	0.9516569076
1.067468317	0.908074752	0.7938957452
1.160295216	0.8321237625	0.6461210028
1.283302303	0.7693159969	0.509282825
1.425562831	0.7208040195	0.3846162811
1.574437169	0.6865892529	0.2734562838
1.716697697	0.6653052949	0.177496482
1.839704784	0.6543171934	0.09913397699
1.932531683	0.6501500673	0.04152114196
1.986953264	0.6492924977	0.008021078653

Appendix C

Workspace THAT

This workspace contains several functions for evaluating and solving the final equations of Chap. 4. The notation used is as follows:

B, BB:	B, Eq. 4-23d,
C:	C, Eq. 4-23e,
DEL:	δ, Eq. 4-22g,
EF:	ε_e,
ER:	ε_r,
ET:	η, Eq. 4-22c,
F:	(fh) normalized frequency GHz·mm
Gl [I;J] ,.....:	$G_{1,ij}$,.... Eqs. 4-33
L:	L, Eq. 4-31
M:	M, Eq. 4-32a and 32c
PH=tan^{-1}(C/L)	C, and L are defined in Eqs. 4-23e and 31
RO:	ρ_n, Eq. 4-25c,
SG:	σ_n, Eq. 4-25,
WI [I]:	W_i, Fig. 4-3,
XI [I]:	ξ_i, Fig. 4-3,
XL [I]:	ξ_{li}, Fig. 4-3,
XU [I]:	ξ_{ui}, Fig. 4-3.

F0

F0 computes ξ_{ij} and ξ_{vj} given the values of ξ_j and W_j.

```
      ▼ F0 WI
[1]   N←⍴WI
[2]   XU←N⍴0
[3]   J←0
[4]  L11:J←J+1
[5]   XU[J]←+/J↑WI
[6]   →(J<N)/L11
[7]   XL←0,¯1↓XU
      ▼
```

D1

D1 computes the matricies with elements

$$(\xi_{vj}-\xi_i),\ (\xi_{yj}-\xi_i),\ (\xi_{vj}+\xi_i+2\eta),\ \text{and}\ (\xi_{yj}+\xi_i+2\eta)$$

used as the arguments of Eqs. 4-33a, c, and d.

```
      ▼ D1
[1]   XI1←XI∘.-XL
[2]   XI2←XI∘.-XU
[3]   Z1←XI∘.+XL+2×ET
[4]   Z2←XI∘.+XU+2×ET
[5]   M←⍴XL
      ▼
```

D2

D2 computes the factors

$$\exp(-\xi_{vj}L),\ \exp(-\xi_{yj}L),\ \exp(-\xi_iL),$$

which appear when integrating Eqs. 4-33.

```
      ▼ D2 L
[1]   EI←(M,M)⍴0
[2]   I←0
[3]  L10:I←I+1
[4]   EI[I;I]←*-L×XI[I]
[5]   →(I<M)/L10
[6]   EX1←(M,M)⍴*-L×XL
[7]   EX2←(M,M)⍴*-L×XU
[8]   LX2←(M,M)⍴L×XU
[9]   LX1←(M,M)⍴L×XL
      ▼
```

D3

D3 computes the matrices SNU and SNL such that correct signs can be allotted to the different terms for evaluating the integral in Eq. 4-33c, for the given conditions

```
      ▼ D3
[1]   SNU←2×¯0.5+XL∘.<XI
[2]   SNL←2×¯0.5+XU∘.>XI
      ▼
```

F1

Using the matrices computed in D1, D2, and D3, F1 forms matricies G1, G2, and G5 with elements $G_{1,ij}$, $G_{2,ij}$, and $G_{5,ij}$ respectively.

```
      ▼ L F1 C
[1]   S←(L*2)+C*2
[2]   SQ←S*0.5
[3]   CLI←C÷L
[4]   PH←¯3○CLI
[5]   LIQ←(PH÷CLI)÷L
[6]   E2←EX2÷2×SQ
[7]   E1←EX1÷2×SQ
[8]   R1←PH-C×XI1
[9]   R2←PH-C×XI2
[10]  R3←-SNU×E2×(LIQ+XI2)×(1○R2)÷R2
[11]  R4←-SNL×E1×(LIQ+XI1)×(1○R1)÷R1
[12]  G2←R3+R4+EI÷S
[13]  R5←PH+C×Z1
[14]  R6←PH+C×Z2
[15]  R7←E1×(LIQ+Z1)×(1○R5)÷R5
[16]  R8←E2×(LIQ+Z2)×(1○R6)÷R6
[17]  G1←R7-R8
[18]  R9←E1[1;]×2○PH+C×ET+XL
[19]  R10←E2[1;]×2○PH+C×ET+XU
[20]  G5←R9-R10
      ▼
```

F2

F2 finds the matrices G3 and G4 (Eqs. 4-33a and b).

```
      ▼ L F2 C
[1]   G4←G3←0
[2]   N←0
[3]  L1:N←N+1
[4]   RS←((○N)*2)-C*2
[5]   RO←RS*0.5
[6]   DR←÷RO×RO+L
[7]   G3←G3+DR×(*-LX1+RO×Z1)-*-LX2+RO×Z2
[8]   G41←EX1×(*-RO×|XI1)
[9]   G41←G41÷RO×L-SNL×RO
[10]  G42←EX2×(*-RO×|XI2)÷RO×L+SNU×RO
[11]  G4I←2×EI÷(L*2)-RS
[12]  G4←G4+G41-G42+G4I
[13]  →(N<MAX)/L1
      ▼
```

F3

Similarly, F3 finds G6 and G7 (Eqs. 4-33f and 2).

```
      ▼ L F3 B
[1]   G6←G7←0
[2]   N←¯1
[3]  L2:N←N+1
[4]   SGS←(B*2)+(○N÷DEL)*2
[5]   SG←SGS*0.5
[6]   BSG←B+SG
[7]   DR←BSG÷SG+L
[8]   G6←G6+DR×(*-LX1+SG×Z1)-*-LX2+SG×Z2
[9]   G71←BSG×EX1×(*-SG×|XI1)÷L-SNL×SG
[10]  G72←BSG×EX2×(*-SG×|XI2)÷L+SNU×SG
[11]  G7I←2×EI÷(L*2)-SGS
[12]  G7←G7+G71-G72+G7I
[13]  →(N<MAX)/L2
      ▼
```

F5

Having the necessary input, F5 assembles the final matrix equation and evaluates the determinant of [G] (Eq. 4-35); DET is a function for evaluating the determinant of

a matrix.

```
     ▼ F F5 EF
[1]  C←C1×F×(ER-EF)*0.5
[2]  BB←C1×F×(EF-1)*0.5
[3]  L F1 C
[4]  L F2 C
[5]  L F3 BB
[6]  G←G1+G2-G3+G4
[7]  H←G5,[1](ER×DEL×BB×G)-G6+G7
[8]  DET 14 14 ↑H
     ▼
```

Fixing the frequency, F5 should be executed few times around the expected ε_e , until the point is found for which the determinant of |G| vanishes.

Appendix D

Workspace RT

The following notation is used in this workspace:

EPS: the precision to which the roots of Eq. 5-6c should be found,

ER: ε_r

F: fh in GHZ·mm,

NX: number of positive roots of Eq. 5-16b to be found,

RO: ρ_m

D

This function evaluates Eq. 5-16b.

```
     ▼ RR←D R1
[1]   RS←R1*2
[2]   MU←(1AS-RS)*0.5
[3]   →(AS<RS)/L1
[4]   F1←MU×5○DEL×MU
[5]   F2←6○DEL×MU
[6]   →L2
[7]  L1:F1←-MU×1○DEL×MU
[8]   F2←2○DEL×MU
[9]  L2:RR←(ER×F1×2○R1)-R1×F2×1○R1
     ▼
```

ROOT

Given a certain frequency, ROOT finds ρ_m, the first NX positive roots of Eq. 5-6c.

```
      ▼ F ROOT NX
[1]    AS←(ER-1)×(CC1×F)*2
[2]    RO←NX⍴0
[3]    N1←N←0
[4]   L0:N←N+1
[5]    →(N>NX)/0
[6]   L1:I←0
[7]    A←○0.5×N+N1-1
[8]    B←○0.5×N+N1
[9]   L2:M←0
[10]   V←A+T×B-A
[11]  L3:M←M+1
[12]   I←I+1
[13]   →(I>IM)/L7
[14]   RS1←D V[M]
[15]   RS2←D V[M+1]
[16]   SN←RS1×RS2
[17]   →(SN<0)/L4
[18]   →(SN=0)/L5
[19]   →(M≥10)/L31
[20]   →L3
[21]  L31:N1←N1+1
[22]   →L1
[23]  L4:A←V[M]
[24]   B←V[M+1]
[25]   →((B-A)>EPS)/L2
[26]   RO[N]←V[M]
[27]   →L0
[28]  L5:→(RS1=0)/L6
[29]   RO[N]←V[M+1]
[30]   →L0
[31]  L6:RO[N]←V[M]
[32]   →L0
[33]  L7:'NO CONVERGENCE'
[34]   'N IS'
[35]   N
[36]   'ITERATION NO. IS'
[37]   I
      ▼
```

Workspace NIN

The notation used in this workspace is as follows:

A: is A, Eq. 5-7c,

C: is C, Eq. 5-7e,

EF: is ε_v,

ER: is ε_r,

ET: is η, Eq. 4-22c,

M1: is M, Eq. 5-10a,

M3: is the number of terms retained in Eq. 5-10a,

MR: is R, Eq. 5-15,

NDB: is $\bar{\bar{\nu}}_m$, Eq. 5-9c,

NMB: is $\bar{\nu}_m$, Eq. 5-9c,

RO: ρ_m,

TH: θ_j, Fig. 5-3,

THL: θ_{lj}, Fig. 5-3,

THU: θ_{uj}, Fig. 5-3.

DATA

Finds θ_{ur}, θ_r, and θ_{lr} (Fig. 5-3).

```
     ▼ DATA
[1]  MV←⍴W
[2]  THU←0,0.5×(¯1↓MR)+MR
[3]  THL←0,¯1↓THU
[4]  SL←1↓THL
[5]  SU←1↓THU
[6]  SM←0.5×SL+SU
[7]  TH←¯1↓SM
[8]  MBB←0.5×TH-THL
[9]  PB←0.5×TH+THL
[10] MDB←0.5×THU-TH
```

```
[11]  PDB←0.5×THU+TH
[12]  SB←1○(GM∘.×MBB)+(MV,MR)⍴PB
[13]  SDB←1○(GM∘.×MDB)+(MV,MR)⍴PDB
      ▼
```

F2

Computes f_2 of Eq. 5-38b. f_1 of Eq. 5-20a is included.

```
      ▼ R2←S F2 SP
[1]   R11←RR1,(1○NMB×RR1),⍟-NDB×RR1←ET×|S+SP
[2]   R12←RR2,(1○NMB×RR2),⍟-NDB×RR2←ET×|S-SP
[3]   R2←R11+R12
      ▼
```

F3

Computes f_3 of Eq. 5-20c.

```
      ▼F3[□]▼
      ▼ R3←S F3 I
[1]   R3←(S F2 SU[I])+(¯2×S F2 SM[I])+S F2 SL[I]
      ▼
```

F0

Computes the coefficients of Eq. 5-10a using the roots of Eq. 5-6c; ρ_m should be copied from RT first.

```
      ▼ F0 C
[1]   M3←⍴RO
[2]   M←0
[3]  L3:M←M+1
[4]   →(M>M3)/L31
[5]   →(C>RO[M])/L3
[6]  L31:M1←M-1
[7]   M←0
[8]  L4:M←M+1
[9]   →(M>M3)/L41
[10]  →(A>RO[M])/L4
[11] L41:MA←M-1
[12]  RS←RO⍟2
[13]  CS←C⍟2
[14]  NU←(|CS-RS)⍟0.5
[15]  NMB←M1↑NU
[16]  NDB←M1↓NU
```

```
[17]  MU←(1AS-RS)*0.5
[18]  MB←MA↑MU
[19]  MD←MA↓MU
[20]  S1B←5○DEL×MB
[21]  S1D←1○DEL×MD
[22]  C1←(6○DEL×MB),2○DEL×MD
[23]  S2←1○RO
[24]  C2←2○RO
[25]  Q1←(S1B,S1D)÷DEL×MU
[26]  Q2←MU×S1B,-S1D
[27]  P1B←RO×S2×Q2
[28]  P3←(ER×DEL×Q1×C2)+(C1×C2×1+ER×DEL)+ER×Q2×S2÷RO
[29]  P3←P3+(C1×S2÷RO)-Q1×RO×S2×DEL*2
[30]  Q←P1B÷P3×NU*3
[31]  Q01←C×1○C
[32]  Q02←(AS-CS)*0.5
[33]  Q03←Q02×5○DEL×Q02
[34]  Q0←Q01×Q03÷(ER×Q03×2○C)-Q01×6○DEL×Q02
[35]  Q←Q0,Q
      ▼
```

FH

Given ε_e , FH finds the determinant of |H| using DET. FH is executed around the expected values of ε_e for a certain fh(for which ρ_m is found in RT) until an ε_e is found for which the determinant of |H| vanishes (Eq. 5-16).

```
      ▽ FH EF
[1]   A←AS*0.5
[2]   C←A×((ER-EF)÷ER-1)*0.5
[3]   F0 C
[4]   H←(MR,MR)ρ0
[5]   I←1
[6]  L0:R←1
[7]  L1:SUM1←SUM2←(M3+1)ρ0
[8]   V←1
[9]  L2:SUM1←SUM1+W[V]×SB[V;R] F3 I
[10]  SUM2←SUM2+W[V]×SDB[V;R] F3 I
[11]  V←V+1
[12]  →(V≤MV)/L2
[13]  H[I;R]←H[I;R]++/Q×(SUM1×MBB[R])+SUM2×MDB[R]
[14]  R←R+1
```

```
[15]  →(R≤MR)/L1
[16]  I←I+1
[17]  →(I≤MR)/L0
[18]  DET H
      ▼
```